HYDROLOGIC IMPLICATIONS OF SNOW-VEGETATION INTERACTIONS IN A SEMIARID MOUNTAIN CLIMATE

by

Maggi Kraft

A dissertation

submitted in partial fulfillment

of the requirements for the degree of

Doctor of Philosophy in Geoscience

Boise State University

May 2023

BOISE STATE UNIVERSITY GRADUATE COLLEGE

DEFENSE COMMITTEE AND FINAL READING APPROVALS

of the dissertation submitted by

Maggi Kraft

Dissertation Title: Snow-Vegetation Interactions in a Semiarid Climate

Date of Final Oral Examination: 14 November 2022

The following individuals read and discussed the dissertation submitted by student Maggi Kraft, and they evaluated the student's presentation and response to questions during the final oral examination. They found that the student passed the final oral examination.

James P. McNamara, Ph.D.	Chair, Supervisory Committee
Hans-Peter Marshall, Ph.D.	Member, Supervisory Committee
Alejandro Flores, Ph.D.	Member, Supervisory Committee
Nancy Glenn, Ph.D.	Member, Supervisory Committee

The final reading approval of the dissertation was granted by James P. McNamara, Ph.D., Chair of the Supervisory Committee. The dissertation was approved by the Graduate College.

DEDICATION

This dissertation is dedicated to Jasper and Star. Thank you for your unwavering love, support, and loyalty.

ACKNOWLEDGMENTS

I would like to thank my family for their support and patience. Thank you to my advisor, Jim McNamara, for your feedback and guidance throughout the PhD program. I would like to thank the following people for their help in the field; Dan Murray, Thomas Othiem, William Rudisill, Megan Mason, Star Wieland, Matt Wieland, Jasper Kraft, Josh Morell, and Monica Vermillion. Additionally, thank you to Dr. Link for loaning me the radiometers. Thank you for to the reviewers in chapter 2 and 3 and my committee for their insightful comments and suggestions. This dissertation was funded in part by the Idaho NASA Idaho Space Grant Association, the National Science Foundation, and Boise State University.

ABSTRACT

Knowledge of the complex interaction between snow, vegetation, and streamflow in semiarid mountain climates is necessary for predicting water resources. The effects of warming temperatures on snow distribution will cascade into vegetation water use and streamflow. Due to our reliance on snow water resources, it is necessary to understand how vegetation affects snow distribution, how vegetation uses snow water inputs and the subsequent effects on streamflow in the current and warming climate. The overall objective of this research is to improve our understanding of snow-vegetation interactions in a semiarid climate. In this dissertation, I use field data to evaluate how vegetation impacts snow accumulation and melt, and how snow distribution and climate parameters affect vegetation. I then apply a physically based model to understand how warming temperatures across the rain-snow transition will affect snow water input for vegetation water use. In the first chapter, I introduce the primary objectives and provide background for the following chapters. In the second chapter, I use field data at two different locations to evaluate how vegetation affects the snow surface energy and mass balance. I found forests accumulate less snow, have a lower cold content to overcome before melting starts and shade the snow surface slowing the melt rate. In the third chapter I estimate evapotranspiration (ET) at five sites spanning the rain-snow transition and I compare ET to climate parameters. Annual ET at the low elevation site is controlled by a balance between spring precipitation and supplying water and energy drivers. The site in the rain-snow transition follows the soil moisture availability, increasing annual ET with

precipitation. Annual ET at the middle and high elevation sites increases with an earlier snow disappearance date. In the fourth chapter, I apply a physically based model to evaluate how warming temperatures alter the rain-snow transition and subsequent ET and streamflow. I found warming temperatures in the fall reduce peak SWE, increase fall streamflow, and shift spring streamflow earlier but have limited effects on ET. Warming temperatures in the spring increase ET and shift spring streamflow timing earlier. Increasing ET rates in the spring lead to reduced ET rates in the summer. Additionally, the forest and seasonal snow zones are most sensitive to warming temperatures. This dissertation advances our understanding of how snow and vegetation interact and how vegetation will respond in a warming climate.

TABLE OF CONTENTS

LIST OF TABLES

LIST OF FIGURES

LIST OF ABBREVIATIONS

BR	Bogus Ridge
BT	Bull Trout
DBH	Diameter Breast Height
DDS	Dynamically Dimensioned Search Algorithm
DEM	Digital Elevation Model
EC	Eddy Covariance
ET	Evapotranspiration
GOF	Goodness of Fit
IDW	Inverse Distance Weight
KGE	Kling Gupta Efficiency
LAI	Leaf Area Index
LDP	Lower Deer Point
LG	Lower Gage
LIDAR	Light Detection and Ranging
LW	Lower Weather
MAM	March April May
MODIS	Moderate Resolution Imaging Spectroradiometer
NDVI	Normalized Difference Vegetation Index
NLCD	National Land Cover Database
RH	Relative Humidity

SH	Shingle Creek
SNOTEL	SNOw TELemetry
SWE	Snow Water Equivalent
TL	Treeline
VPD	Vapor Pressure Deficit
WY	Water Year

CHAPTER ONE: INTRODUCTION

In the mountainous areas of the western United States snow is the primary source of environmental and societal water resources (Trujillo *et al.*, 2012; Li *et al.*, 2017). Hydrologists rely on mountain snowpack observations to provide water resource predictions for farmers, hydropower, and resource managers (Church, 1933; Martinec *et al.*, 1983; Garen, 1992). The complex landscape of mountains imposes challenges to hydrologic prediction with heterogeneous topography, vegetation, and subsurface properties that create equally complex snow distribution patterns and snow-to-streamflow transmittance. Watersheds spanning the rain-snow transition, where precipitation shifts from rain to snow, and ecosystems shift from relying on rain to snow dominated hydrologic regimes, complicate the snow-vegetation-streamflow interactions (Richardson *et al.*, 2013; Hammond *et al.*, 2019; Harrison *et al.*, 2021). Yet, despite the reliance on snow water resources, we lack a complete understanding of snow-vegetation-streamflow interactions in semiarid environments (Dickerson-Lange *et al.*, 2021).

In semiarid climates of the western United States, evaporation, and transpiration (ET) comprise about half the hydrologic budget (Aishlin and McNamara, 2011; Kormos *et al.*, 2014; Hammond *et al.*, 2019) with most of the water falling as snow during the winter months. Trees rely on snow water, sourcing up to 87.5% of their water from snow, and are affected by the timing of soil water inputs and rates (Martin *et al.*, 2018; Hammond *et al.*, 2019). Variability in snowmelt timing and snow water availability potentially alter vegetation water use and productivity (Hu *et al.*, 2010; Knowles *et al.*,

2018). Warming temperatures will shift the snowmelt timing earlier in the spring and raise the rain-snow elevation, altering the current hydrologic regime (Tague *et al.*, 2009; Klos *et al.*, 2014). In the western United States, 25% of the land surface has an intermittent snowpack (present partially through the winter), while a seasonal snow pack (present all winter) covers 13% of the region (Moore *et al.*, 2015). With a disproportionate amount of streamflow coming from the seasonal snow zones (Hammond *et al.*, 2018a; Harrison *et al.*, 2021). In the same region, two-thirds of the water supply originates from forested environments (Brown *et al.*, 2008). Consequently, a shift in the rain-snow elevation and intermittent snow zone in forested environments can have a large impact on downstream water resources. Therefore, understanding vegetation-snow interactions spanning the rain-snow transition is necessary to make informed predictions of the hydrologic water balance.

The overall goal of this research is to evaluate how vegetation affects snow distribution, how snow distribution affects vegetation, and the subsequent impacts on the hydrologic system in a semiarid climate spanning the rain-snow transition. This research incorporates field data and a modeling approach to analyze the spatial and temporal variability of snowmelt and vegetation water use. This research improves understanding of the snow surface energy balance and resulting snowmelt variability at both the plot and watershed scale spanning the rain-snow transition.

Background

Forests alter the snow surface energy and mass balance compared to open areas creating variable snowmelt rates (Fig. 1.1; Sicart *et al.*, 2004; Ellis and Pomeroy, 2007; Seyednasrollah *et al.*, 2013; Malle *et al.*, 2019). Forests increase longwave radiation

(Lundquist *et al.*, 2013), and tree debris decreases the snow albedo (Hardy *et al.*, 2000; Webster and Jonas, 2018) resulting in increased net total radiation. Conversely, forests can decrease net radiation at the snow surface by shading the surface from shortwave radiation (Ellis *et al.*, 2013; Malle *et al.*, 2019), and protect the surface from wind and increased sublimation rates (Pomeroy, 1994; Dickerson-Lange *et al.*, 2017; Roth and Nolin, 2017). Additionally, forests intercept snowfall reducing snow accumulation (Hedstrom and Pomeroy, 1998; Dickerson-Lange *et al.*, 2017; Roth and Nolin, 2017). Forest cover effects on the snow energy and mass balance have been widely observed, but the role and degree of different snow processes affecting snow distribution vary by climate (Lundquist *et al.*, 2013), and latitude (Molotch *et al.*, 2009).

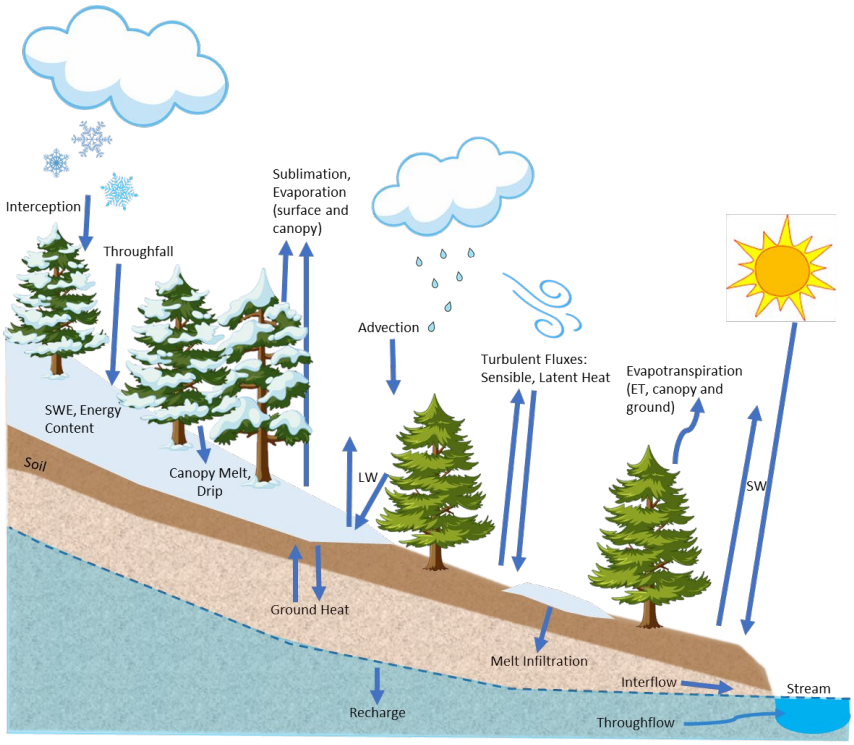

Figure 1.1 Schematic illustration of snow energy and mass balance processes in vegetated environments.

Snowmelt timing initiates the peak soil moisture (McNamara *et al.*, 2005; Smith *et al.*, 2011) and therefore the synchrony of soil moisture availability with energy drivers and early season ET rate (Poulos *et al.*, 2021). The effects of the synchronicity between snowmelt and energy have been observed along an elevational gradient with lower ET rates on low elevations and south facing slopes that melt earlier compared to high elevations and north facing slopes (Barnard *et al.*, 2017; Poulos *et al.*, 2021; Seyfried *et al.*, 2021). We would expect a similar relationship between different vegetation types; vegetation in areas with earlier snowmelt having lower ET rates early in the season (Fellows *et al.*, 2019). If snow melts later in the forest, peak soil moisture occurs when temperatures are higher supporting soil water necessary for tree establishment. Partially canceling the effects of later soil moisture availability, forests intercept snow, reducing the snow water accumulation and meltwater availability (Pomeroy *et al.*, 1998; Gleason *et al.*, 2021). The heterogeneity of snowmelt timing also affects the ET rates. Uniform snowmelt results in a single pulse of melt water saturating the soil. Heterogeneous snowmelt allows ET to occur as snow patches are melting leading to a longer period with increased soil moisture and ET (Hammond *et al.*, 2019). These examples demonstrate the interconnectedness of snow and vegetation highlighting the need to know the primary role of forests on the snow surface energy balance and spatiotemporal variability of snowmelt. We can apply an understanding of snow-vegetation interactions to evaluate how and why ET varies and how warming temperatures will affect snow water resources across an elevational gradient.

Dissertation Summary

The following chapters in this dissertation address three topics: 1) How does vegetation impact snowmelt timing and distribution? 2) What controls ET at different elevations spanning the rain-snow transition? 3) How will warming temperatures across the rain-snow transition alter snow and rain surface water inputs and subsequent ET and streamflow?

Chapter 2 evaluates how vegetation affects snow accumulation and snowmelt. We used field data to analyze snow surface energy inputs and snow depth in different vegetation covers. Our results indicate during the accumulation period the forests accumulated less snow and had a lower cold content to overcome before melting started. During the melt period, the low-density forests shade the snow surface slowing the melt rate. The snow melted uniformly between forest covers unless there was a large spring storm adding variability in the snow depths prior to snow disappearance.

Chapter 3 we use field data to estimate actual ET at sites along an elevation gradient and compare annual and daily ET to environmental parameters of soil moisture, air temperature, vapor pressure deficit, snow cover and precipitation. We observed three trends with ET across the watershed. ET at the low elevation site was a balance between spring precipitation supplying soil moisture into the summer season and precipitation limiting the energy drivers in the spring. The sight in the rain-snow transition followed the soil moisture availability, increasing ET rates as soil moisture increased. The middle and high elevations sites were limited by the growing season length, thus ET increased as snowmelt timing shifted earlier.

Chapter 4 applies a modeling framework to evaluate how warming temperatures affect snow disappearance timing and ET. Modeled ET suggested warmer fall temperatures reduced the peak SWE, increased fall streamflow, and shifted spring streamflow timing earlier but had limited effects on ET due to asynchrony between energy and soil moisture availability. Warmer temperatures in the spring increased ET and shifted streamflow timing earlier. Increased ET early in the spring led to reduced ET rates in the summer and fall. Across the rain-snow transition, ET rates in the forest and seasonal zones were the most sensitive to increased temperatures.

CHAPTER TWO: FOREST IMPACTS ON SNOW ACCUMULATION AND MELT IN A SEMIARID MOUNTAIN ENVIRONMENT

This Chapter has been published as: Kraft, M., McNamara, J. P., Marshall, H.P., Glenn, N.F. (2022). Forest Impacts on Snow Accumulation and Melt in a Semi-arid Mountain Environment. *Front. Water* 4:1004123. Doi: 10.3389/frwa.2022.1004123

Abstract

Snowmelt is complex under heterogeneous forest cover due to spatially variable snow surface energy and mass balances and snow accumulation. Forest canopies influence the under-canopy snowpack net total radiation energy balance by enhancing longwave radiation, shading the surface from shortwave radiation, in addition to intercepting snow, and protecting the snow surface from the wind. Despite the importance of predicting snowmelt timing for water resources, there are limited observations of snowmelt timing in heterogeneous forest cover across the Intermountain West. This research seeks to evaluate the processes that control snowmelt timing and magnitude at two paired forested and open sites in semi-arid southern Idaho, USA. Snow accumulation, snowmelt, and snow energy balance components were measured at a marginal snowpack and seasonal snowpack location in the forest, sparse vegetation, forest edge, and open environments. At both locations, the snow disappeared either later in the forest or relatively uniformly in the open and forest. At the upper elevation location, a later peak in maximum snow depth resulted in more variable snow

disappearance timing between the open and forest sites with later snow disappearance in the forest. Snow disappearance timing at the marginal snowpack location was controlled by the magnitude and duration of a late season storm increasing snow depth variability and reducing the shortwave radiation energy input. Here, a shorter duration spring storm resulted in more uniform snowmelt in the forest and open. At both locations, the low-density forests shaded the snow surface into the melt period slowing the melt rate in the forest. However, the forest site had less cold content to overcome before melting started, partially canceling out the forest shading effect. Our results highlight the regional similarities and differences of snow surface energy balance controls on the timing and duration of snowmelt.

Introduction

Snowmelt is an important component of the hydrologic cycle for environmental and economic use. The accumulation and melting of snow are impacted by many factors including climate (Molotch *et al.*, 2009; Musselman *et al.*, 2021), vegetation (Dickerson-Lange *et al.*, 2017), and topography (Kormos *et al.*, 2014). Local controlling factors such as the distribution of forested and open areas (Lundquist *et al.*, 2013), aspect (Kormos *et al.*, 2014), and wind (Winstral *et al.*, 2009) can influence snow distribution differently depending on regional climate factors. Developing an understanding of the governing controls on snow accumulation and melt in different hydroclimatic regions is essential to predicting current and future water resources.

Several studies have addressed the different drivers of snow accumulation and melt across climate regions. In warm regions over 20% of the annual snow water resources melt during the accumulation season while in cold regions, <5% of the annual

snow water resources mobilize before spring melt (Musselman *et al.*, 2021). The average annual snow accumulation in the region contributes to whether a snowpack will melt or accumulate snow during warm storms. During warm storms, deep low density snowpacks accumulate snow rather than melt snow (Haleakala *et al.*, 2021a). Accumulation of Snow Water Equivalent (SWE) at warmer, marginal snowpack locations are governed by temperature while higher, colder locations are more limited by precipitation (Haleakala *et al.*, 2021a). Additionally, regional air temperature influences the effect of forest canopy on accumulation and melt. In warmer regions, the magnitude of forest interception tends to be greater than open areas reducing the under canopy snow accumulation (Dickerson-Lange *et al.*, 2021). During the melt period, forest shading in combination with spring temperatures influences whether a region will retain snow in the forest or open longer (Dickerson-Lange *et al.*, 2021; Safa *et al.*, 2021). Several studies demonstrate the regional differences in snow accumulation and melt between forests and open (Dickerson-Lange *et al.*, 2021; Safa *et al.*, 2021) and warm and cold climates (Haleakala et al., 2021; Musselman et al., 2021).

Snow and weather observations are typically made in the open, however in the Western United States two-thirds of the water supply originates from forested environments (Brown *et al.*, 2008; Lundquist *et al.*, 2013). The distribution of forest openings within a forest influence snow accumulation and melt across a landscape, resulting in spatially heterogeneous snow depth and snowmelt timing (Moeser *et al.*, 2014; Mazzotti *et al.*, 2019; Koutantou *et al.*, 2022). Forest openings increase snow water storage retention where vegetation is not intercepting snow, and surrounding vegetation protects these areas from wind and solar radiation (Dickerson-Lange *et al.*, 2017). The

structure of forest gaps influences the snow depth with mean snow depths higher when the open fraction is concentrated in larger gaps rather than numerous, fragmented smaller gaps (Mazzotti *et al.*, 2019). Canopy snow interception reduces the sub-canopy snow accumulation, indicating that canopy density is a first-order process in snow accumulation (Roth and Nolin, 2019). Snow that is intercepted by a forest canopy may sublimate, melt, or release onto the surface depending on meteorological conditions, decreasing the snow available to melt and streamflow (Storck *et al.*, 2002). Where wind influences snow accumulation and melt, snow depth is greater and persists longer in the forests compared to non-forested areas (Roth and Nolin, 2019; Hojatimalekshah *et al.*, 2020). Additionally, forest structure alters the snow surface net radiation, impacting snow accumulation and melt (Hardy *et al.*, 2004; Lawler and Link, 2011; Lundquist *et al.*, 2013). Net radiation is enhanced in small gaps or near the forest edge from the contribution of shortwave radiation and longwave radiation (Seyednasrollah and Kumar, 2014; Webster *et al.*, 2016). High emissivity and increased forest temperatures increase longwave radiation from vegetation compared to open areas creating a variable snowpack energy balance in forested environments (Pomeroy *et al.*, 2009; Lundquist *et al.*, 2013). Counteracting increased longwave radiation, forests can shade the snow surface from incoming shortwave radiation, decreasing the incoming shortwave radiation compared to open areas (Malle *et al.*, 2021). At the forest edge shading can vary by edge exposure with north forest edges shading the snow surface (Currier and Lundquist, 2018). These canopy influences on snow processes create uncertainty when estimating the snow surface energy balance and are challenging to represent when simulating snowmelt and ecohydrological processes throughout watersheds.

Understanding when and where snow is accumulating and melting is important for predicting the movement of meltwater in watersheds. Earlier snowmelt is associated with an earlier start of the growing season (Harpold, 2016; Poulos *et al.*, 2021), increased plant transpiration early in the season (Kraft and McNamara, 2022), and reduced streamflow (Hammond *et al.*, 2018b; Milly and Dunne, 2020). Peak soil moisture occurs on or within a few days of snow disappearance and declines into the summer season (Smith *et al.*, 2011; Hammond *et al.*, 2019). An earlier start of the soil moisture recession potentially results in greater vegetation water use early in the season but extends the summer plant water stress (Harpold, 2016; Poulos *et al.*, 2021). Elevation is a primary control on snow distribution and the magnitude of snow for streamflow. For example, Rice et al. (2011) found high elevations contributed about one-third of snowmelt to streamflow, while middle elevations contributed 40-60% of annual snowmelt. However, the contribution of snow from different elevations likely varies due to physiographic differences between watersheds. Additionally, the uniformity of the snowpack affects the melt rate and streamflow contribution. In an alpine catchment in Colorado, Badger et al. (2021) indicated a more spatially uniform snowpack melts earlier due to greater energy exposure per unit of SWE, resulting in decreased streamflow. The effects of a more uniform snowpack on decreased streamflow were more sensitive in years with lower mean SWE. This indicates that sites with shallower snowpacks may be more susceptible to changes in streamflow and a more uniform snowpack could reduce soil water availability into the summer months. Due to the spatial variability of snow distribution, knowledge of the watershed scale snow distribution is critical to predicting streamflow for environmental and societal water use. Understanding the processes controlling snow

accumulation and snowmelt rate and timing at fine scales is important for improving model predictions of snow water resources (Broxton *et al.*, 2021).

The impact of vegetation on snow cover duration varies in different vegetation types, latitudes, and snow climates (Dickerson-Lange *et al.*, 2021). Snowmelt spatial variability has been explored in maritime climates (Dickerson-Lange *et al.*, 2015; Hubbart *et al.*, 2015; Roth and Nolin, 2017), high Rocky Mountain cold continental climates, (Fang and Pomeroy, 2016; DeBeer and Pomeroy, 2017), and the semi-arid southern Rockies (Molotch *et al.*, 2009; Broxton *et al.*, 2015) but, only a few studies have considered snow distribution in an intermountain semi-arid environment.

Previous research on snow distribution in a semi-arid environment highlighted the effects of aspect on snow water inputs (Kormos *et al.*, 2014), rain-on-snow events (Marks *et al.*, 2001), model structure (Havens *et al.*, 2019), and local differences in vegetation (Marks and Winstral, 2001). Relatively little attention has been given to how vegetation and regional differences in climate affect the spatiotemporal variability of snowmelt in the intermountain, semi-arid environment which supplies streamflow for reservoirs and summer water use. In these climates it has been hypothesized that the dominant role of forests is to shade the snow surface rather than intercept snow or enhance longwave radiation (Dickerson-Lange *et al.*, 2021; Safa *et al.*, 2021). However, there are limited studies quantifying the under canopy snow surface energy balance in the cold semi-arid intermountain climates. Dickerson-Lange et al. (2021) highlighted the need for additional research of forest-snow observations in these climates where forest effects can flip from forests shortening to lengthening snow duration.

Within the cold intermountain climate region, snow distribution can range from a marginal (<1 m deep) and intermittent snow cover lasting for four months or less to a relatively deep (>2 m) seasonal snowpack, remaining for eight months out of the year. The variability of snow cover season and depths potentially leads to differences in the sensitivity of the snow surface energy and mass balance within the region (Jennings *et al.*, 2018). Marginal and warm snowpacks, with wintertime temperatures close to 0°C, are more sensitive to a unit increase in snow depth and energy compared to a cold and deep, seasonal snowpacks (Lopez-Moreno *et al.*, 2017; Jennings *et al.*, 2018). The marginal snowpacks produce mid-season snowmelt, begin melting earlier in the spring season, and are more susceptible to rain-on-snow events compared to deep, seasonal snowpacks (Kormos *et al.*, 2014; Bilish *et al.*, 2019). The different snowpack energy states in marginal and seasonal snowpacks highlight the need to evaluate both snowpack states to understand forest-snow processes.

This research evaluates processes controlling snowmelt timing and magnitude in forested, forest edge, sparse vegetation, and open sites at a marginal snowpack and seasonal snowpack location in semi-arid southern Idaho, USA. Specifically, we ask the following question: (1) What are the relative importance of canopy interception, forest-enhanced longwave radiation, and reduced shortwave radiation by shading in snow accumulation and melt in marginal and seasonal snowpacks?

Methods

Study Sites

Bull Trout Study Location

The Bull Trout study location (BT), located in the Bull Trout Lake Watershed in

southern Idaho (Fig. 2.1), has instrumentation distributed on the western edge of a flat meadow at an elevation of 2133 m, and the Banner Summit SNOTEL is 2 km away (Fig. 2.2). The Banner SNOTEL and BT watershed have a seasonal snowpack, receiving an average of 2 m of snow per year with the winter/spring snow cover season lasting from November to early June. The dominant winter (DJFMA) precipitation phase is 61% snow and daily average winter air temperatures range from -19.0 to 6.5 °C with an average of -6.0 °C. Winter precipitation constitutes about 68% of the annual precipitation. During the study period (snow covered period between October 2019 and June 2021) wind speeds ranged from 0.0 to 3.0 m/s with an average wind speed of 0.7 m/s. The dominant vegetation type includes subalpine fir with an understory of coarse woody shrubs. The mean canopy height at the location is 7.0 m and the Leaf Area Index (LAI) in the forested site is 2.0 m^2m^{-2}. To measure LAI and Sky View Factor (SVF), 360-degree photographs using the Ricoh Theta X 360-degree camera were taken below each sensor. Methods for capturing, processing, and changing the images into hemispherical photographs follow Honjo et al. (2019) and the Hemisfer program was used to calculate SVF and LAI above each sensor (Schleppi *et al.*, 2007).

We installed a weather station in the open at the Bull Trout location on 2019-11-23 recording hourly air temperature, relative humidity, incoming and outgoing longwave and shortwave radiation, wind speed and direction, and snow surface temperature. Additionally, the BT study location is located 2 km from a SNOTEL station at an elevation of 2145 m at Banner Summit. The SNOTEL station collects hourly SWE, soil moisture, and temperature at 2.0, 8.0, and 20.0 cm depths below the surface, air

temperature, wind speed and direction, and relative humidity. Soils at the SNOTEL station and the BT location are loamy sand (Soil-Survey-Staff, 2013). Average daily air temperatures at the Bull Trout weather stations were biased by 2.8 °C and average daily snow depth at the BT location was biased by -2.2 cm compared to the SNOTEL station.

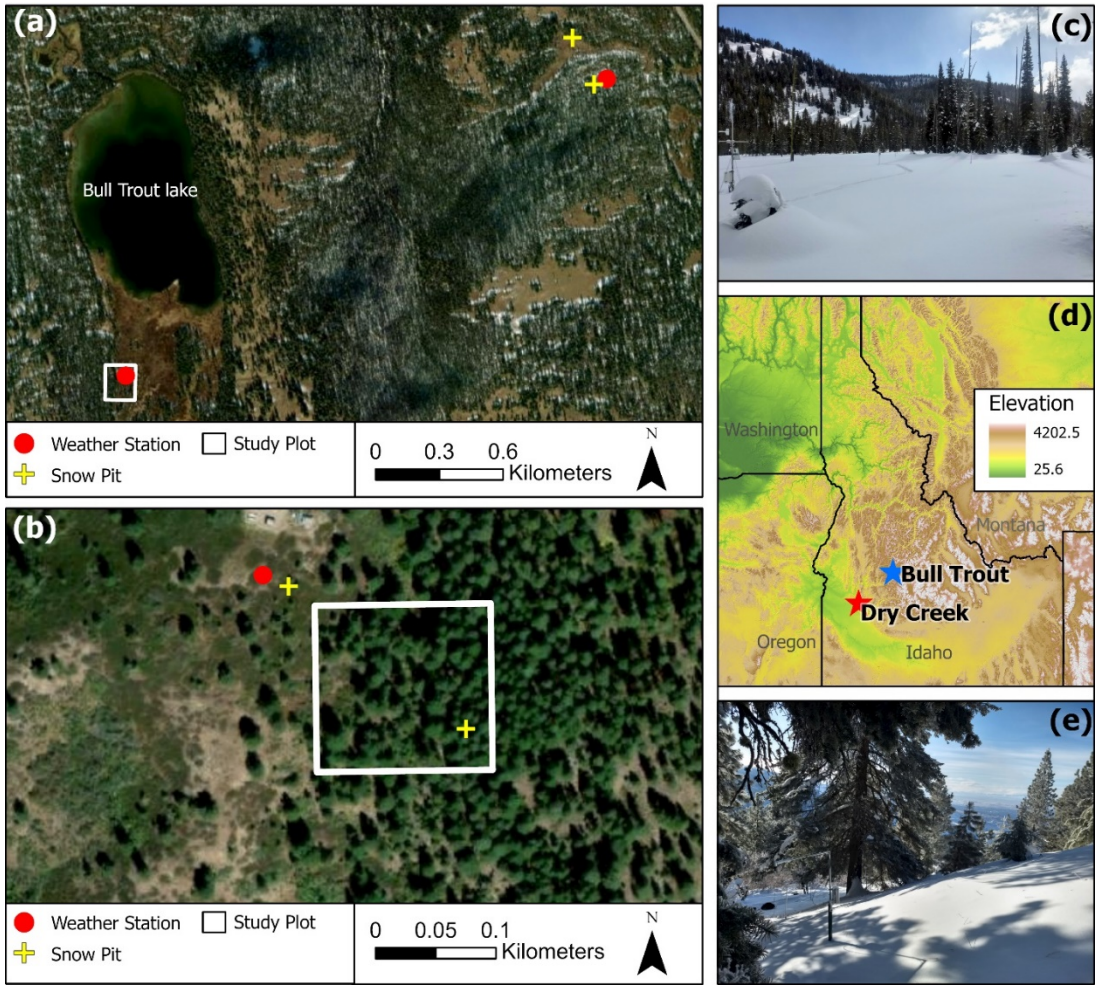

Figure 2.1 Locations with aerial images (Esri, 2017) of the Bull Trout (a) and Dry Creek (b) study location in southern Idaho, overview location of the two study sites (d) and pictures of the BT study location looking south east toward the open site (see Figure 2a) (c) and LDP study location looking south toward the sparse vegetation snow depth sensor (see Figure 2b) (e). The white squares represent the location of the snow depth sensor array and radiometer array (LDP only). The red dots are weather station locations, and the yellow crosses are SnowEx snow pit sites.

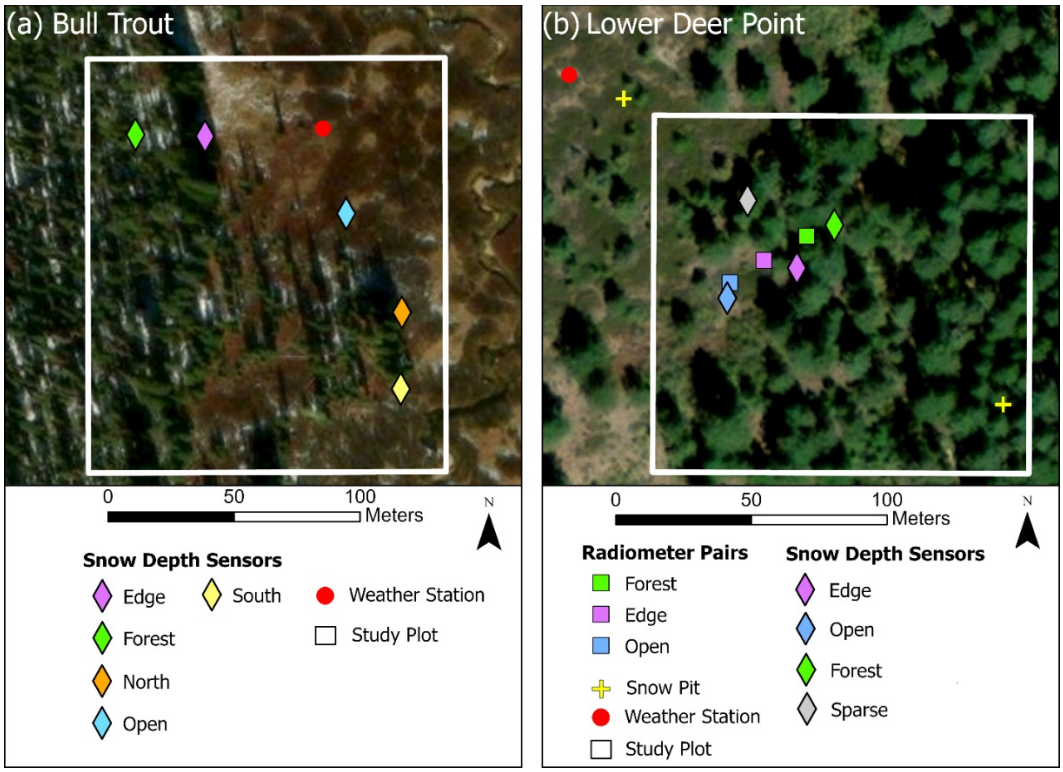

Figure 2.2 Locations with aerial images (Esri, 2017) of sensors at the Bull Trout study location (a) and Lower Deer Point study location (b). The white squares correspond to the white square study locations in Fig. 2.1.

Lower Deer Point Study Location

The Lower Deer Point study location (LDP) located in the Dry Creek Watershed in southern Idaho (Fig. 2.1), has instrumentation distributed across the southeast aspect of the hillslope at an elevation of 1585 m (Fig. 2.2). The LDP location has a marginal snowpack, receiving about 1 m of snow per year with a winter snow cover season from December through early April. The dominant winter (DJFM) precipitation phase is 77% snow and daily average winter air temperatures range from -12.0 to 10 °C with an average of -2.0 °C. Winter precipitation constitutes about 53% of the annual precipitation. During the study period (snow covered period between October 2019 and May 2021) wind speeds ranged from 0.0 to 6.0 m/s with an average wind speed of 2 m/s. The dominant vegetation type includes Douglas fir, Ponderosa pine trees, and an

understory of coarse woody shrubs. The mean canopy height at the plot is about 10 m and the LAI is 2 m^2m^{-2}.

The LDP location has previously been used to monitor snow accumulation and melt (e.g. Anderson et al., 2014) and is located 0.1 km from a weather station. The weather station is located in the open and records hourly measurements of air temperature, precipitation, snow depth, relative humidity, soil moisture, soil temperature, wind speed and direction, and incoming and outgoing longwave and shortwave radiation. However, air temperatures were not recorded due to equipment failure in November 2019. Additionally, soil moisture and temperature are recorded at 2.5, 20, and 33 cm depths adjacent to the weather tower. The soil moisture sensors include Campbell Scientific CS616 Water Content Reflectometers, and soil temperature is measured using thermocouples. The soil at the site is sandy loam, less than one meter deep overlying fractured crystalline bedrock, and porosity at the site is approximately 0.36 (Kelleners *et al.*, 2010; Geroy *et al.*, 2011).

Snow Pits and Sensors

Five ultrasonic snow depth sensors (Maxbotix) were installed at the BT location and four ultrasonic snow depth sensors were installed at the LDP location. The snow depth sensors were installed across a range of forest structures characteristic of the area (Fig. 2.2). At the BT location sensors were in the forest (SVF 41.5%), south canopy edge (SVF 56.5%), north canopy edge (SVF 70.7%), east canopy edge (SVF 71.9%) and in the open (SVF 97.1%). At LDP the sensors were in the forest (SVF 22.3%), open (SVF 81.4%), on the west canopy edge (SVF 52.4%) and in sparse vegetation (SVF 60.2%). The canopy edge was considered the area between SVF 50% and 75%, while the open

was mostly clear of trees (over 75% SVF), and the sparse vegetation had openly spaced trees (about 60% SVF) while the forested sites were in dense forested vegetation (less than 50% SVF). To distinguish between edge and sparse sensor locations, the edge sensors were in the transition between forest and open areas. While the sparse sensor was in an area with trees spaced far enough apart to where their branches did not touch.

The ultrasonic snow depth sensors' record length was from 2019-11-21 through 2021-05-11 at the LDP location and 2019-10-25 through 2021-06-21 at the BT location recording through water years (WY) 2020 and WY 2021. Gaps in the snow depth sensor datasets were due to battery or equipment failures. The nearby weather station snow depth or other snow depth sensors were used to fill gaps based on a linear regression between the weather station and each sensor. Some gaps were not filled due to weather station failure or during periods of weather patterns when the rate of vegetation interception and accumulation was uncertain. Data gaps consisted of 11.9% of the total observations at BT and filled values consisted of 4.9% of the total observations and 7.0% of the observations remained unfilled. The longest gap filled was for the open and north edge site at BT for 27 days in January 2020. Other data gaps filled were for periods less than one week. Data gaps at the LDP location consisted of 9.9% of the total observations and of these observations 6.5% were filled. The longest data gap filled was for 16 days in January 2020 at the west edge site. An additional 11 snow depth sensors were installed in other vegetation structures but were not included in the analysis due to sensor or battery failure. Daily changes in snow depth were calculated at each sensor, classifying all positive changes in the snow depth as snow accumulation and all negative changes in snow depth as snowmelt.

At LDP weekly to bi-weekly snow pits were surveyed between 2020-01-22 to 2020-03-11 and 2021-01-15 to 2021-03-23, as part of the NASA SnowEx Mission. Through both seasons snow pits were surveyed in the open (elevation 1852 m) near the weather station and in the forest in a stand of Ponderosa pine trees (elevation 1809 m) about 120 m from the open site. At the BT location weekly to bi-weekly snow pits were dug at the Banner Summit SNOTEL (2 km from the BT location and referred to as the SNOTEL) between 2019-12-18 to 2020-03-12 and 2021-01-15 to 2021-03-22 and an open site 0.15 km from the SNOTEL site during winter 2020 (also part of the SnowEx Mission). Measurement protocols at both sites follow the NASA SnowEx 2020-21 Experimental Plan (Marshall *et al.*, 2019b). Two profiles of snow density were measured every 10.0 cm using a wedge-shaped density cutter. The snow temperature was recorded every 10.0 cm and the snow depth was measured at each side of the snow pit. The snow pit measurements enable the calculation of SWE (equation 1) and cold content (E_{cc}) (equation 2) for each layer:

$$SWE = \frac{\rho_s}{\rho_w} d_s \qquad \text{(equation 1)}$$

$$E_{cc} = c_i \rho_s d_s (T_s - T_m) \qquad \text{(equation 2)}$$

where ρ_s and ρ_w are the density of the snow and liquid water (kg/m^3), respectively, $d_s$is the snow depth (m), E_{cc} is the cold content (W/m^2), c_i is the specific heat of ice, T_s and T_m are the snow temperature (°C) and melting temperature of snow (0 °C), respectively.

Radiometers

In addition to the four-component radiometers at the LDP and BT weather stations, we installed three paired incoming shortwave and longwave radiometers at the LDP study location on 2019-02-24 (Fig. 2). The radiometers were distributed on the west exposure of the forest edge, in the open and in the forest. The west exposed forest edge had a SVF of 53%, the radiometer pair in the forest had a SVF of 22% and the open site had a SVF of 80%. We assumed the sensors were covered in snow during or immediately following snowstorms and thus data was removed during snowstorms and an hour after the storm ends. Additionally, we installed timelapse cameras to identify and remove data when the radiometers were snow covered for extended periods of time. Additional data gaps were due to battery or sensor failures. Data gaps in the open sensor were filled using the weather station data. We split the incoming radiation measurements into the accumulation (Dec - Feb) and snowmelt (March - April) periods.

Calculated Energy Balance Components

The snow surface energy balance was calculated at a daily timestep using the aggregated hourly weather data from LDP and BT.

$$\Sigma Q = \frac{\Delta E}{\Delta t} \quad \text{(equation 3)}$$

where ΣQ (W/m^2) is the net flux of energy per unit area to the snowpack from the atmosphere and ground (W/m^2), ΔE is the change in the energy state of the snowpack per unit area (W/m^2) and Δt is a specific duration (s).

The net energy flux is described as

$$\Sigma Q = Q_k + Q_L + Q_E + Q_H + Q_G + Q_R \quad \text{(equation 4)}$$

where Q_k is the net shortwave radiation (W/m^2), Q_L is the net longwave radiation (W/m^2), Q_E is the latent heat (W/m^2), Q_H is the sensible heat (W/m^2), Q_G is the ground heat flux (W/m^2) and Q_R is the conductive and advective energy fluxes (W/m^2). Q_R is the conductive and advective energy fluxes and assumed to be negligible at both sites. The net longwave and shortwave radiation were directly measured using four-component radiometers at each site. All other terms were calculated using the station weather data. For parameters not recorded at the BT weather station, we used the nearby SNOTEL data.

The change in energy state of the snowpack depends on if the average snowpack temperature is at or below the freezing temperature.

$$If\ snowpack\ temperature < 0\ °C\text{:}\ \Delta E = \Delta E_{cc}\ ,$$

$$If\ snowpack\ temperature = 0\ °C\text{:}\ \Delta E = \Delta E_{melt}$$

E_{cc} is the internal energy of the snowpack at a given time, commonly known as the cold content (equation 2 above). E_{melt} is the energy associated with phase change (W/m^2)

$$E_{melt} = (SWE)\rho_w \lambda_f \qquad \text{(equation 5)}$$

where λ_f is the latent heat of freezing, and all other variables have previously been defined.

Turbulent Flux

The sensible heat exchange was calculated as

$$Q_H = \frac{0.622\ \rho_a\ c_p\ k^2\ u_{zm}(T_a - T_s)C_s}{[\ln\left(\frac{z_m - z_d}{z_0}\right)]^2} \qquad \text{(equation 6)}$$

where k = 0.4, ρ_a is the density of air (kg/m^3), c_p is the heat capacity of air (MJ/kg K), z_m is the measurement height above the snow surface (m), z_d is the zero-plane displacement

height (m), z_0 is the surface-roughness height (m), u_{zm} is the wind speed (m/s), T_a is the air temperature (°C) and T_{ss} is the snow surface temperature (°C). We assume that z_d is negligibly small, z_m is 2 m, and z_0 is 0.002 m (Morris, 1989; Dingman, 2015). The snow surface temperature was measured at BT station but estimated at the LDP weather station using the longwave radiation measured at the weather station. We found the outgoing longwave radiation and snow surface temperature to be highly correlated at BT (R^2= 0.99).

$$T_s = \left(\frac{L_{out} - L_{in}\,(1 - \varepsilon_{ss})}{\varepsilon_{ss}\sigma}\right)^{1/4} \quad \text{(equation 7)}$$

where L_{out} is outgoing longwave radiation, L_{in} is incoming longwave radiation ε_{ss} is the snow surface emissivity and is set at 0.98, and σ is the Stefan Boltzmann constant.

The stability state of the air above the snow surface was determined by the dimensionless bulk Richardson number, Ri_B.

$$Ri_B = \frac{g * z_m * (T_a - T_s)}{0.5 * (T_a + T_s) * u_{zm}^2} \quad \text{(equation 8)}$$

where g is the gravitational acceleration (9.81 m/s^2) and all other terms have previously been defined.

The turbulent exchange rates can be adjusted by a stability correction factor in stable and unstable conditions (Andreadis *et al.*, 2009). Positive values of Ri_B indicate stable conditions where the warm air and cool snow surface impede turbulent mixing. Negative values of Ri_B indicate unstable conditions where the air is colder than the surface and free convection exists causing increased mixing. We applied equations 9 – 11 as the general stability correction equations (Andreadis *et al.*, 2009; Dingman, 2015).

Unstable Conditions (Ri_B)<0): $C_s = (1 - 16 * Ri_B)^{0.5}$ (equation 9)

Stable Conditions (Ri_B)>0: (equation 10)

$$Ri_u = \frac{1}{\ln\left(\frac{z_m}{z_0}\right)+5}$$

For $0 < Ri_B \leq Ri_u$, (equation 11a)

$$C_s = (1 - \frac{Ri_B}{0.2})^2$$

And for $Ri_B > Ri_u$ (equation 11b)

$$C_s = (1 - \frac{Ri_u}{0.2})^2$$

The latent heat exchange was calculated as

$$Q_E = \frac{0.622\ \rho_a\ \lambda\ k^2\ u_{zm}(e_{zm} - e_s)C_s}{\mathrm{p} * \rho_w * [\ln\left(\frac{z_m - z_d}{z_0}\right)]^2} \quad \text{(equation 12)}$$

where λ is the latent heat of sublimation (MJ/kg), ρ_w is the density of water (kg/m^3), p is atmospheric pressure (kpa), e_{zm} is vapor pressure at the measurement height (kpa), e_s is the vapor pressure at the snow surface (kpa).

Ground Heat

The ground heat was calculated following (Marks *et al.*, 1998)

$$G = \frac{2k_s k_g (T_g - T_s)}{k_g\ z_s + k_s z_g} \quad \text{(equation 13)}$$

where k_g is the thermal conductivity of the soil (W/m K), (k_g = 1.12 W/m K for both sites), k_s is the thermal conductivity of the lower snow layer (W/m K), T_g is the soil temperature (°C), T_s is the bottom snow layer thickness (m) and z_g is the distance below the ground surface (m), z_s is the thickness of the bottom snow layer (m). We used the

measured soil temperature from the SNOTEL near BT at 2 cm depth and the soil measurement site next to the LDP weather station at 2.5 cm depth. The k_s was estimated as 0.3 W/m K (Gray and Male, 1981) for both sites based on the lower snow layer density of 330 kg/m^3. The lower snow layer density was estimated using the average value from the deepest snow density measured in the snow pits. The temperature of the bottom snow layer was estimated using the snow pit temperature profiles and linearly interpolating between each snow pit date. The lower snow pit layer thickness was set at 10 cm.

The measured and calculated energy balance components were split into accumulation and melt periods based on when the energy and mass balances shifted from negative to positive energy flux and the snowpack began to melt. At BT the accumulation period was December through March and the melt period wasApril to snow disappearance at the end of June. At LDP, the accumulation period was December through February, and the melt period was March to snow disappearance in April.

Results

Snow Depth

Bull Trout

At the seasonal snowpack, BT location peak snow depth ranged from 175 cm (WY 2020) and 208 cm (WY 2021) in the open and 152 cm (WY 2020) to 139 cm (WY 2021) in the forest (Fig. 2.3). The timing of peak snow depth was the same for all vegetation covers occurring in early April (WY 2020) and February (WY 2021) (Table 1). On average, the forested sites accumulated 77% less snow, indicating the forest canopy intercepted 23% of the peak snowfall. In both years snow melted out earliest at the south exposed site and latest from the north exposed site (in WY 2021) or forested (in

WY 2020) sites. Snow disappearance ranged from 2020-05-22 to 06-11 (20 days) and 2021-05-13 to 06-03 (21 days) from all sites. However, in WY 2021 all except the north exposed edge site was melted out within 9 days of each other (05-13 to 05-22). The melt rates were lowest in the forest (average 1.6 cm/day since 1 April), highest in the open and south exposed edge sites (average 3.1 cm/day since 1 April), and the east edge site melt rate was closer to the south exposed edge and open sites (average 3.0 cm/day since 1 April). The melt rates at the different sites were similar between the two years except for the forest site where the melt rate was 0.7 cm/day slower in WY 2021.

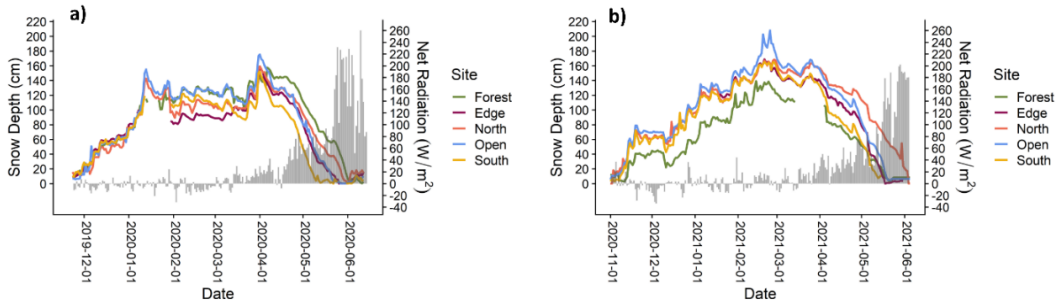

Figure 2.3 Snow depth with net total radiation at the BT location during winter 2020 (a) and winter 2021 (b). Net total radiation was measured at the weather station located in an open canopy cover site.

Lower Deer Point

At the marginal snowpack, LDP location values for peak snow depth ranged from 103 cm (WY 2020) and 117 cm (WY 2021) in the open and 69 cm (WY 2020) and 70 cm (WY 2021) in the forest (Fig. 2.4). On average, the forest accumulated 63% less snow, and the forest canopy intercepted 37% of the snow accumulation. The timing of peak snow depth occurred at the same time for all vegetation covers in mid (WY 2020) to late (WY 2021) February (Table 2.1). Snow melted latest at the forest (WY 2020) and west edge (WY 2021) sites and earliest at the open (WY 2020) and sparse (WY 2021) sites. In both years snow melted out in the open before the forest site, however, in 2021 the

difference was only one day. Snow disappearance timing from all sites ranged from a 19 day difference (WY 2020) to a 7 day difference (WY 2021). The snowmelt rate from the snow depth peak to snow disappearance and 1 March to snow disappearance were both faster in all vegetation covers in 2021 with an average melt rate of 2.5 cm/day in 2021 and 1.4 cm/day in 2020. The fastest melt rate was at the open site (average 2.4 cm/day since 1 March) and the slowest melt rate was at the forest site (average 1.4 cm/day since 1 March).

Table 2. 1 Bull Trout and Lower Deer Point snow depth and melt rates and timing.

	Site	Year	Snow Disappearance Date	Peak Snow Depth Date	Peak Snow Depth (cm)	1 April Snow Depth (cm)	Snowmelt Rate (cm/day, 1 April to snow disappearance)	Snowmelt Rate (cm/day, peak to snow disappearance)
Bull Trout (BT)	Forest	2020	6/9	4/4	158	156	1.7	2.2
	Forest	2021	5/19	2/21	139	94	1	1.3
	Edge	2020	5/24	3/30	158	158	2.9	2.9
	Edge	2021	5/16	2/18	169	140	3	1.9
	North	2020	5/30	3/30	159	159	2.6	2.6
	North	2021	6/3	2/25	169	157	2.4	1.7
	Open	2020	5/25	3/30	175	175	3.1	3.1
	Open	2021	5/20	2/22	208	154	3	2.4
	South	2020	5/20	3/30	152	152	2.9	3
	South	2021	5/11	2/18	165	132	3.1	2.01
	Site	Year	Melt Date	Peak Snow Depth Date	Peak Snow Depth (cm)	1 March Snow Depth (cm)	Snowmelt Rate (cm/day, 1 March to snow disappearance)	Snowmelt Rate (cm/day, peak to snow disappearance)
Lower Deer Point (LDP)	Open	2020	4/11	2/16	103	77	1.9	1.9
	Open	2021	4/7	2/27	117	108	3	2.9
	Sparse	2020	4/24	2/16	112	69	1.3	1.3
	Sparse	2021	4/3	2/26	96	90	2.7	2.8
	Edge	2020	4/14	2/19	91	72	1.7	1.7
	Edge	2021	4/10	2/27	96	93	2.3	2.3
	Forest	2020	4/26	1/15	69	48	0.6	0.9
	Forest	2021	4/8	2/26	70	68	1.7	1.8

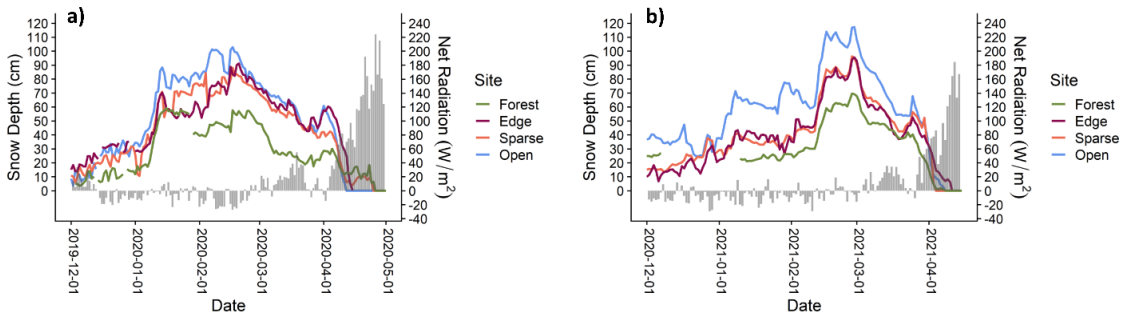

Figure 2.4 Snow depth with net total radiation at the LDP location during winter 2020 (a) and winter 2021 (b). Net total radiation was measured at the weather station located in an open canopy cover site. Note the axis limits are different compared to Figure 2.3.

Energy Balance

Weather Stations

Bull Trout

During the accumulation phase net shortwave and net longwave came close to canceling each other out in both WY 2020 and WY 2021 (Table 2.2). The turbulent fluxes, sensible and latent energy, were both positive and of similar magnitude in both years. During the accumulation periods in WY 2020 and WY 2021, latent energy contributed 2.4% and 3.4% to net energy, respectively, (equation 3) while sensible energy contributed 10.1% and 14.5% in the same period. During the melt phases, in WY 2020 and WY 2021, the latent heat flux contributed 2.2%, respectively, while the sensible heat flux contributed 5.2% and 5.9% in the same period. The ground energy flux was less than 2.7% of the total energy flux through the accumulation and melt periods in both years. During the melt period in both years, net shortwave radiation contributed the most to the energy flux (60.3% and 56.5%). The net longwave flux during the melt period in WY 2020 and WY 2021 was 22.7 W/m^2 and 38.8 W/m^2 lower than the accumulation period. During the melt period, the outgoing longwave radiation was on average 47.8 W/m^2

greater than the accumulation period while the incoming longwave radiation was on average 6.0 W/m^2 less. The greater outgoing longwave radiation during the melt period led to the lower net longwave flux during the melt periods. Overall, the net energy flux was greater during the melt period in WY 2021 compared to WY 2020 from increased net shortwave radiation, and turbulent fluxes in WY 2021. We expect the energy balance at the open site to be different than the other canopy cover sites. As forest density increases, we would expect the net shortwave radiation to decrease and net longwave radiation component to increase. While the energy balance at the open site is different than the sites with canopy cover, evaluating how the snow surface energy balance changes throughout the season will provide insight into how the snow surface processes change through time.

Table 2.2 Daily average snow surface energy balance at the weather station and SNOTEL for the BT and LDP accumulation and melt periods for each year, the difference between the years (2020 - 2021) and accumulation and melt periods. The accumulation period was from December - February at LDP and December – March at BT. The melt period was from March- snow disappearance at LDP and April – snow disappearance at BT.

	Energy Balance Terms W/m^2	**Accumulation**			**Melt**			**Accumulation Minus Melt**	
		2020	2021	Difference	2020	2021	Difference	2020	2021
Bull Trout (BT)	Incoming Shortwave, Kin	61.1	60.0	1.1	200.9	212.4	-11.5	-139.8	-152.4
	Outgoing Shortwave, Kout	48.7	49.2	-0.5	128.9	133.0	-4.1	-80.2	-83.8
	Incoming Longwave, Lin	252.5	253.9	-1.3	255.5	242.3	13.1	-2.9	11.5
	Outgoing Longwave, Lout	268.7	264.4	4.3	294.5	291.8	2.7	-25.8	-27.4
	Net Shortwave, K	12.4	10.7	1.7	72.0	79.5	-7.5	-59.6	-68.8
	Net Longwave, L	-15.7	-10.2	-5.5	-38.4	-49.0	10.7	22.7	38.8
	Net Total Radiation, K+L	-3.3	0.5	-3.8	33.6	30.5	3.2	-36.9	-29.9
	Sensible, H	3.3	3.7	-0.4	6.2	8.3	-2.1	-2.8	-4.6
	Latent, LE	0.8	0.9	-0.1	2.6	3.1	-0.5	-1.8	-2.2
	Ground, G	0.9	-0.2	1.1	-1.1	-0.3	-0.8	2.0	0.2
	Net Energy (K+L+LE+H+G)	1.0	5.1	-4.1	42.2	41.9	0.3	-41.2	-36.8
	K+L+LE+H	0.8	5.1	-4.3	42.4	41.9	0.5	-41.5	-36.7
Lower Deer Point (LDP)	Incoming Shortwave, Kin	81.1	92.9	-11.9	196.1	220.9	-24.8	-115.1	-128.0
	Outgoing Shortwave, Kout	66.7	73.2	-6.5	138.3	146.9	-8.6	-71.6	-73.7

	Incoming Longwave, Lin	274.6	265.7	8.9	265.7	254.2	11.5	8.9	11.5
	Outgoing Longwave, Lout	294.7	292.5	2.2	302.4	302.8	-0.3	-7.7	-10.3
	Net Longwave, L	-20.1	-26.8	6.7	-36.8	-48.6	11.8	16.7	21.8
	Net Shortwave, K	14.4	19.7	-5.3	57.9	74.1	-16.2	-43.5	-54.4
	Net Total Radiation, K+L	-5.7	-7.1	1.3	21.1	25.5	-4.4	-26.8	-32.6
	Sensible, H	15.3	13.1	2.2	10.7	15.1	-4.4	4.6	-2.0
	Latent, LE	6.5	5.4	1.1	4.8	6.9	-2.1	1.7	-1.6
	Ground, G	4.8	4.8	0.0	3.4	5.3	-1.9	1.5	-0.5
	Net Energy (K+L+LE+H+G)	20.9	16.2	4.7	39.9	52.8	-12.8	-19.1	-36.6
	K+L+LE+H	16.0	11.3	4.7	36.6	47.5	-10.9	-20.5	-36.1

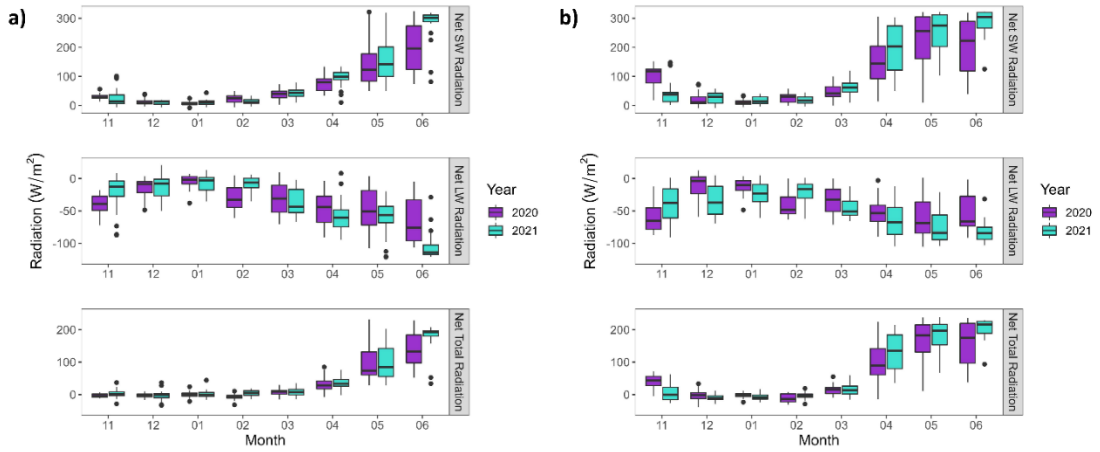

Figure 2.5 Daily average net longwave (LW), net shortwave (SW) and net total radiation (NR, LW+SW) at the BT (a) and LDP (b) locations for each month and year. All measurements are from the weather station located in open canopy cover sites at each study location.

At the BT weather station in the open, November longwave radiation was greater in WY 2021 creating greater net total radiation early in the 2021 winter (Fig. 2.5a). Through December and January, both years had similar radiation values and net total radiation was near zero. The largest difference between years in net total radiation occurred in February when longwave radiation was greater in WY 2021 resulting in higher net total radiation compared to WY 2020 and median positive net total radiation. Through March, April, and May in WY 2021 longwave radiation tended to be lower and Both shortwave radiation and net median net total radiation tended to be higher compared to WY 2020.

When comparing the net total radiation at the weather station to the continuous sensor snow depth measurements in the different canopy covers through the accumulation period, the net total radiation varied between positive and negative values. Near 1 April the net total radiation became predominantly positive (Fig. 2.3). In WY 2021 near the end of March the net total radiation was higher compared to WY 2020 resulting in snowmelt before the beginning of April and a lower snow depth on 1 April 2021 (mean snow depth WY 2020 was 160 cm and WY 2021 was 135 cm).

Lower Deer Point

The net energy flux (equation 3) during the accumulation phase was similar between years (difference of 4.5 W/m^2). During the accumulation phase in WY 2020 and WY 2021, the magnitude of the net longwave radiation was greater than the net shortwave radiation, reducing the net energy flux by 5.7 W/m^2 and 7.1 W/m^2. In the same accumulation periods, the ground heat flux contributed 7.9% and 6.9% to the net energy flux while the turbulent fluxes contributed a combined 35.6% and 26.4% to the net

energy flux. Net longwave was less (6.7 W/m^2) and net shortwave was greater (5.3 W/m^2) in WY 2021 compared to WY 2020. The net energy flux during the melt phase was greater in WY 2021 than in WY 2020 (a difference of 17.3 W/m^2). During the melt period in WY 2020 and WY 2021, net shortwave radiation contributed the most to the net energy flux (51.0% and 49.4%). Consistent with the accumulation period, in the melt period net longwave was less (11.8 W/m^2) and net shortwave was greater (16.2 W/m^2) in WY 2021 compared to WY 2020. The longwave flux during the melt period was 36 W/m^2 lower in both years compared to the accumulation period. During the melt period, the outgoing longwave radiation was on average 26.4 W/m^2 greater than the accumulation period while the incoming longwave radiation was on average 1.2 W/m^2 greater. The greater outgoing longwave radiation during the melt period led to the lower net longwave flux during the melt periods. The ground heat flux was positive in both years contributing 3.0% and 3.5% to the net energy flux.

At the weather station in the open, November and December net total radiation was greater in WY 2020 compared to WY 2021 (Fig. 2.5b). In January, net longwave radiation was lower in WY 2021 reducing the net total radiation. In February the pattern shifted with higher longwave radiation values and median net total radiation in WY 2021. Through March the net radiation was similar, and the median was positive. In March 2021, the net shortwave radiation was greater and net longwave radiation was lower.

When comparing the accumulation period net total radiation at the weather station to the continuous snow depth measurements in both years net total radiation was predominantly negative and similar to the BT location, becoming positive near 1 March (Fig. 2.4). The positive net total radiation coincided with the start of the snowmelt period.

The 1 March snow depth in WY 2021 was 31 cm greater than 1 March 2020 but, net total radiation through the first half of March was greater in WY 2021, resulting in increased snowmelt rates. During the storm near the end of March, energy input was reduced, and snowmelt was delayed for 10 days in WY 2020 and 3 days in WY 2021.

Radiation Observations in Different Forest Types at Lower Deer Point

During the accumulation and snow melt periods the average daily incoming shortwave radiation was lowest in the forest (30.5 W/m^2) and highest in the open (74 W/m^2) (Table 3, Fig. 2.6). However, the average daily incoming longwave radiation was highest in the forest (297 W/m^2) and lowest in the open (283 W/m^2) (Fig. 2.6). During the accumulation period, total incoming radiation (SW + LW) in WY 2021 was lower at the open and west edge sites than the forest site compared to WY 2020. During the melt period, incoming radiation was higher at all sites in WY 2021 but the open site had the largest difference between years (60.6 W/m^2).

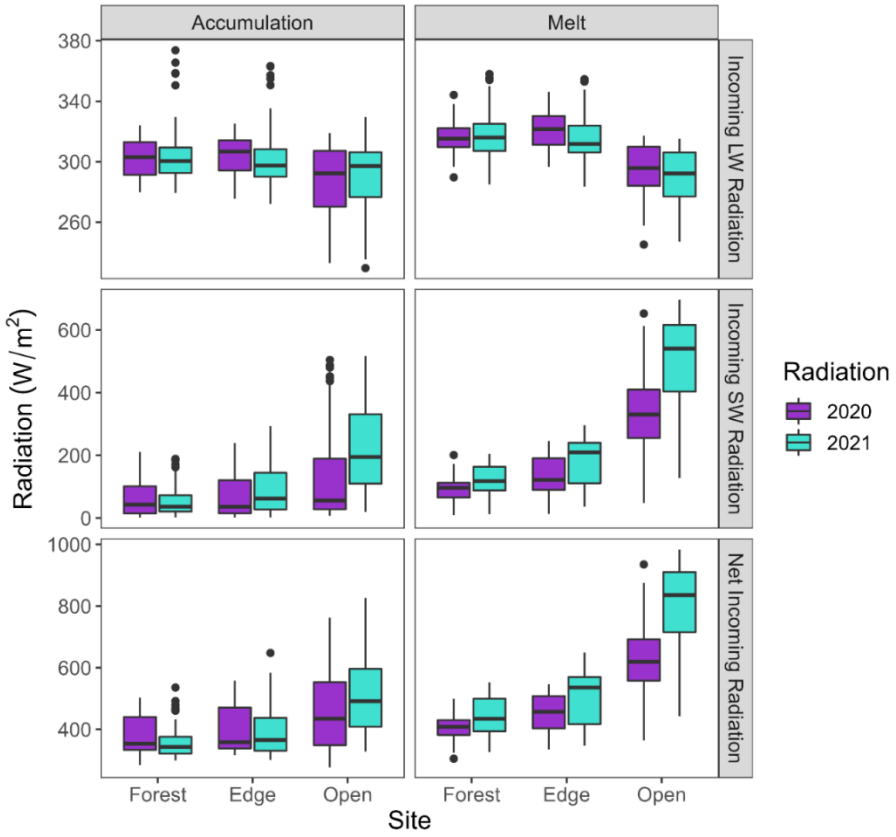

Figure 2.6 Daily average longwave radiation, incoming shortwave radiation and net incoming radiation for WY 2020 and WY 2021 in the forest, open and edge sites during the accumulation and melt periods at the LDP study location. Daily values were split over the accumulation period from December - February and during the melt period from March - snow disappearance.

Table 2.3 Daily average measured incoming shortwave and longwave radiation at the LDP study site split into accumulation and melt periods. The accumulation period was from December - February and the melt period was from March- snow disappearance.

		LDP Radiometers Accumulation			LDP Radiometers Melt		
Energy Balance Terms (W/m^2)	Site	2019	2020	2021	2019	2020	2021
Incoming Longwave, Lin	Forest	NA	297.9	296.7	311.5	310.5	311.9
Incoming Shortwave, Kin	Forest	NA	39.3	21.8	41.1	44.8	56.6
combined, Kin + Lin	Forest	NA	337.2	318.5	352.6	355.3	368.5
Incoming Longwave, Lin	Edge	NA	299.1	295.1	310.9	317.4	310.0
Incoming Shortwave, Kin	Edge	NA	30.4	36.7	55.2	65.4	84.7
combined, Kin + Lin	Edge	NA	329.5	331.9	366.1	382.8	394.7
Incoming Longwave, Lin	Open	NA	283.4	282.2	279.6	288.1	281.9
Incoming Shortwave, Kin	Open	NA	56.4	91.9	177.0	147.4	214.2
combined, Kin + Lin	Open	NA	339.8	374.0	456.6	435.5	496.1

Soil Moisture and Temperatures

The soil temperatures were sensitive to air temperature and snowmelt timing in both years and locations. At the SNOTEL near BT, snow depth was less than 10 cm in November WY 2020 but greater than 10 cm in November of WY 2021. During November soil temperatures in 2019 were -1.07 °C and in 2020 were -0.27 °C (Figure 7a). Mean daily air temperatures in November 2019 were -1.8 °C and in 2020 were -3.9 °C. In both years the soil temperatures remained at or just below 0 °C until snow disappearance in late May or early June. In 2019 the ground froze before wetting-up and remained at about a 12% lower soil moisture through the winter season compared to WY

2021. Marking the onset of snowmelt, the soil moisture began to increase 6 days after peak SWE in WY 2020 and 6 days earlier than peak SWE in WY 2021. The soil temperature on peak SWE in WY 2020 was less than 0 °C while it was 0 °C in WY 2021. In both years, as the snow melted the soil moisture increased to a peak near 33%. Peak soil moisture occurred on 2020-04-30 and 2021-05-31. The soil moisture remained near the peak until snow disappearance and dropped near 2020-06-22 and 2021-06-02.

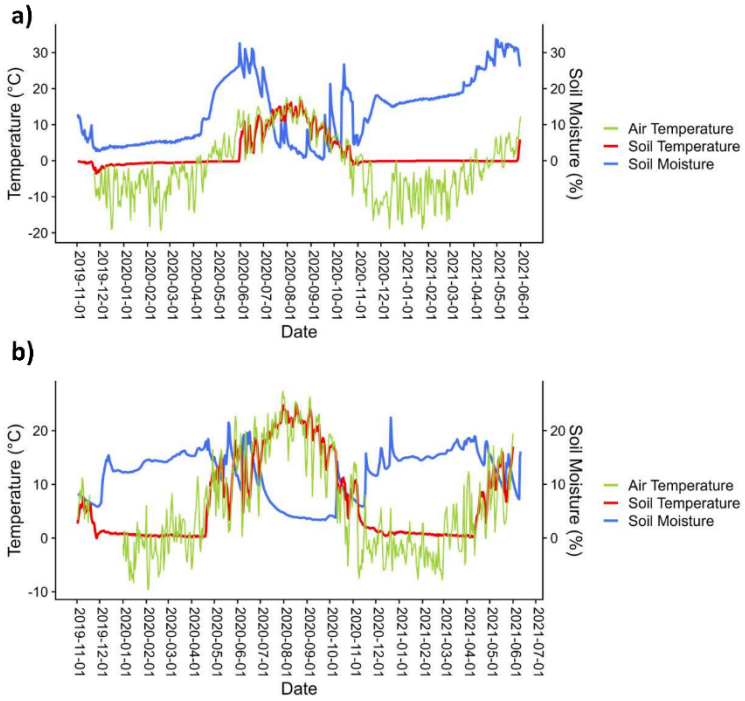

Figure 2.7 Daily average soil moisture, soil temperature and air temperature in open canopy cover at the SNOTEL located near the BT study location (a) and at the LDP weather station (b). Note the axis limits are different between the two panels.

At the LDP location, mean daily November soil temperatures were 4.04 °C in 2019 and 4.07 °C in 2020 (Fig. 7b). During both snow covered seasons (DJFMA), soil temperature remained above zero and increased sharply as the snow melted in April. During the fall the soil moisture increased and remained at about 15% soil moisture through the winter season. The soil moisture began to increase on 2020-03-01 and 2021-

03-04 indicating the onset of the snowmelt period. As the snow melted, the soil moisture increased to a peak near 20%. Peak soil moisture occurred on 2020-05-20 and 2021-04-11.

Table 2.4 Cold content (E_{cc}) timing and rate of increase towards isothermal at the LDP and BT snow pit sites for 2020 and 2021.

Site	Year	Peak E_{cc} Date	Isothermal Date	Peak E_{cc} (W/m^2)	average rate of increase from peak E_{cc} (W/m^2 / day)
LDP open	2020	2/20/2020	3/4/2020	-23.1	1.9
LDP open	2021	1/26/2021	3/9/2021	-14.7	0.3
LDP forest	2020	2/20/2020	3/4/2020	-6.7	0.5
LDP forest	2021	2/23/2020	3/9/2021	-6.5	0.4
BT SNOTEL	2020	2/19/2020	NA	-46.3	1.1
BT SNOTEL	2021	2/25/2021	NA	-55.3	2.1
BT Open	2020	2/19/2020	NA	-35.9	1.0

Snow Pits

Including all years, sites and pits, cold content was negatively correlated with snow depth, decreasing as snow depth increased (R^2 =0.60 p-value<0.001) (Fig. 2.8). Comparing the individual sites, the slope of E_{cc} versus snow depth was greater at the SNOTEL pit site near BT and for greater snow depths (Table 2.4). For snow depths less than 60 cm the E_{cc} tends to be less than -0.5 W/m^2 except for two early season snow pits at the SNOTEL pit site near BT. Above 60 cm snow depth, the cold content decreased by -3.3 W/m^2 per 10 cm increase in snow depth (increase by -3.3 W/m^2 per 10 cm decrease in snow depth) through the snow pit measurement periods.

Peak snowpack cold content, E_{cc}, occurred six days earlier in WY 2020 compared to WY 2021 at the SNOTEL pit site located near BT (Table 2.4, Figure 2.9a). However, peak E_{cc} was correlated with snow depth and the peak snow depth occurred after snow pits were completed for WY 2020. Peak E_{cc} was 10.4 W/m^2 magnitude greater at the SNOTEL compared to the open site in WY 2020 and 9 W/m^2 greater magnitude in 2021. The rate of increase from peak E_{cc} to 0 °C was 1.1 W/m$^{2/}$day faster in WY 2021. Compared to the LDP location, peak E_{cc} near BT was 12.8 to 48.8 W/m^2 greater.

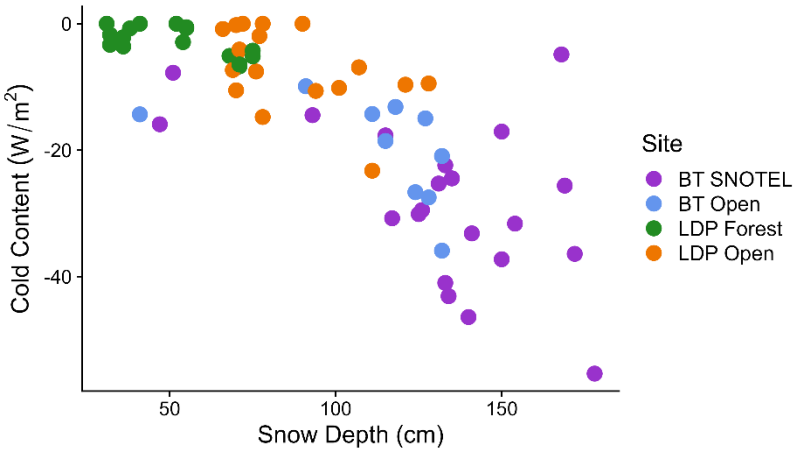

Figure 2.8 Snowpack cold content versus snow depth for each snow pit and site for WY2020 and WY2021. There were two snow pits at each location (BT and LDP).

At the LDP location peak snowpack cold content occurred at the same time in the open and forest site in WY 2021 and earlier in the open site compared to the forested site in WY 2020 (Fig. 2.9b). Peak cold content occurred within the same week in the forest in WY 2020 and WY 2021 and 25 days earlier at the open site in WY 2021. The peak E_{cc} was greater magnitude in the open site both years with 2020 having the highest magnitude peak E_{cc} at the LDP location (8.4 W/m^2 greater in 2020 than 2021). The dates the snowpack became isothermal were the same for both the forest and open sites and within the same week in WY 2020 and WY 2021. In WY 2020, the rate of increase from

peak E_{cc} to isothermal was at least 1.6 W/m^2/day greater in the open site compared to 2021.

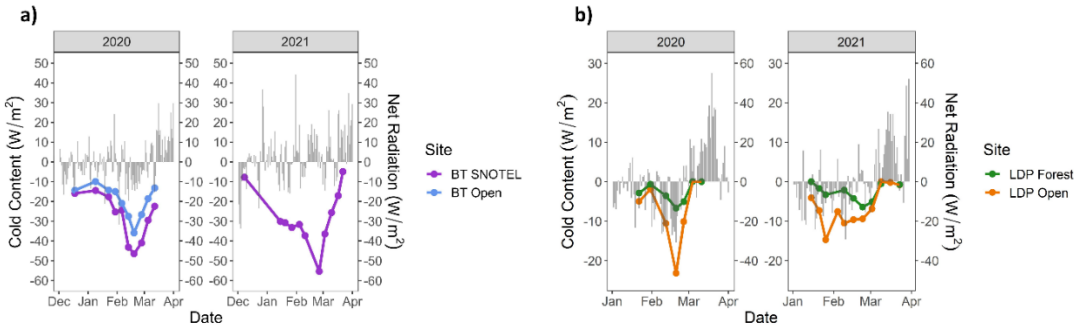

Figure 2.7 Snowpack cold content at the BT pit sites (a) and LDP pit sites (b) with net total radiation at each site.

Discussion

Snow Accumulation Period: Controlled by Forest Canopy Interception

At both locations, less snow accumulated in the forest compared to the open. Similar to Dickerson-Lange *et al.* (2017), we hypothesize that interception causes this difference in peak snow accumulation. During the accumulation season, the dominant energy balance component in the forest was incoming longwave radiation while the dominant energy balance component in the open was incoming shortwave radiation. Measured incoming longwave radiation at the snow surface was consistent between years and between forest covers (forest, west edge, open) at the LDP location. Incoming shortwave radiation was more variable than incoming longwave radiation between years and forest covers but was lower compared to the longwave radiation for all forest covers. The net energy at the weather stations in the open during the accumulation period tended to be negative or near zero at both locations (BT and LDP) (Fig. 10). The low net energy input in the open and low incoming radiation in the forest during the accumulation period suggests that snow interception processes are a first-order process contributing to mass balance differences

in different vegetation covers. However, net total radiation was only measured in the open and is likely different in different vegetation covers. The forested site likely had greater daily net longwave radiation compared to the open site and lower net shortwave radiation as indicated by the incoming radiometer measurements at LDP.. The snow surface energy differences are likely a second-order process during the accumulation phase.

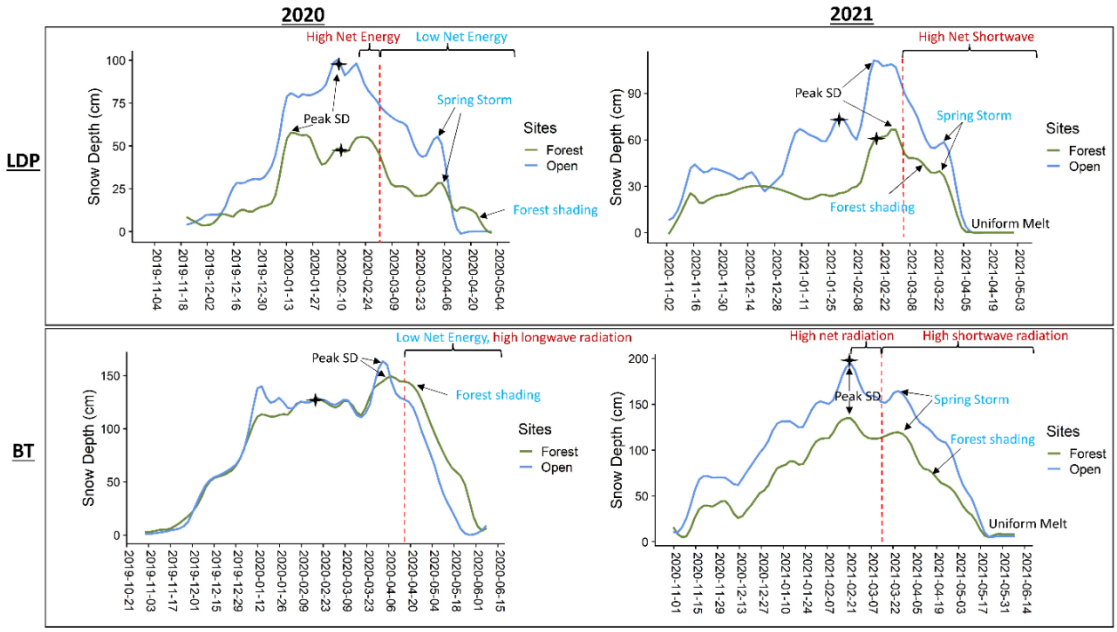

Figure 2.8 Annotated loess smoothed snow depth at the forest and open sites at both study locations and years. The red dotted line represents the start of snowmelt infiltrating the soil profile. The black stars are timing of peak Ecc during the snow pit data collection periods. Variables that slow the snowmelt rate and lead to later snow disappearance are in blue while variables that increase the snowmelt rate and lead to earlier snow disappearance are in red. Net energy is the net energy flux defined in equation 3.

The greater incoming longwave radiation compared to the open site contributed to a greater cold content in the forest compared to the open site at LDP. The greater cold content and lower snow depth in the forested sites resulted in less energy and mass required to reach an isothermal state and initiate the snowmelt period. Both open and

forest sites reached isothermal states and the start of the melt period within the same week. Increased shortwave radiation and therefore net total radiation, increased the cold content in the open at a faster rate, resulting in similar timing of isothermal states in the open and forest. At the end of the accumulation period, both the snowpacks were in isothermal states, thus, the primary difference between the forest and open snowpacks was the mass of snow.

The seasonal snowpack (BT) location reached lower cold content than the marginal snowpack (LDP) location. This is expected considering the marginal snowpack location is colder and has a deeper snowpack. Comparing the relationship between E_{cc} and snow depth at each location we observed a steeper slope between snow depth and cold content in the colder location. The steeper slope indicates a greater change in cold content per unit snow depth. Similar to Jennings and Molotch (2020) this suggests that in warmer, lower snow accumulation sites the contribution of snowfall to E_{cc} was less compared to colder climates.

Snowmelt Period: Controlled by Forest Shading and Spring Storms

The snowmelt period established whether the snow disappeared later in the forest or relatively uniformly between vegetation covers. Incoming longwave radiation was the dominant contributor to snowmelt in the forest. However, the greater longwave radiation in the forest did not offset the lower incoming shortwave radiation compared to the open site. Rather, the forest site shaded the snow surface, reducing the incoming shortwave radiation resulting in a slower snowmelt rate in the forest compared to the open (Fig. 10). The slower snowmelt rates in the forest site combined with less snow mass to melt resulted in a similar snow disappearance timing as the open site. The edges and sparse

vegetation sites melted at a slower rate compared to the open but faster rate compared to the forest. Similarly, the slower snowmelt rate combined with the lower snow depth resulted in a uniform melt timing with the open and forest sites.

A spring storm offset the snow depths and snow surface energy in the different vegetation covers resulting in a difference in snow disappearance timing between the open and forested sites. For instance, the spring storm in WY 2020 paused the melt at the LDP location by 10 days and resulted in greater snow accumulation in the open site compared to the forest site. The spring storm was likely warm resulting in canopy intercepted snow melting and dripping off the canopy rather than accumulating and sublimating (Storck *et al.*, 2002) expanding the difference in snow depth between the open and forest before snow disappearance. However, we did not measure snow interception but assumed the difference in snow accumulation between the open and forest was due to forest interception. Despite the lower snow accumulation in the forest sites, the relatively low forest sites canopy density shaded the snow surface, slowing the melt rate following the storm and resulting in later snow disappearance in the forest compared to the open (Sicart *et al.*, 2004; Musselman *et al.*, 2008). The spring storm in WY 2021 also paused snowmelt but for only three days and accumulated less snow compared to WY 2020 spring storm. The short duration and lower accumulation storm were not enough to establish a difference in snow disappearance timing between the forest and open sites. Similarly, at the BT location, a late peak snow depth attributed to spring storms set a difference in accumulation between the open and forest sites at the onset of an isothermal state snowpack and the start of the snowmelt period. The slower snowmelt rate in the forest due to forest shading compared to the open and the difference

in storm accumulation late in the winter season led to variability in melt timing across vegetation covers.

The behavior of the late peak snow depth was not the same for the marginal snowpack (LDP) and seasonal snowpack (BT) locations. The BT location had more snow to melt and a longer melt period. The seasonal snowpack, BT location had lower net total radiation in April compared to LDP. Although we did not measure radiation in the forest at BT, the lower net shortwave radiation and colder temperatures likely resulted in a lower net longwave component at BT compared to the LDP location. The lower net total radiation in the forest and open at BT, combined with a greater snow depth led to a later start of the snowmelt period compared to LDP. The longer melt period in WY 2021 allowed the snow depth at the forest and open sites to reach similar snow depths at the end of the spring and snow disappeared uniformly. In WY 2020 the melt period was shorter and the shading effect of the trees slowed the melt rate compared to the open delaying the snow disappearance date. Conversely, at the LDP location, the late snow depth peak resulted in a uniform snow disappearance. The high net shortwave radiation in WY 2021 resulted in rapid melt following the snow depth peak and less variability between the snow depths in the different vegetation covers in mid-March. Since there is less snow to melt at the LDP location, the forested snow depth was able to catch up to the open snow depth near the snow disappearance timing.

These results support previous research hypothesizing where and why snow melts later in the forest compared to the open. Previously, Lundquist et al. (2013) set a -1°C mean December-January-February air temperature threshold where forest cover shifts from the dominant effect of shading to longwave radiation. Additionally, Dickerson-

Lange et al. (2021) flow chart hypothesized that for cold environments forests act to shade the snow cover, slowing snowmelt in the forest and set up a longer snow cover season in forested environments. Here, both study locations mean December-January-February air temperatures were below the -1°C threshold classifying both locations as cold environments according to the Dickerson-Lange et al. (2021) flow chart. Our results corroborate the previously hypothesized role of shading on snowmelt rates in these cold environments.

Soil Moisture and Temperature

Similar to other studies we found soil moisture peaked immediately following snow disappearance (Molotch *et al.*, 2009; Smith *et al.*, 2011). At the BT location, the soil froze before the snow cover season and through the accumulation season, the soil temperature increased. As the snow began to melt the soil moisture increased, reaching a similar saturation level as the 2021 season. Regardless of the soil moisture state at the start of winter, we observe a similar moisture level at the beginning of the snow-free season. At the LDP location, soil temperatures remained near or above zero through the winter snow cover season. This result contradicts Molotch et al. (2009) who found colder soils at the warmer site.

More uniform snow disappearance in different vegetation covers has consequences for the uniformity of peak soil moisture. Since the soil moisture peak coincides with the snow disappearance date, less spatiotemporal variability in snow disappearance timing will cause less spatiotemporal variability in peak soil moisture and soil moisture availability into the summer season. Reduced snow water storage from

snowmelt variability could extend the period when soil is dry and the length of vegetation water stress into the summer season (Harpold, 2016).

Uncertainties and Assumptions

Uncertainties due to meteorological data and field measurements are present. The incoming shortwave and longwave radiometers at LDP were not heated and thus required snow to melt off of them or to be cleaned off following snowfall. Because of this, we removed incoming radiation data during snow storms which may result in higher shortwave radiation and lower longwave radiation measurements. However, when comparing the open radiometer measurements to the heated radiometer at the weather station we did not observe a significant difference in the range of measurements. Additionally, the radiometers were installed on poles ranging from 1 to 1.5 m off the ground surface. The height of the radiometers did not change throughout the snow season thus, we assumed the incoming radiation 1-1.5 m above the surface was the same as the incoming radiation on the snow surface. Additionally, Maxbotix snow depth sensors have a 1 mm resolution and do not work when the sensor height is between 30-50 cm. To avoid the no data range we installed the snow depth sensors at least 2 m above the ground. At each snow depth sensor, we are not able to account for the changes in snow depth due to densification (i.e., settling and metamorphism) thus are focused on changes in snow depth.

The ground heat flux energy balance calculation used soil data from the SNOTEL site 2 km away. The climate conditions between the SNOTEL and the weather station at BT did not vary greatly, thus we assumed the ground temperature and moisture were similar at the BT location. The turbulent fluxes were calculated using the weather station

data. We did not measure relative humidity at the snow surface which could result in an overestimate of latent heat at the surface. However, a sensitivity analysis adjusting the relative humidity by +/- 5% did not greatly change the latent heat flux. Additionally, the results of this study are based on two years of field data at nine points in southern Idaho. While these points are representative of the dominant vegetation type and climate in the region, the points may not imitate the heterogenous landscape in the region.

Conclusion

Forests can enhance snowmelt rates via longwave radiation and reduce snowmelt rates by shading the snow surface from shortwave radiation (Varhola *et al.*, 2010). These energy balance processes can cancel each other out, but changes to the forest structure from landcover changes such as fire and bark beetle will alter the dominant forest energy balance process. We find that shading suppresses the effect of shortwave radiation in relatively low-density forests, increasing the snow duration in the forest. However, snowpack cold content is greater in forested areas than in open areas, requiring less energy to bring the snowpack to an isothermal state, which partially cancels the shading effect. At the seasonal snowpack (BT) location, the magnitude and timing of the snow depth peak were important for predicting the variability of snowmelt. The marginal snowpack (LDP) location was controlled by the magnitude and duration of a late season storm adding snow depth variability and reducing the snow surface energy input. At both sites, the forests shade the snow surface into the melt period.

The results of this study have broader implications for the effects of forest cover on snow persistence and water availability in semiarid regions. These results support the decision tree framework to understand how vegetation influences snow distribution

(Dickerson-Lange *et al.*, 2021). Developing an understanding of the dominant controls on snowmelt across the region is applicable for forecasting the timing and quantity of snow water availability for environmental and societal water and forest management. These results will support practitioners by having a baseline understanding of dominant controls on snow water availability. Landcover change due to gap thinning or forest fire will likely increase the snowmelt rates in the forest site. However, in relatively low density forests, standing dead trees potentially still attenuate incoming shortwave radiation leading (Burles and Boon, 2011). Similarly, gap thinning will increase the amount of total radiation at the snow surface increasing snowmelt rates (Seyednasrollah *et al.*, 2013). These results presented here provide regionally specific observations to support resource management in a changing climate and environment. Future research will focus on the larger scale analysis to identify how landcover changes will affect the snow distribution. Such an analysis will support how the controls on snow distribution will change due to landcover changes such as fire, bark beetle, and vegetation succession.

CHAPTER THREE: EVAPOTRANSPIRATION ACROSS THE RAIN-SNOW TRANSITION IN A SEMIARID WATERSHED

This Chapter has been published as: Kraft, M., & McNamara, J. P. (2022). Evapotranspiration across the rain–snow transition in a semi-arid watershed. *Hydrological Processes*, *36*(3). https://doi.org/10.1002/hyp.14519

Abstract

The snowpack regime influences the timing of soil water available for transpiration and synchrony with the evapotranspiration (ET) energy demand (air temperature, VPD, and shortwave radiation). Variability of snowmelt timing, soil water availability, and the energy demand results in heterogeneous ET rates throughout a watershed. In this study, we assessed how ET and growing season length vary across five sites on an elevational gradient in the Dry Creek Watershed, ID, USA. We compared trends of daily and annual ET between 2012 and 2017 to environmental parameters of soil moisture, air temperature, vapor pressure deficit, snow cover, and precipitation. Trends between parameters and ET were evaluated at each site and compared between sites. We observed three trends in ET across the watershed. The first trend is at the low elevation site where the snow cover is not continuous throughout the winter and rain is the dominant precipitation form. The first day of the growing season and ET occurs early in the season when the energy demand is low and soil water is available. Annual ET at the low elevation site is a balance between spring precipitation providing soil water into the summer season and limiting the ET energy demand. The second trend occurs at the

middle elevation site located in the rain-snow transition. At this site, ET increases with snow depth and spring precipitation extending the soil water availability into the summer season. At the higher elevation sites, ET is aligned with the energy demand and limited by growing season length. At the high elevation sites, decreasing snow depth and spring precipitation and increasing spring air temperatures result in greater annual ET rates. The observations from this study highlight the influence of environmental parameters and the potential sensitivity of ET to climate change.

Introduction

Mountain forests rely on snowmelt for recharging soil moisture and groundwater sources that provide water for transpiration into the growing season (Hu *et al.*, 2010). In cold, snow dominated environments when trees are dormant during the snow cover months, the timing of snowmelt and soil warming initiates evapotranspiration (ET) and the start of the growing season (Harpold, 2016). Vegetation type and density alter the accumulation of snow, duration of the snowmelt season, and partitioning of snow water to streamflow and ET (Molotch *et al.*, 2009; Kormos *et al.*, 2017). In snow dominated environments, the snowmelt timing occurs with or just before peak soil moisture and the initiation of the soil moisture drawdown period (Smith *et al.*, 2011). Initially, water is available in the shallow soil layers but as the growing season progresses, the soil profile continually dries down to the water stress point (McNamara *et al.*, 2005; Smith *et al.*, 2011). Throughout the growing season, different vegetation types utilize different water stores in the soil profile leading to varying reliance on snow water inputs within a watershed (Bales *et al.*, 2011; Petersky *et al.*, 2019). The different reliance on water sources and precipitation phases causes varying vulnerability of vegetation to changes in

dominant precipitation phase and snowmelt timing altering the soil water availability into the growing season.

Watersheds within the rain-snow transition rely on winter precipitation in the form of rain in low elevations, a mix of rain and snow in mid elevations and snow in the high elevations. The rain-snow transition elevation range is bound by the upper portion of the zone being predominantly snow and lower boundary as rain. The elevation of the rain-snow transition zone depends on temperature and humidity, and thus varying by region, latitude, and storm event. In the Western U.S. mid-latitude regions, the rain-snow transition zone ranges from 1000-2000m (Marks *et al.*, 2013; Cui *et al.*, 2020). Warming temperatures have resulted in a declining fraction of wintertime precipitation falling as snow (Knowles *et al.*, 2006) potentially shifting the rain-snow transition and hydrologic regime.

Changes to snowmelt timing due to climate change may change the soil moisture availability into the growing season. As the climate warms, there are earlier snowmelt timing and downward trends in April 1st Snow Water Equivalent (SWE) in the western U.S. (Hamlet *et al.*, 2005; Zeng *et al.*, 2018; Milly and Dunne, 2020; Robles *et al.*, 2021). Regions that receive snow as the dominant phase of precipitation are expected to transition to receiving more rain, which will increase snow ephemerality (Hinckley *et al.*, 2014), and the snow cover duration (Klos *et al.*, 2014), altering the timing of soil water available for vegetation (Harpold, 2016; Petersky *et al.*, 2019). Previous studies found that earlier snowmelt in response to warming is not always synchronous with the timing of earlier canopy green-up (Richardson *et al.*, 2013; Grogan *et al.*, 2020). The asynchrony between snowmelt and phenological events results in longer winter-spring transition

periods and earlier spring runoff timing (Grogan *et al.*, 2020). Lengthening the time between snowmelt and the emergence of buds and leaves results in a longer period with increased surface albedo and ET earlier in the growing season (Milly and Dunne, 2020). Earlier snowmelt potentially results in an earlier start of the soil moisture recession, extending summer plant water stress (Harpold, 2016; Poulos *et al.*, 2021). Spring precipitation extends the wet soil conditions beyond the snow disappearance date, but the contribution depends on precipitation timing (Smith *et al.*, 2011) and may not be enough to compensate for earlier springs and shallower snowpacks (Hu *et al.*, 2010). Lower snow accumulation and earlier snowmelt timing have been correlated with decreased vegetation productivity and peak NDVI or greenness (Hu *et al.*, 2010; Trujillo *et al.*, 2012; Potter, 2020). Later snowmelt is associated with higher plant growth rates over the growing season possibly due to increased snow cover period reducing soil evaporation and increasing soil moisture levels for plant growth in the summer months when insolation and temperatures are higher (Wang *et al.*, 2013; Potter, 2020).

The effect and variability of earlier snowmelt will vary across elevation, aspects, and climatic regimes which control the energy for ET. Elevation is a strong predictor of snow depth in forest and shrub areas (Harshburger *et al.*, 2010; Tennant *et al.*, 2017) influencing the watershed water budget, snowmelt date, and ET timing. In the Sierra Nevada, previous studies found the elevation gradient has a strong control on ET. Modeled ET at low elevations were water limited while higher elevations retained a snow cover longer, were limited by growing season length (Christensen *et al.*, 2008; Lundquist and Loheide, 2011) and middle elevations with moderate precipitation and snow depths had the highest transpiration rates (Christensen *et al.*, 2008). When considering aspect,

Cooper et al. (2020) observed transpiration on south aspects were controlled by air temperature while north sites were controlled by vapor pressure deficit (VPD). The timing of peak sap flow was linked to soil water limitations, which were regulated by the timing of snowmelt (Cooper *et al.*, 2020). Aspect and elevation control the peak snow accumulation and melt timing within the watershed. South aspects and lower elevations accumulate less snow and tend to melt earlier than higher elevations and northerly aspects (Kormos *et al.*, 2014; Tennant *et al.*, 2017). Thus, the watershed scale variability of ET is a product of the variability of snow processes and terrain controlling the complex interaction with soil moisture availability, and energy demand.

There are a limited number of observations of ET in semiarid ecosystems in the western U.S. limiting our understanding of the effects of how climate change may impact vegetation water use in these systems. Some work has been conducted in the Reynolds Creek Experimental Watershed (RCEW) in southern Idaho. Here, Flerchinger et al. (2020) analyzed gross ecosystem production (GEP) and ET at four sagebrush dominated sites on an elevational gradient across the rain-snow transition. At the highest elevation sites, GEP was negatively correlated to precipitation, and the date of snowmelt and GEP at the low elevation sites were strongly controlled by annual precipitation. In the RCEW, (Fellows *et al.*, 2019) evaluated ET, climate variables, and soil moisture at an aspen dominated site and sagebrush dominated site. Their results indicate that soil properties rather than weather and climate controlled water availability at each site with greater water limitations at the sagebrush site. The previous research in this region provides an initial evaluation of how ET may change with elevation or vegetation however they did not explore the vegetation gradient from sagebrush steppe into a pine dominated forest. In

the semiarid Dry Creek Watershed in southern Idaho, (Poulos *et al.*, 2021) analyzed soil moisture and temperature with NDVI derived productivity and found that lower elevations had earlier snowmelt resulting in reduced growth intensity and earlier peak productivity. At lower elevations there was a greater amount of time when soils were dry and warm while at the high elevations there was a greater amount of time when soils were wet but cold. The greater soil reservoirs on north slopes at high elevations provide water later in the year when air temperatures and insolation are high. (Poulos *et al.*, 2021) considered the elevational and aspect variability in vegetation productivity across different vegetation types but, they did not quantify changes in ET or the relationships between ecosystem productivity and climate variability between years.

The Dry Creek Watershed is in the rain-snow transition zone where temperatures are expected to shift from snow conducive temperatures to rain (Klos *et al.*, 2014). By the mid 21st century it is predicted that increased temperatures will reduce the snow cover months from five months to three or fewer months per year (Klos *et al.*, 2014). Previous research analyzed the variability of ET to climate parameters but did not evaluate the variability of ET across an elevational gradient, from sagebrush-steppe to forested ecosystems in a semiarid environment. This research will address this knowledge gap of how and why ET varies in a semiarid watershed across and within the rain-snow transition. Our research objective was to improve our understanding of the impacts of temperature, precipitation, and snow on ET by analyzing the variability in ET at different elevations over six years. We address two questions using field observations: 1) What controls ET at different elevations? 2) How does an ephemeral snowpack and earlier snowmelt impact annual ET?

Methods

Study site

The Dry Creek Experimental Watershed (DCEW) is a 27 km^2 long term study watershed (elevation 1100 – 2200 m) located in southwest Idaho, USA (Fig. 3.1) (McNamara *et al.*, 2018). Precipitation in the semiarid watershed occurs mostly during the winter and is in the snow-rain transition zone with a snowpack accumulating above the Treeline (TL) study site. Vegetation ranges from sagebrush-steppe vegetation at lower elevations and on south facing slopes to pine forests at higher elevations and north facing slopes. The soil on hillslopes is shallow (<2m deep) and gravely loams to gravelly sands (Williams *et al.*, 2009).

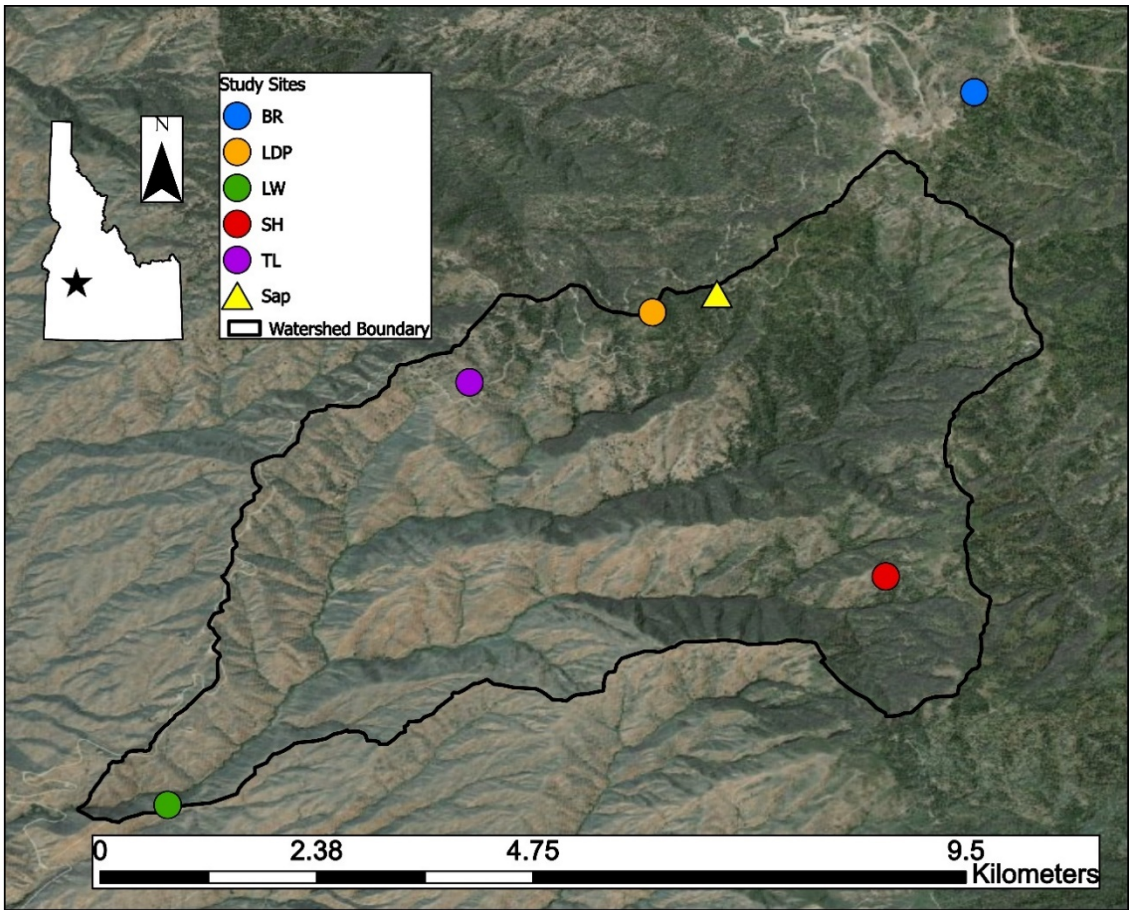

Figure 3.1 Map of Dry Creek watershed located in southern Idaho. There are five study sites at low, middle, and upper elevations in the watershed, one sap flux station located near the LDP site and an EC station located near the SH site.

This study will focus on five meteorological and soil moisture study sites within the DCEW (Table 1, Fig. 3.1). The lowest elevation site is Lower Weather (LW), the Treeline site (TL) is at the rain-snow transition, Shingle Ridge (SH) is located just above TL, followed by Lower Deer Point (LDP) and the Bogus Ridge site (BR) is the highest elevation site in the watershed. The DCEW is located across the rain-snow transition with sites spanning the different precipitation regimes. The low elevation site (LW) receives about 75% of the total precipitation as rain and does not have a consistent snow cover through the winter season (Fig. 2). Vegetation at this site consists of grass, forbs, and sagebrush (*Artemisia tridentata)*. At the TL site, about 50% of the annual precipitation

falls as rain and has the greatest fraction of the precipitation as sleet (20%). The TL site has an average peak snow depth of 51 cm and snow cover season from January to March. Vegetation at the TL site includes sagebrush, forbs, grass, and scattered Douglas fir (*Pseudotsuga menziesii*) trees and is the start of the upward tree line. The SH site is on the upper edge of the rain-snow transition receiving about 50% of the annual precipitation as rain but has a greater proportion of precipitation falling as snow and greater average peak snow depth compared to the TL site (Table 3.1). Vegetation at the SH site includes grass, sagebrush (*Artemisia tridentata)*, Ponderosa pine (*Pinus ponderosa*) and Douglas fir (*Pseudotsuga menziesii*). The LDP site receives 40% of the mean annual precipitation as rain, an average peak snow depth of 79 cm and snow cover season from December through early April. Vegetation at the LDP site includes grass and forbs, shrubs, Ponderosa pine (*Pinus ponderosa*) and Douglas fir (*Pseudotsuga menziesii*). The highest elevation site, BR, receives about 54% of the annual precipitation as snow and about 27% of the annual precipitation as rain. The BR site has the highest peak snow depth and longest snow cover season. Vegetation at the BR site is dominated by Douglas fir (*Pseudotsuga menziesii*), Ponderosa pine (*Pinus ponderosa*) and understory shrubs.

Table 3.1 Climate properties, modeled ET, growing season, and predictor variables at each site (data between 2012 and 2017).

	Bogus Ridge (BR) (Highest elevation)	Lower Deer Point (LDP)	Shingle Creek (SH)	Treeline (TL)	Lower Weather (LW) (Lowest elevation)
	Mean ± STD	Mean ± STD	Mean ± STD	Mean ± STD	Mean ± STD
Elevation	2114	1850	1720	1610	1151
Air Temperature (°C)	6±9.8	8.3±10	8.9±10.3	9.8±10.3	11.1±10.5
Peak Snow Depth (cm)	183.3±35.5	79.3±25.9	69±16	51±12	17.4±8.6
Annual ET (mm/yr)	384.0±54.6	456.1±83.7	427.9±59.6	324.2±74.3	187.0±63.6
Growing Season Length (Days)	35.2±17	82.8±21.3	76±27.2	88±18.5	86.7±44.6
Cumulative Precipitation (mm/yr)	728.6±205.3	548.3±72.7	624.2±70.7	629.7±131.4	392.5±82.5

Day of Peak NDVI (Julian Day)	187±11	179±9	171±6	169±11	139±14
Peak NDVI	0.8±0	0.8±0	0.8±0	0.7±0	0.5±0.1
Day of Water Stress (Julian Day)	156.8±16.11	147.8±15.8	118.3±13.8	167±10.1	165±10.9
Average March Temperature (°C)	-0.11±1.64	2.46±1.61	3.93±1.86	4.34±1.52	6.66±0.96
Average April Temperature (°C)	2.36±1.95	5.15±1.79	6.02±1.91	7.06±1.72	9.27±1.44
Average May Temperature (°C)	7.47±0.7	10.13±0.62	10.95±0.64	11.83±049	13.64±0.5
Days since Oct 1 to Peak SD	139.6±32.9	135.5±21.5	116.8±24.5	119.6±24.5	103.9±11
Snowmelt Day (Julian Day)	124±15	88±20	75±21	69±18	nan
Average MAM VPD (kpa)	0.4±0.04	0.5±0.04	0.6±0.09	0.6±0.05	0.7±0.04

Number of Snow Covered Days	182.1±38.6	158.6±15.8	134.8±41.8	122±22.6	67.1±16.2
Cumulative MAM Precipitation (mm)	266.6±96.4	197.9±59.3	214.5±80.8	226.8±85.7	133.2±47
Growing Season Start (Julian Day)	131±13	101±17	97±16	90±13	80±18

Each site consists of measurements of incoming and outgoing shortwave and longwave radiation, air temperature, relative humidity, wind speed and direction, precipitation, snow depth, and soil pits measuring volumetric water content (VWC) and soil temperature. Additionally, a sap flux sensor is located 0.75 kilometers from the LDP site, and an eddy covariance (EC) tower is next to the SH site. Long term meteorological data were available at each site but soil data was limited to 2012-2017. Small data gaps were filled using the study site's average value from all other years while long data gaps were filled using data from the closest station or the site and year were not included in the analysis. Data gaps consisted of less than 10% of the measured data for air temperature, wind, and relative humidity. Net radiation was not available at the TL site due to sensor failure from 2013 through 2016 and was replaced with radiation values from the LDP site. Using radiation data from 2018-2020 we found an R^2 of 0.93 between the radiation

at LDP and TL sites. The SH site did not include 2012-2014 in the analysis due to missing soil temperature data in 2012 and 2013. At sites with missing peak snow depth data, ET was calculated however the site and year were not included in the statistical analysis. An EC system at the SH site consisted of a three-dimensional sonic anemometer (Model CSAT3, Campbell Scientific, Inc.. Logan UT) and an open path infrared gas analyzer (IRGA: Model LI-7500a, LI-COR, Inc. Lincoln, NE) sampled at 10 Hz. The thirty-minute fluxes were processed using the EasyFlux® DL software (Campbell Scientific, In., Logan Ut, https://www.campbellsci.com/easyflux-dl) with default processing options. Small data gaps were interpolated between measurements. Large data gaps (2015/5/19 – 2015/6/17) due to battery failure were not used in the analysis. The water fluxes were summed daily and by water year to obtain daily and annual ET.

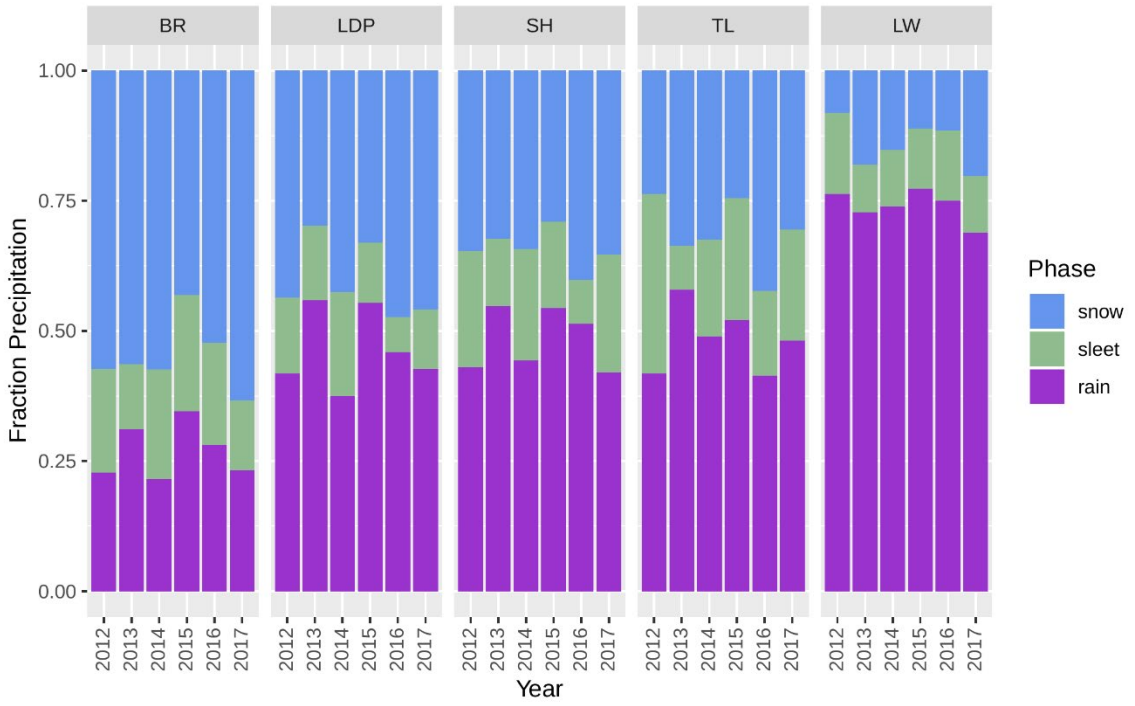

Figure 3.2 Fraction precipitation phase at each site and year. The lower bars (purple) represent the fraction of annual precipitation falling as rain, the middle bars (green) are the fraction as sleet and the upper bars (blue) are the fraction of precipitation as snow. The TL site is within the rain-snow transition where about 50% of the annual precipitation falls as rain and has the greatest proportion of precipitation as sleet

This study was conducted across six years, from 2012-2017. The watershed average cumulative water year precipitation during this time was 616 mm with the driest year occurring in 2012 with 476 mm precipitation and the wettest year occurring in 2017 with 777 mm. Average peak snow depths ranged from 20 cm at LW, to 174 cm at BR and a basin average peak snow depth of 71 cm between 2012 and 2017 (Table 3.1).

Evapotranspiration

Actual ET was calculated for each site using the Penman-Monteith Equation (equation 3.1).

$$ET = \frac{\Delta(K+L) + \rho_a c_p \frac{(e_s - e_a)}{r_a}}{\lambda_v(\Delta + \gamma(1 + \frac{r_a}{r_s})} \qquad \text{equation 3.1}$$

where r_s is the canopy conductance calculated using Stewarts model as a function of climate conditions (Stewart, 1988), ra is aerodynamic resistance, *K* is net shortwave radiation, *L* is net longwave radiation, Δ is the rate of change of saturation vapor pressure with air temperature, γ is the psychrometric constant, c_p is the specific heat of air, ρ_a is air density, and λ_v is the latent heat of vaporization.

To calculate actual ET we used a Jarvis-type model (equation 2) to calculate canopy conductance (Jarvis, 1976; Harris *et al.*, 2004; Rodrigues *et al.*, 2016). Stewart (1988) developed simple functional forms for several meteorological variables based on leaf-level observations, however, we assume the model is scalable to canopy scale using the leaf area index (LAI) (Harris *et al.*, 2004; Rodrigues *et al.*, 2016). The form of this model is:

$$g_c^{mod} = g_c^{max} f(R) f(T) f(D) f(W) \qquad \text{equation 3.2}$$

Where g_c^{mod} is the estimate of leaf conductance (m s^{-1}) and g_c^{max} is the maximum leaf conductance (m s^{-1}). The functional scalars are between 0 (minimum) and 1 (maximum) and describe how rates of g_c^{max} vary with shortwave radiation ($f(R)$), air temperature ($f(T)$), vapor pressure deficit of the atmosphere ($f(D)$), and soil moisture ($f(W)$). The functional forms are given by (Jarvis, 1976; Cox *et al.*, 1998) (equations 3.3-3.6):

$$f(R) = \left(\frac{R_S}{1100}\right) * \frac{1100 + a_1}{R_S + a_1} \quad \text{equation 3.3}$$

$$f(T) = \frac{\left((T - T_0) * (T_m - T)\right)^{\tau}}{\left((a_2 - T_0) * (T_m - a_2)\right)^{\tau}} \quad \text{equation 3.4}$$

$$\tau = \frac{T_m - a_2}{a_2 - T_0}$$

$$f(D) = exp(-a_3 * VPD) \quad \text{equation 3.5}$$

$$f(W) = \frac{\theta_w - a_4}{a_5 - a_4} \quad if\ a_4 < \theta_w < a_5 \quad \text{equation 3.6}$$

$$= 0 \ \ if\ \theta_w < a_4$$

$$= 1 \ \ if\ \theta_w < a_5$$

The coefficients ($a_1 - a_5$ and g_c^{max}) were estimated using multivariate optimization. The maximum and minimum temperatures, T_m and T_0, were set values of 40 and 0 for the upper and lower cut-off (Harris *et al.*, 2004; Rodrigues *et al.*, 2016). The daily actual ET was calculated by summing the modeled hourly ET. The model was optimized at each site by minimizing the sum of square errors between computed ET and MODIS, 500 m, 8-day composite ET (MOD16A2). The soil moisture parameters were adjusted using the soil moisture field data at each site. The optimized model was then compared to EC measurements at the SH site between 2013 and 2017.

We used the LAI at each site to scale the leaf conductance to the canopy scale. The canopy conductance is given by (equation 7):

$$r_s = LAI * k * g_c^{mod}$$ equation 7

Where k is a shelter factor accounting for leaves sheltered form the sun and wind will transpire at lower rates. We assumed k was equal to 0.5 for all sites (Dingman, 2015).

Growing Season Length

Growing Season was defined as beginning the day after mean daily soil temperatures of the upper 5 cm were over 5°C for 5 days (Tor-ngern *et al.*, 2017). The length of the growing season was estimated by the number of days the soil profile was above the water stress point (Smith *et al.*, 2011; Harpold, 2016). We defined the water stress point as the point at which the rate of water extraction is limited by the soil rather than the climate and plant water stress begins (Eagleson, 1978). The water stress point at each site was estimated by identifying the change in the slope of the VWC dry down curve. At this inflection point, it is assumed this is the point at which the rate of water extraction begins to decline (Smith *et al.*, 2011). When the soil profile was below 5°C for 5 days marked the end of the potential growing season. At all sites the upper 15 and 30 cm VWC levels were used except at Shingle Ridge where only the 5 cm depth was available.

NDVI

To analyze the timing and magnitude of peak greenness at each site, we use the Normalized difference vegetation index (NDVI), a remotely sensed vegetation index correlated with plant productivity (Running and Nemani, 1988). The NDVI index ranges between 0 and 1 with high values indicating greater productivity or greenness. We used daily NASA Modis (Moderate Resolution Imaging Spectroradiometer) 500 m resolution

(MOD09GA) atmosphere-corrected product (https://lpdaac.usgs.gov/products/mod09gav006/). The daily data was filtered for image quality thresholds to reduce scatter due to snow cover, aerosols, and clouds. NDVI was calculated at each site following the normalized ratio of the near-infrared (nir) and red bands (equation 3.8).

$$NDVI = \frac{Rnir - Rred}{Rnir + Rred} \quad \text{equation 3.8}$$

In Dry Creek watershed NDVI peaks earliest at lower elevations and on average 16 days earlier on southern aspects compared to northern aspects (Poulos *et al.*, 2021). The magnitude of peak NDVI varies with elevation and aspect with the highest elevations peaking over 0.64 and the lowest elevations maximum values near 0.41. Northern aspects average peak NDVI occur near 0.56 while southern aspects exhibit average peaks of 0.47.

Sap Flux

A thermal dissipation sap velocity (Dynamax FLGS-TDP XM1000) sensor was installed in 2012 in a Douglas-fir tree (*Pseudotsuga menziesii*) near the LDP meteorological station. The sensor has been operating intermittently from 2012 – 2017, decommissioned in the winter, and restarted each spring season. We followed the standard Granier (1985) method of determining sap velocity (V, cm/hr) (equation 3.9).

$$V = 0.0119 * \left(\frac{\Delta T_m - \Delta T}{\Delta T}\right)^{1.231} * 3600 \quad \text{equation 3.9}$$

The thermal dissipation sap flow sensors estimate tree-scale transpiration by measuring the temperature difference (ΔT) between two probes in the sapwood of a tree. The value ΔT_m, is the value of the maximum temperature difference or value when no sap flow occurs during the predawn period (between two and five). Thermal conduction

increases with sap velocity, therefore, as the sap velocity increases, the heat dissipation increases, and the heat source cools. When the temperature differences between the two sensors are maximal the sap flow is near zero or at a minimum. To reduce uncertainty in calculating transpiration rates we analyzed mean daily sap velocity (cm/day) and focus on changes in the timing of sap velocity rather than the magnitude of sap velocity. Sapwood area is required to convert sap velocity to transpiration rate for water balance calculations. Assumptions in the sapwood area potentially introduce large errors (Looker *et al.*, 2016).

Statistical Analysis

At individual sites, we calculated the Spearman correlation coefficient and p-values between modeled ET and predictor variables. The significant predictors were determined for each site based on p-values ≤ 0.10 and a site's strongest predictor was determined as the site's predictor with the lowest p-value. We used simple linear regression to fit the best fit line and find the slope and R^2 of each significant ET-predictor relationship.

We performed a regression tree analysis to identify the importance of predictor variables on annual ET values. The regression tree was based on all variables except snowmelt date because the LW site does not have a consistent snow cover throughout the season and therefore does not have a single spring snowmelt date. Regression trees have been used to estimate growing season length and water stress timing (e.g. Harpold, 2016). We grew a regression tree until additional splits no longer improved the cross-validated r^2 by 0.001. The complexity parameter was computed using 10-fold cross-validation and

pruned to optimal complexity by selecting the number of splits corresponding to 1 standard error of the minimum mean squared error (Breiman, 1984; R Core Team, 2021).

Results

Validating ET Calculations

We validated the modeled Penman-Monteith actual ET using three different measurements of transpiration and fluxes: We (1) compared EC measured ET to calculated ET, (2) compared the timing of sap flux velocity to calculated ET, and (3) analyzed timing and magnitude of remote sensing derived NDVI to daily and calculated annual ET at each site.

We compared the calculated values with EC data from the SH site from 2013 through the fall of 2016. The RMSE of daily ET was 1.33 mm. The modeled ET tends to overestimate the daily ET rate. The MODIS data compared to the EC data differed by RMSE of 0.96 mm/day. The MODIS ET tends to overestimate the peak ET but captures the timing of the EC measured ET (Fig. 3.3).

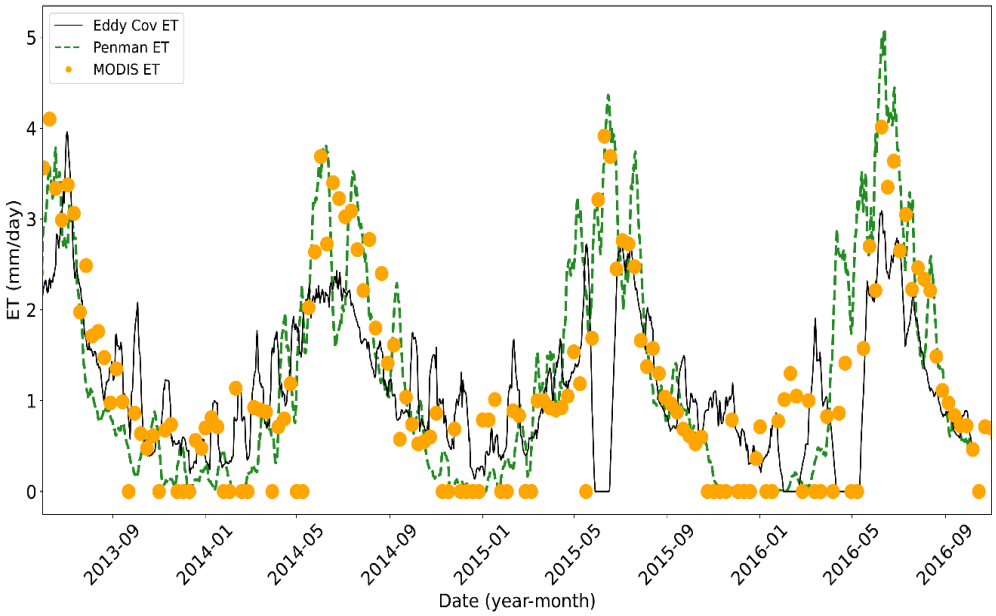

Figure 3.3 Fraction precipitation phase at each site and year. The lower bars (purple) represent the fraction of annual precipitation falling as rain, the middle bars (green) are the fraction as sleet and the upper bars (blue) are the fraction of precipitation as snow. The TL site is within the rain-snow transition where about 50% of the annual precipitation falls as rain and has the greatest proportion of precipitation as sleet.

The modeled ET, air temperature, soil moisture, soil temperature, precipitation, and VPD, at LDP were compared to the sap velocity at a station approximately 0.75 km from the LDP weather station site. The peak sap flux rate was greatest in the year 2014 and lowest in 2016. The peak sap flux occurred between June 15th and July 12th and aligned with peak air temperatures until the beginning of July (Fig. 3.4). Through the summer season, the sap flux decoupled from the air temperature profile, steadily declining and increasing in response to summer rain events. The sap flux approached 0 in the fall when soil moisture is the driest and temperatures are approaching zero.

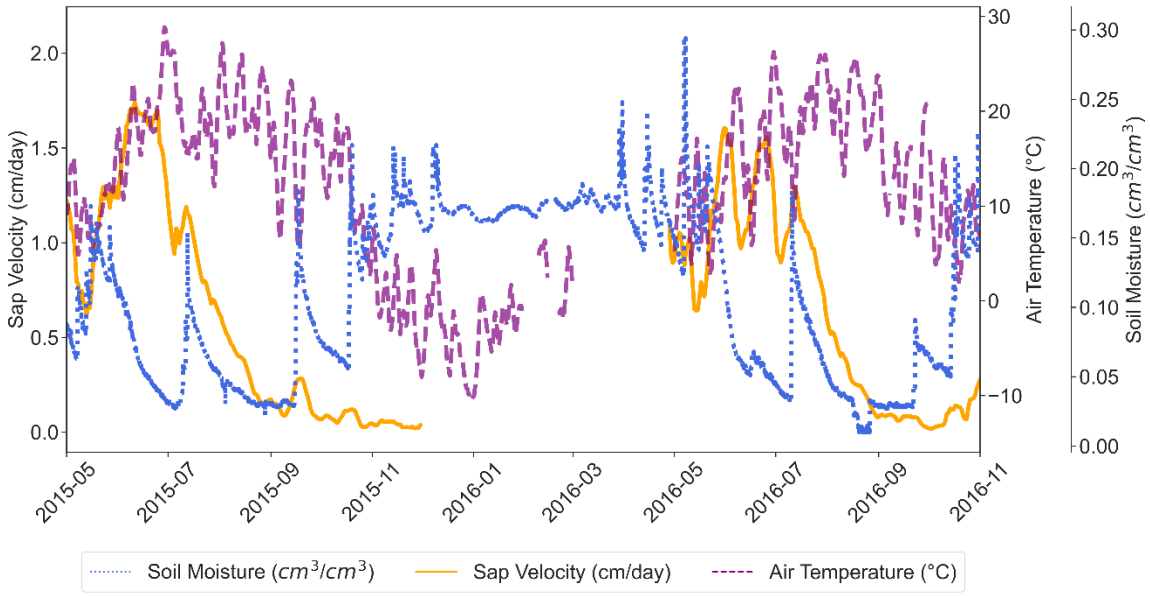

Figure 3.4 Sap flux (solid orange) with air temperature (dashed purple) and soil moisture (dotted blue) from 2015-05-01 to 2016-11-1. The sap flux station is located 0.75 km from the LDP study site.

Next, the modeled ET was compared to NDVI at each site. The peak greenness measured using MODIS NDVI, was positively correlated with annual ET (R^2= 0.59, p-value<0.001). The lowest NDVI was at LW, while the highest NDVI was at LDP and SH consistent with the sites with the highest annual ET (Table 1). The BR and TL sites were between the two. The timing of peak daily ET was positively correlated with the peak NDVI (R^2 = 0.33, p-value<0.001) such that later the peak ET, the greater the max daily ET rate. LW had the lowest NDVI and earliest peak ET rate while BR, LDP, and SH had the highest NDVI and latest peak ET. The timing of peak NDVI is negatively correlated to March, April, and May average temperatures however both the timing and max NDVI are the most correlated with average May temperatures (R^2 = 0.60, p-value<0.001). The timing of peak NDVI is positively related to peak snow depth (R^2 = 0.42, p-value<0.001) such that as snow depth increases, the peak NDVI is later.

ET Variability Within and Between Sites

The highest annual ET and mean average daily ET rates are at the mid-elevation sites, LDP and SH. The highest elevation site, BR has an average ET of 384 mm while the lowest elevation sites (TL and LW) have the lowest annual ET (324 and 187 mm) (Table 3.1, Fig. 3.5, and Fig. 3.6). Interestingly, although annual ET and the average daily ET are lowest at LW (0.4 mm/day), the growing season and the mean number of days that average daily ET is above 0.01(mm/day) is highest at that site (296 days). The average daily ET is highest at LDP (1.2 mm/day) (Fig. 3.6).

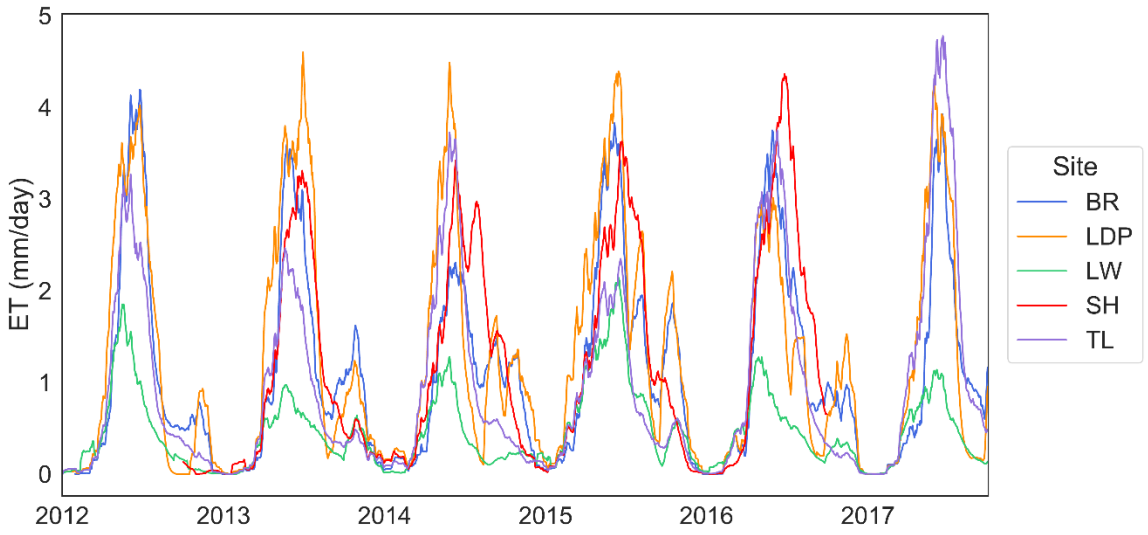

Figure 3.5 Smoothed daily ET rate (mm/day) from 2012 through 2017 at each site.

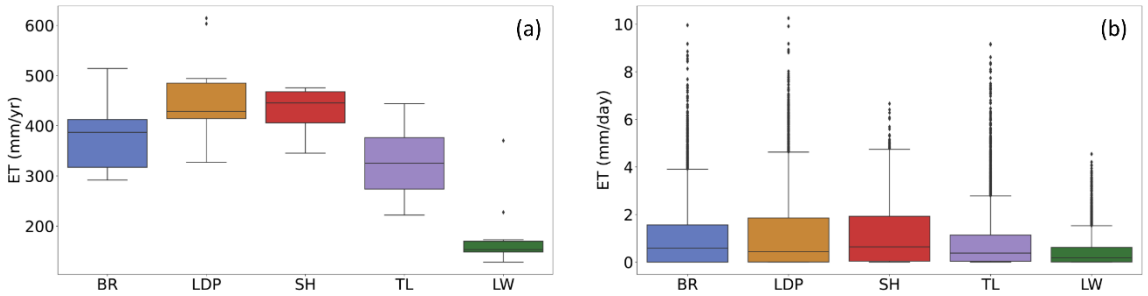

Figure 3.6 Annual ET rate (a) and average daily ET rate (b) at each site.

The LW site becomes snow free the earliest of all sites in the watershed. This site has the highest average March, April, May (MAM) temperatures (10.8°C), lowest peak snow depth (35.2 cm), and the earliest start of the growing season (Table 3.1). The LW site peak ET occurred on average on May 23rd, about 15 days earlier than the TL site and 16 days before the BR site. At the site level, ET at LW was negatively correlated with spring precipitation, decreasing as spring precipitation increased (R^2 =0.67, p-value=0.05) (Fig. 3.7). Comparing the ET with soil moisture, the ET peak occurs before the peak temperatures and follows the decline in soil moisture (Fig 3.8). During the higher snow or precipitation years, the temperatures tend to be cooler reducing incoming shortwave radiation, temperatures, and VPD resulting in low daily ET rates and lower annual ET compared to years with drier precipitation and lower peak snow depth (Fig. 3.8). The highest annual ET of 298 mm occurs in 2015 with the second lowest MAM cumulative precipitation, while the lowest annual ET of 160 mm occurs in 2012 along with the highest MAM cumulative precipitation.

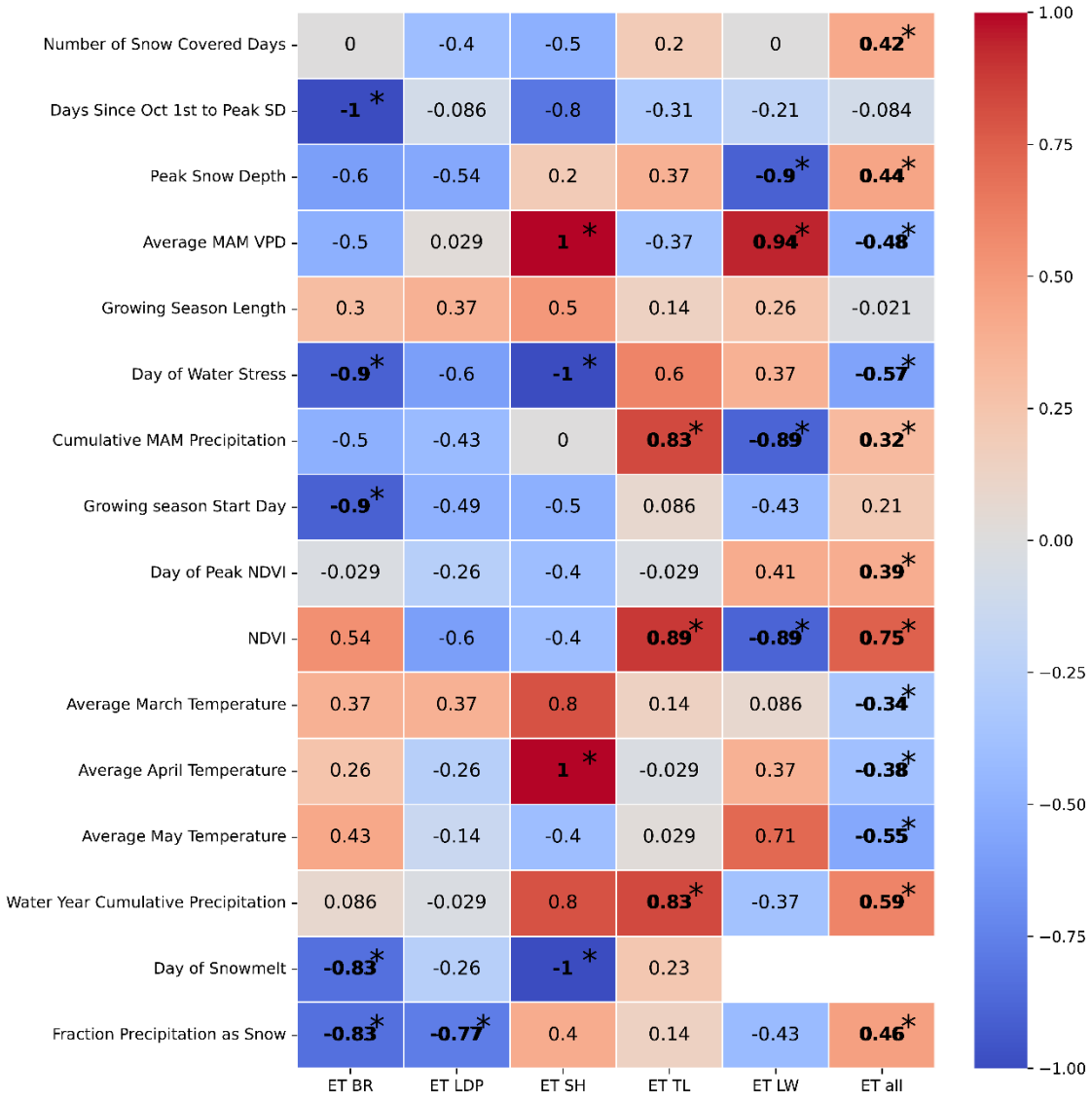

Figure 3.7 Spearman correlation coefficient between annual ET and parameters calculated at each site and all sites combined. Bolded values with an asterisk indicated significant correlations (P-Value ≤ 0.10). Sites are ordered from the highest elevation (BR) to the lowest elevation (LW) and ET all represents the ET from all sites and years combined.

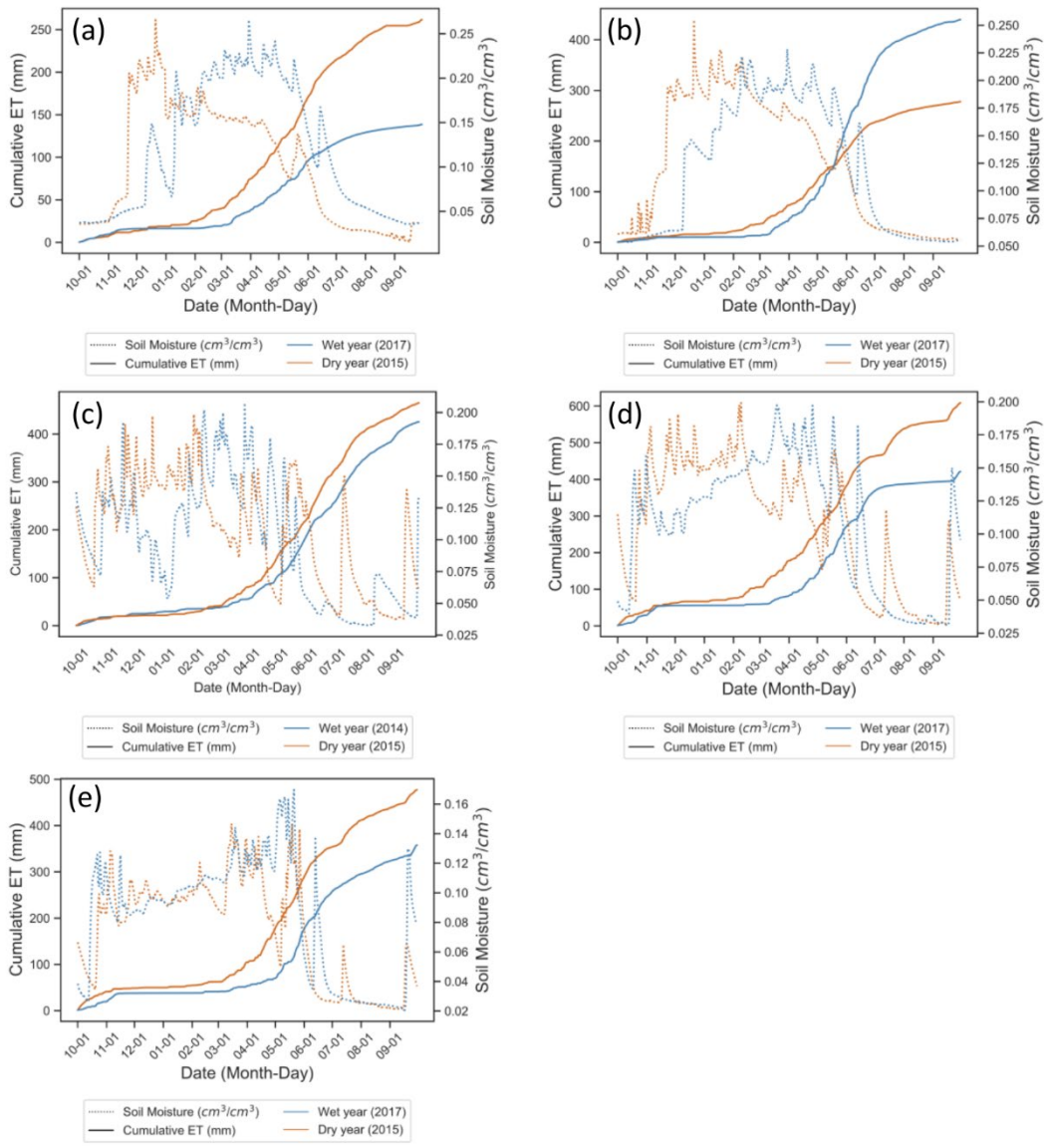

Figure 3.8 Cumulative ET (solid) and soil moisture (dotted) for a dry year and wet year at LW (a), TL (b), SH (c), LDP (d), BR (e).

The TL site is in the rain-snow transition zone, with an average peak snow depth of 50 cm, and consistent snow cover for about 125 days during the winter season (Table 3.1). The average annual ET is 324 mm, and peaks on June 8th. The highest ET of 425 mm occurred in 2017 along with the highest MAM precipitation, while the lowest mean annual ET (230 mm) occurred in 2013 with the lowest MAM cumulative precipitation. At the TL site, cumulative MAM precipitation and water year cumulative precipitation were

positively correlated with annual ET (R^2 = 0.71 p-value = 0.04 and R^2 = 0.87 p-value <0.01) (Fig. 3.7). In 2013, MAM precipitation was the lowest, resulting in a greater rate of decline of soil moisture and lower annual ET compared to the wetter years. When the snow cover period is longer or if there is higher spring precipitation, the growing season starts later, the ET rate early in the season is lower and the soil moisture stays relatively high through the spring season (Fig. 3.8). The high soil moisture at the beginning of the summer season aligns with the increased energy demand and results in increased ET rates.

The middle elevation sites (SH and LDP) had the greatest total ET and average daily ET rates. At these sites, the growing season began later in the spring, aligning the energy demand and soil water availability. The daily ET rate follows the temperature trend, declining as the temperatures begin to decline and soil moisture is at its driest state. The annual ET was greatest when temperatures were higher in the spring, snow depth was lower creating an earlier start to the growing season. Consistent with this trend, the fraction of water year precipitation falling as snow was negatively correlated with annual ET at the LDP site (R^2 = 0.54, p-value =0.10), and average March temperatures were positively correlated with ET (R^2 = 0.65) such that a one degree increase in average March temperatures increases annual ET by 40 mm (Fig. 3.7). The SH site was not significantly correlated to any climate parameters but we observed a trend between annual ET and snowmelt date (R^2 = 0.85) and cumulative water year precipitation (R^2 = 0.69).

The BR site is the high elevation site with the highest average peak snow depth (189 cm), longest snow cover season (183 days), coldest year round temperatures, latest

growing season start date (May 10th), and earliest growing season end date (Oct. 7th) compared to all other sites (Table 3.1). Annual ET was on average, 384 mm with the peak ET occurring on average on June 9th. The highest ET of 477 mm occurred in 2015 while the lowest ET of 341 mm occurred in 2014. At BR, the timing of peak snow depth was negatively correlated with ET (R^2=0.94, p-value<0.01), and the average spring air temperatures were positively correlated with annual ET with March air temperatures showing the strongest correlation (R^2 = 0.84) (Fig. 3.7). The lowest ET occurred during the year with the highest MAM cumulative precipitation, lowest September precipitation, and lowest average May temperatures. The fraction of water year precipitation falling as snow was negatively correlated with annual ET (R^2=0.70, p-value =0.04). The later snowmelt date aligns the energy demand of increased air temperatures, VPD, and shortwave radiation with soil moisture availability.

Watershed Analysis

Predicting Annual ET

A regression tree analysis predicting average annual ET at all sites and years showed that April and May air temperature explained 86% of the variability in ET in 4 branches (Fig. 3.9). The first branch was based on average May air temperature greater or less than 13°C. When temperatures are above 13°C in May, the average ET is 165 mm. However, when May temperatures are less than 13°C but March air temperatures are below 4.2° C, the average ET is 356 mm. When the average April temperature was greater than 4.2° C, the average ET is 464 mm.

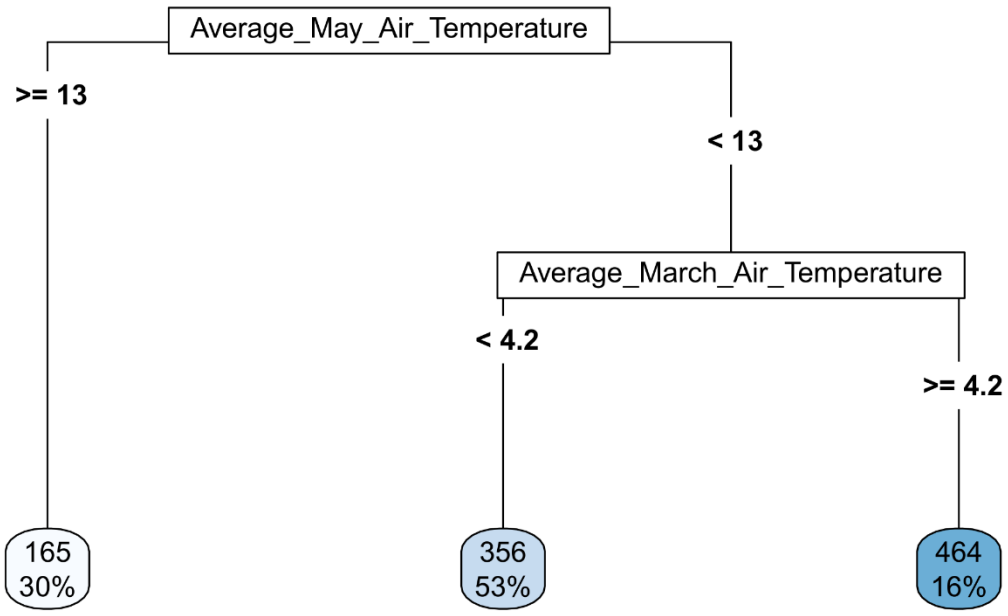

Figure 3.9 Regression tree results for predicting average annual ET using climate variables. The pruned tree explains 86% of the variability in ET in four branches based on air temperatures. The numbers on each branch leg show the decision for each branch and the final number in the lower boxes show the average predicted ET and percent of observations in the branch.

Watershed Correlations

We used simple linear regression to compare predictor variables and ET at all sites and years in the watershed (Fig. 3.7). The first day of water stress and NDVI had the highest correlations with annual ET. The timing of water stress is negatively correlated with ET, such that ET increases with an early water stress date (Fig. 10). We observe a diverging relationship between the timing of water stress and ET for years and sites with average May temperatures below 13° C as indicated by the regression tree analysis. When air temperatures are above 13° C, the timing of water stress is positively correlated with annual ET and annual ET values are below 200 mm. When air temperatures are below 13° C annual ET is negatively correlated with the timing of water stress. The negative correlation between ET and water stress is driven by the upper elevation, cooler

sites (BR, LDP and SH). At the middle to upper elevation sites, a one day increase in water stress results in a -2.5 mm decrease in annual ET. At the middle to high elevation sites, earlier water stress indicates an earlier start of the growing season, higher spring temperatures and greater annual ET.

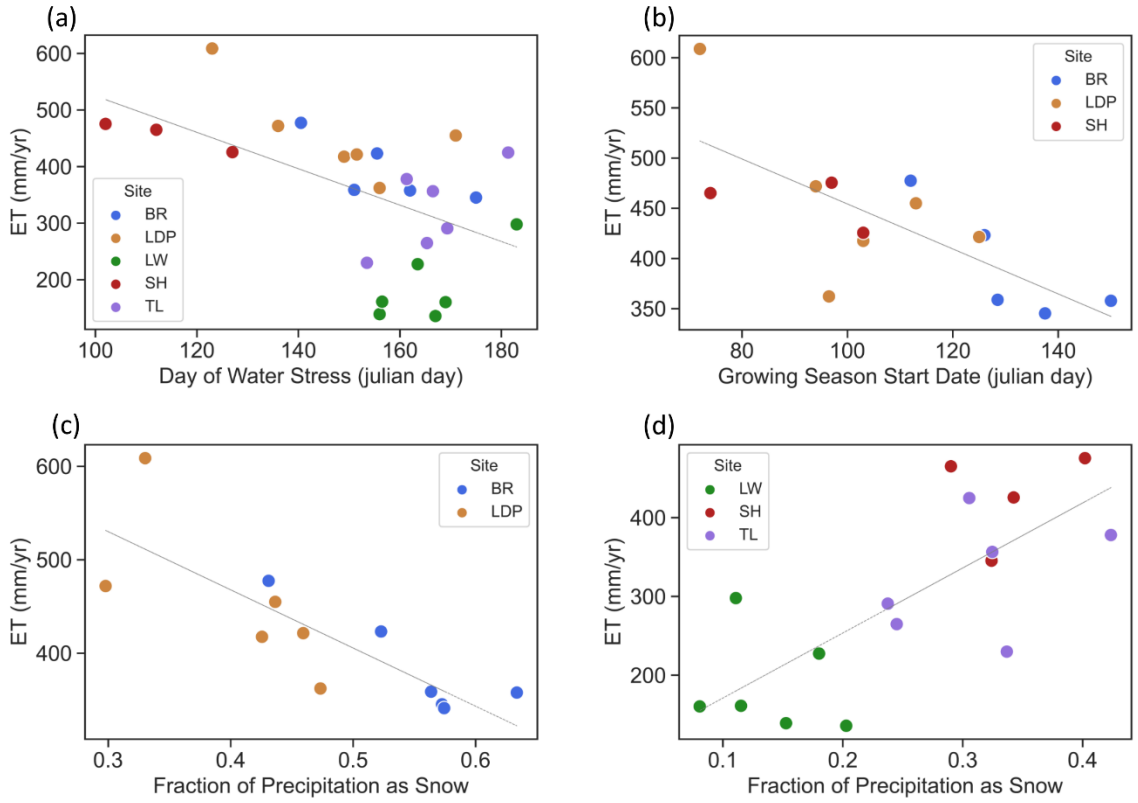

Figure 3.10 Annual ET versus the first day of water stress at each site (a), growing season start date at BR, LDP, and SH sites (b), and the fraction of precipitation as snow at the LDP, and BR sites (c), and SH, TL, and LW sites (d).

We also observe a trend with higher average April temperatures and earlier growing season start dates (R^2 = 0.41, p-value=0.02) across all sites and years. The slope of average April temperatures with growing season start date indicates that 1° C increase in average April temperatures results in a 5 day earlier growing season start date. Annual ET is not significantly correlated with growing season start date at the watershed scale, but the growing season start date at the upper elevation sites (LDP, SH, BR) are

correlated with annual ET (R^2 = 0.54, p-value < 0.01) (Fig. 10). At the upper elevation sites a two day later growing season start date results in about a 5 mm decrease in annual ET.

The fraction of precipitation falling as snow was significantly correlated with ET. At the watershed scale ET increased as the fraction of precipitation as snow increased. However, the relationship between the precipitation phase and annual ET varied when splitting the watershed into upper elevation (LDP and BR) and lower elevations (TL, SH and LW). At the upper elevations the fraction of precipitation falling as snow was negatively correlated with annual ET (R^2 = 0.67, p-value <0.01), while the lower elevations were positively correlated with the fraction of precipitation as snow (R^2 = 0.56, p-value<0.1) (Fig. 3.10).

Discussion

The modeled ET rate at each site is controlled by the synchrony of soil water availability with air temperature, shortwave radiation, and VPD. At the high elevations and low elevations, we observe higher annual ET when peak snow depth is lower, spring temperatures are warm and there is a greater fraction of precipitation as rain (higher elevations), although, the cause for each trend differs by elevation. In the rain-snow transition, however, we observe the opposite trend. ET increases with increasing snow depth and MAM precipitation (Fig. 11). The upper elevation sites are energy limited while the lower elevation sites are soil moisture limited. At all sites, the timing of peak ET and NDVI is earlier as spring temperatures increase. These results highlight the variability of annual ET and parameters influencing ET on an elevational gradient through the rain-snow transition. The rain-snow transition is vulnerable to warmer

temperatures and a shift in the rain-snow transition potentially altering the growing season length and changing the timing of phenological events (Richardson *et al.*, 2013). The ET rate and timing of ET may shift in response to changes in snow disappearance and energy drivers. This research builds upon previous studies analyzing the variability of ET by using field data to evaluate ET trends in a semiarid watershed in the rain-snow transition.

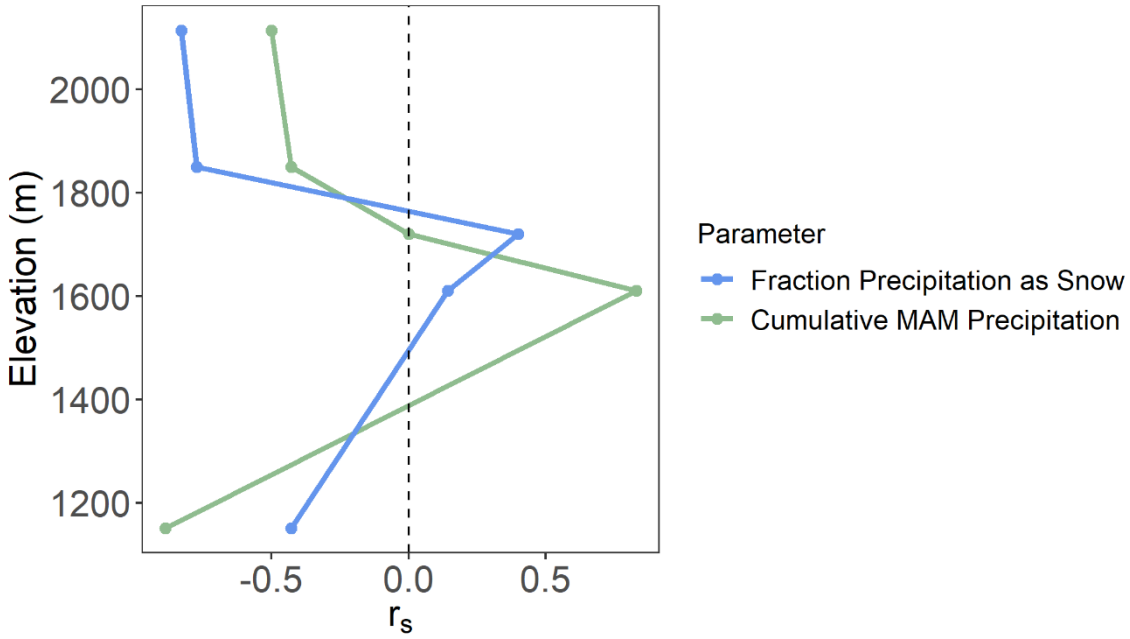

Figure 3.11 Spearman correlation coefficient between site elevation and cumulative March, April and May (MAM) precipitation and the fraction of annual precipitation as snow. High and low elevations are negatively correlated while the mid elevations are positively correlated with precipitation and the fraction of precipitation as snow.

Climate and Soil Moisture Availability Control ET

ET is either moisture or energy limited depending on elevation, latitude, or landcover type (Tague and Band, 2004; Lundquist and Loheide, 2011). Here we find three different trends in ET depending on elevation and snow cover (Fig 3.12).

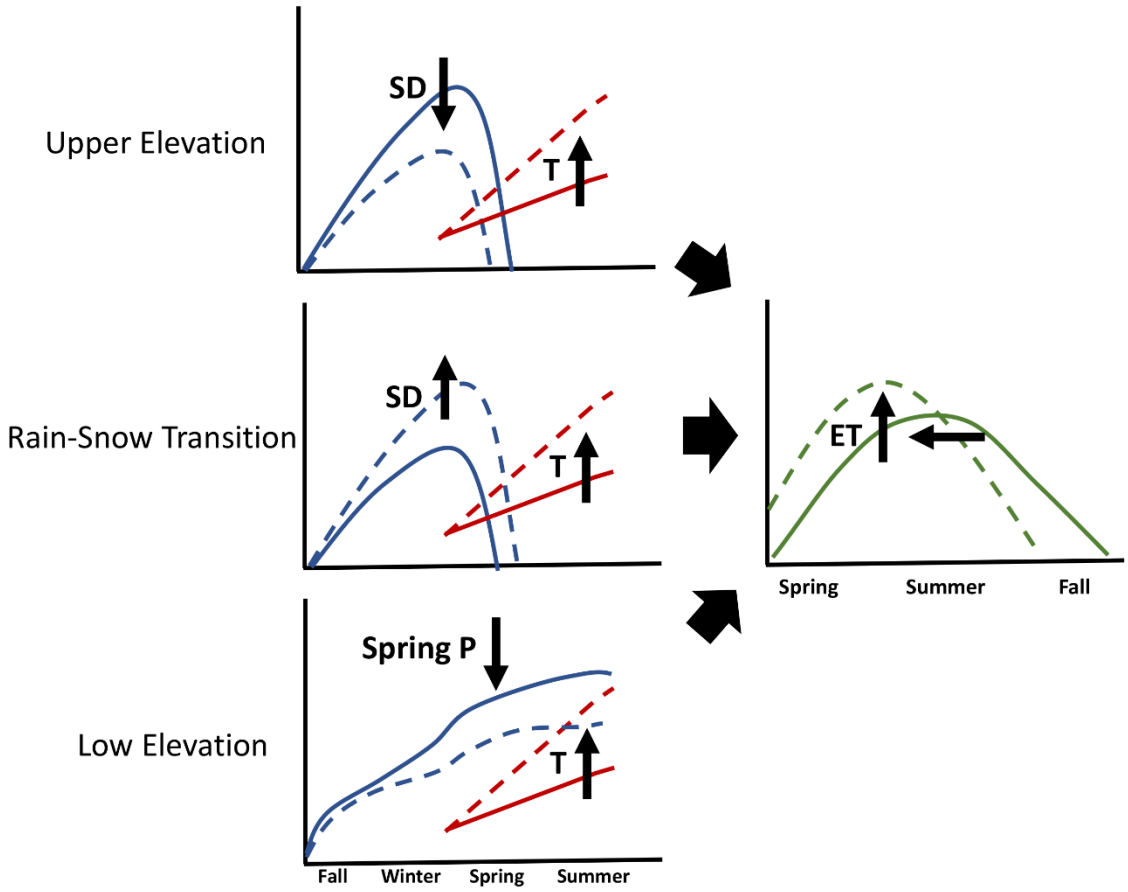

Figure 3.12 Conceptual model of parameter influencing ET magnitude and timing at each elevation. The solid lines represent the current parameter state, and the dotted lines represent a change to the current state. The blue lines are snow depth (SD) and March, April, May precipitation (Spring P). The red lines are air temperatures (T) in the spring and moving into the summer season and the green line is evapotranspiration (ET). Each scenario and change to precipitation and temperature depicted is predicted to increase ET and move the timing of ET earlier.

The first trend is at the low elevation site, LW, where ET is limited because soil moisture is available when the energy demand (air temperature, VPD, and shortwave

radiation) is low. The snow cover is not consistent, the dominant form of precipitation is rain (Fig. 3.2) and the first day of ET occurs early in the season when the energy demand is low, limiting the daily ET rate. For instance, in 2015, the cumulative March, April, and May precipitation was low. Years with low spring precipitation are negatively correlated with average MAM VPD, and average May air temperatures leading to increased daily ET rates early in the season. The relatively low precipitation is enough to supply soil moisture later into the season (Fig 3.8). Compared to a high snow year in 2017, the early season ET rates are lower due to lower energy demand. Once spring precipitation begins to decline and the air temperatures increase, the ET peaks and is limited by soil moisture into the summer season. The earlier snowmelt and greater length of time the soil is warm result in a longer period when the soil is warm but dry and ET is limited at lower elevations (Poulos *et al.*, 2021). The LW site depends on the balance between spring precipitation providing soil moisture and spring precipitation limiting the energy drivers. This relationship follows Christensen et al. (2008), who found transpiration in a watershed in the Sierra Nevada was sensitive to water availability at low-middle elevations. Years with high and low precipitation had low annual transpiration while the moderate precipitation years had the highest transpiration.

The second trend occurs at the rain-snow transition site, TL, where the annual and daily ET rates are limited by soil moisture and change between resembling the low elevation sites (LW) or the higher elevation sites (e.g. LDP). The timing of peak soil moisture is correlated with snowmelt (Smith *et al.*, 2011) and the soil water stress timing is explained by the timing of snow disappearance (Harpold, 2016). At the TL site, the variability between high and low ET years occurs due to changes in snow years and

spring precipitation controlling the soil moisture recession and water availability into the summer season. In contrast to the other sites, the TL site exhibits a decrease in ET with decreasing snow depth and spring precipitation due to soil moisture limitations. A wet spring or water year results in greater soil moisture for ET into the summer season. During a low water year or dry spring, ET is limited by soil moisture when the energy demand is high. For instance, at the TL site, 2017 was a wet water year, had a relatively high peak snow depth, and a relatively late water stress date (Fig. 3.8). Initially, the daily average ET rates were low, but as the growing season progressed, the energy demand increased and was in sync with the soil moisture availability increasing the daily average ET rates and annual ET. In contrast, during a dry water year (2015) the daily average ET rate was higher early in the growing season compared to the wet year. The lack of spring precipitation in 2015 resulted in an earlier start to water stress, lower daily ET rates as the growing season progressed, and a lower annual ET. Other studies in the nearby Reynolds Creek Experimental Watershed (RCEW) observed a similar relationship between soil moisture availability and ET. Fellows et al. (2019) found soil moisture and soil properties strongly controlled Gross Ecosystem Exchange (GEE) at a sagebrush dominated site and aspen dominated site. The early snowmelt reduced spring water input and advanced the GEE onset and soil moisture withdrawal resulting in late-summer water stress.

The third trend is with the middle to high elevation sites where annual ET is energy limited. These sites tend to have average May temperatures below 13°C and a decrease in annual ET with later soil water stress due to a shorter growing season length (Fig. 3.8). At these sites, we expect increased spring temperatures and earlier snow disappearance will increase annual ET due to the longer growing season length. The soil

water availability at the middle elevation sites (SH and LDP) is more closely aligned with the energy demand compared to BR, TL, and LW but is limited by energy and snow cover. At LDP, the highest annual ET occurred during the drier years, earlier snowmelt, and warmer springs (Fig. 3.8). The longer growing season length and higher energy demand result in a greater number of days ET is occurring, higher daily ET rates, and higher annual ET. At SH, we observe the same trend with increased annual ET during warm springs when the snowmelts earlier. However, the SH site differs from LDP by displaying a positive correlation with annual ET and annual precipitation and does not have a strong correlation with the precipitation phase.

At the BR site, the start of the growing season begins later, and ends earlier, compared to all other sites, and is energy limited. The later growing season start date and earlier start of the snow covered season at the BR site resulted in fewer days that ET occurs and lower average monthly temperatures result in lower daily average ET rates compared to LDP. However, the later start date led to a greater amount of water availability during peak ET demand and greater average daily ET rates compared to LW and TL sites (Poulos *et al.*, 2021). The timing of soil water availability and energy demand for ET are aligned, but cooler summer temperatures, lower VPD, lead to less annual ET compared to the middle elevations. When comparing a wet year and drier year (Fig. 3.8), the earlier snowmelt and growing season start date during the dry year lead to greater annual precipitation compared to the wetter year with a later snowmelt date.

The hypothesis that ET at middle and high elevation is limited by energy rather than soil moisture until mid-summer is consistent with the timing of sap flux compared to the soil moisture and air temperature at the LDP site. The sap flux follows the VPD and

air temperature profile, peaking near peak air temperature and reaches peak sap flux when soil moisture is near the wilting point (Fig.3. 4). The coupling of sap flux with air temperature and VPD indicates the tree was not limited by soil moisture despite low soil moisture levels early in the summer season (Looker *et al.*, 2018). Through the summer season, air temperature remains high and the sap flux rate decouples from the air temperature trend and begins to decline as a result of soil moisture limitation (Cooper *et al.*, 2020). The sap flux does not drop to near 0 until the winter months indicating the trees are using deep soil water at a reduced rate due to water conservation strategies by the plant such as decreased stomatal conductance (Looker *et al.*, 2018). Previous studies in Dry Creek watershed found plant water was isotopically distinct from streams and groundwater but they were inconclusive regarding the vegetation water source (McCutcheon *et al.*, 2017). In western Montana, Martin et al. (2018) found winter precipitation accounted for 87.5% and 84% of tree growth with lower elevation sites more dependent on winter precipitation than higher elevations. Considering the LDP site sits just above the rain-snow elevation line and on a southeast facing slope, the primary water source for LDP is likely from deeper snow derived soil water. However, increases in soil moisture result in increases in sap flux rates suggesting the tree can shift to shallow water sources in response to summer rain.

Implications for Climate Change

The declining trend of snowpack in the United States (Zeng *et al.*, 2018) and the importance of winter snowpack for vegetation water use into the summer season (Hu *et al.*, 2010) highlights the importance of quantifying the trends in ET timing and magnitude in a changing climate. Petersky et al. (2019) found in the Great Basin, an increase in 2°C

during the winter will reduce the season snow extent by 14.7%, and a 4°C increase in air temperatures resulted in about a 40 day less snow duration in Douglas Fir and Ponderosa Pines trees. The reduced snow water availability and strong link between ET and spring air temperatures lead to the question*: what does lower snowpack and increased spring temperatures mean for vulnerable watersheds in the rain-snow transition?* In this study, there was a high correlation between spring temperatures, max snow depth, and annual ET, and peak ET timing. However, annual ET diverged depending on elevation and snow cover. For example, comparing 2015 and 2017 TL ET (Fig. 3.8), the years were similar in growing season start date. However, 2015 had a lower snow year, and temperatures were 1.8°C higher in the spring. This difference resulted in 160 mm less in annual ET during the dry year. This difference at TL, implies that as temperatures increase, and snow cover duration decreases at the TL site we might see decreased ET due to an earlier start of the soil moisture recession and greater offset with peak energy demand. But, the lack of correlation between ET and precipitation phase at TL and high correlation between spring precipitation and ET indicate spring precipitation of any form can supplement the earlier start of the soil moisture recession.

At the high elevation sites, the positive correlation between average May temperature and ET and negative correlation between snow depth and ET indicates annual ET will increase as temperatures increase, peak ET will be earlier, and peak greenness will be lower (Christensen *et al.*, 2008). When considering BR, LDP, and SH, a 1°C increase in average March air temperature results in a 20 mm increase in annual ET. At the site level, at BR in 2012 and 2015, a 2°C increase in average May temperatures resulted in a 132 mm increase in annual ET. As the temperatures warm, we

expect the precipitation phase to shift from snow to rain. The upper elevation sites, LDP and BR, were negatively correlated with the fraction of water year precipitation falling as snow. These results indicate as temperatures rise and snow changes to rain at these upper elevation sites, we expect an increase in annual ET assuming the same amount of precipitation.

At the LW site air temperature was not significantly correlated with annual ET but we observed a positive trend between annual ET and average May and March air temperatures. The strongest correlation between air temperatures and annual ET resulted in a 70 mm increase in ET per 1°C increase in May temperatures. However, in a warming climate, assuming the same precipitation, annual ET will likely not change considerably at the LW site due to soil moisture limitations. The timing of peak ET will be earlier and the daily ET rate will be higher (Flerchinger *et al.*, 2020).

At the watershed scale, as spring temperatures increase, the decrease in modeled ET at TL will likely not be sufficient to offset the combined increasing ET rates at the lower and higher elevations. This implies that as spring temperatures increase and snow depth decreases, the watershed annual ET will be higher compared to the observed years in this study. The increased ET rate reduces water availability for groundwater recharge, streamflow, and hydrologic connectivity of the watershed (Kleine *et al.*, 2021; Segura, 2021). Previous research in the Dry Creek watershed estimated deep drainage accounted for 34% of the total precipitation (Kormos *et al.*, 2015) in the TL sub-catchment and that the watershed streamflow was largely groundwater dominated (Tetzlaff *et al.*, 2015). In Dry Creek watershed, increased watershed ET rates due to rising temperatures will

potentially reduce the snow water availability for groundwater recharge and consequentially reduce the water available for streamflow.

A shift in the precipitation regime from snow to rain will affect elevations differently depending on whether a site is energy or water limited (Flerchinger *et al.*, 2020). Sites that historically had a seasonal snowpack and are energy limited such as the LDP, SH, and BR sites, will be the most challenged under a hydrologic regime characterized by earlier and more episodic water inputs (Petersky *et al.*, 2019). The sap flux station exhibits a reliance on deep groundwater, likely supplied by snowmelt that might challenge vegetation accustomed to these water sources. As the snow melts it slowly regenerates deep groundwater storage, but with a shallower snowpack, greater rain precipitation, the deep groundwater stores might not regenerate (Bales *et al.*, 2011). The change in the hydrologic regime will result in changes in vegetation productivity. As the number of snow covered days decreases, March, April, and May temperatures increase we observe decreased NDVI and earlier peak NDVI and ET timing across all sites and years. The changes to a more ephemeral snowpack and longer duration of water stress may result in reduced regeneration success, plant mortality, and shifts in species composition.

Conclusion

We have highlighted how ET is controlled by the alignment of soil water availability and energy demand at five sites along an elevational gradient. We found three different trends with how ET changes with soil water availability and climate parameters across the watershed. The first trend is at the low elevation site, LW, where ET occurs early in the season when the energy demand is low, limiting the daily ET rate and

depleting the soil moisture availability into the summer season. The LW site depends on the balance between spring precipitation providing soil moisture and precipitation limiting the energy drivers during the spring months. The second trend occurs at the rain-snow transition site, TL, where the annual and daily ET rates are soil moisture limited, and the annual ET increases with increasing precipitation. In contrast to the other sites, the TL site increases in ET with increasing snow depth and spring precipitation due to greater soil moisture availability. The third trend is with the middle to high elevation sites where annual ET is energy limited. Annual ET at these sites increases with earlier snow disappearance and longer growing season lengths.

The results of this study have implications for the partitioning of water in the hydrologic cycle in a changing climate. As temperatures increase, we expect watershed scale annual ET will increase. However, contradicting the watershed scale increase in ET, we expect ET at the rain-snow transition will decrease due to an earlier start of the soil moisture recession and soil moisture limitations into the summer season. Changes in water use and availability at different elevations will affect vegetation productivity and species composition. Information about the differing reactions to climate parameters at each elevation can be used to define areas more susceptible to changes in climate

CHAPTER FOUR: THE SENSITIVITY OF EVAPOTRANSPIRATION TO WARMING TEMPERATURES ACROSS THE RAIN-SNOW TRANSITION

This Chapter is expected to be published as: Kraft, M., McNamara, J. P., Flores, A.N., Rudisill W., Marshall, H.P., Glenn, N.F., Maneta, M. (2023). The Sensitivity of Evapotranspiration to Warming Temperatures Across the Rain-Snow Transition.

Abstract

Vegetation in water limited, semiarid regions rely on snow melt to support vegetation into the summer season. Across the rain-snow transition, warming temperatures will shift snow to rain dominated hydrologic regimes, altering the timing and distribution of soil moisture available for vegetation. Our objective was to assess how changing temperatures will alter the snow water input, streamflow, and evapotranspiration (ET) and how the seasonal variability in warming temperatures affects ET. To improve our understanding of how warming temperatures will affect snowmelt, ET, and streamflow, we applied the physically based EcH_2O model to the Dry Creek Watershed in southern Idaho, USA which spans the rain-snow transition. Air temperatures were perturbed by 2°C during the snow cover season from October through May and in individual months of November, December, March, and April to explore how the seasonal variability of warming temperatures will affect snow water equivalent (SWE), ET, and streamflow. We found that warming temperatures in the fall decreased peak SWE and therefore shifted the snowmelt timing and streamflow earlier in the spring.

Soil moisture and energy for ET were not synchronized limiting the ET rates. Warming temperatures in the spring shifted snowmelt earlier, streamflow timing earlier and ET rates increased due to synchronized soil moisture availability and energy drivers. In all scenarios, high ET rates in the spring reduced soil moisture availability and ET rates later in the summer season. Across the rain-snow transition, ET rates were the most sensitive in the forest and seasonal zones because of the later snow disappearance timing aligning with soil moisture and energy drivers. These results expand our understanding of how warming temperatures will affect hydrologic processes in complex semiarid mountain climates spanning the rain-snow transition.

Introduction

The hydrologic regime of snow dominated mountainous regions is controlled by the amount and timing of snow water input (Molotch *et al.*, 2009; Hammond *et al.*, 2019). Climate variability impacts snowmelt timing and distribution, which impacts how snowmelt water partitions between evapotranspiration (ET), soil moisture and groundwater recharge, and streamflow, impacting the downstream water supply (Rasouli *et al.*, 2022) and dependent ecosystems (Petrie *et al.*, 2015; Grogan *et al.*, 2020). In semiarid ecosystems, most of the annual precipitation occurs during the winter, concentrating the timing of soil moisture availability for ET and streamflow. The effects of climate variability are greater in these climates than in a wet climate because of the limited time soil saturation occurs (Hammond *et al.*, 2019). Adding complexity in semiarid mountainous regions, the impacts of warming temperatures on snowmelt and subsequent snow water availability vary across elevation, aspect, and vegetation.

The rain-snow transition is the area bounded by a rain dominated and snow dominated hydrologic regime. Within the rain-snow transition zone, a thin ephemeral snowpack, generally less than 1 m deep develops that generally begins to melt soon after snowfall (Sturm and Liston, 2021). The thin snowpack is more susceptible to warm storm events and incoming energy compared to a deep snowpack (Jennings and Molotch, 2020; Haleakala *et al.*, 2021b). Changes in the precipitation phase due to warming temperatures will alter the rain-snow elevation shifting the extent of the ephemeral snowpack and reducing the total months of snow conducive temperatures in the current rain-snow transition zone (Klos *et al.*, 2014).

Changes from a seasonal to an ephemeral snowpack will cascade into changes in snowmelt driven hydrologic processes. Previous research found that warming temperatures will likely decrease spring snow water equivalent (Mote *et al.*, 2018), increase annual ET (Goulden and Bales, 2014), and decrease the water available for streamflow (Milly and Dunne, 2020; Rasouli *et al.*, 2022). Warmer temperatures earlier in the season initiate the snowmelt period, but snow water inputs are released at a slower rate earlier in the season (Musselman *et al.*, 2017). Peak soil moisture and plant water availability coincide with snow disappearance timing, after which the soil moisture begins to decline (McNamara *et al.*, 2005; Smith *et al.*, 2011). An earlier snow water input and snow disappearance lead to an earlier peak soil moisture, potentially lengthening the growing season, but as a tradeoff with potentially longer summer soil water stress (Petrie *et al.*, 2015; Harpold, 2016). However, response to snowmelt timing and soil moisture availability to warming temperatures will vary across the landscape with local topography and subsurface conditions.

Snow and vegetation processes vary spatially and temporally with topography, soil, and vegetation. Slope and aspect affect the incident solar radiation with higher solar radiation and surface energy on southerly slopes increasing snowmelt rates (Kormos *et al.*, 2014), initiating an earlier peak soil moisture (McNamara et al., 2005), and increasing evaporative demand compared to northerly slopes (Seyfried *et al.*, 2021). Along an elevational gradient, higher elevations receive greater snow water inputs and have later snow disappearance dates than low elevations (Tennant *et al.*, 2017). As a result of the synchronicity of water and energy, ET varies along the elevational gradient (Christensen *et al.*, 2008; Kraft and McNamara, 2022). Additionally, localized variability in snow water input and soil characteristics affect soil water availability for vegetation into the summer season (Williams *et al.*, 2009; Geroy *et al.*, 2011). In semiarid regions, forest cover shades the snow surface from solar radiation, slowing the snowmelt rate compared to open areas (Malle *et al.*, 2019). The slower snowmelt rate leads to snow disappearance timing and peak soil water availability, coinciding with increased energy sustaining more intense ET rates. Deeper soil depth on north aspects compared to south aspects support greater soil moisture storage into the summer months, provide water for ET when the energy demand is high (Poulos *et al.*, 2021), and provide hydrologic conditions suitable for tree establishment (Fellows *et al.*, 2019). Additionally, snow and vegetation processes can vary with season. Fall determines the initial soil conditions but doesn't necessarily contribute to spring and summer soil water availability for ET (Smith *et al.*, 2011). During the winter, low temperatures and solar radiation limit the ET rate and snow melt water for streamflow (Kormos *et al.*, 2014; Tor-ngern *et al.*, 2017; Bowling *et al.*, 2018). The variability of landscape characteristics with seasonal shifts in hydrologic processes

creates uncertainty when predicting how ET will respond to warming temperatures and a change in the rain-snow elevation.

Vegetation in water limited semiarid regions is particularly sensitive to environmental change because of the reliance on snow (Trujillo *et al.*, 2012; Hammond *et al.*, 2019). But warming temperatures will alter snow's spatial variability and distribution and the subsequent snow disappearance timing. In Reynolds Creek Experimental Watershed (RCEW) in semiarid southern Idaho, Marshall et al. (2019) found warming temperatures altered snow drift disappearance timing reducing the snow melt heterogeneity and subsequently leading to increased water limitation in an aspen site. The sensitivity of ET to warming temperatures and shifts in the hydrologic regime varied spatially and temporally depending on site characteristics and reliance on snow water inputs. Across the rain-snow transition, Flerchinger et al. (2020) found that increased temperatures shifted the timing of water availability with higher, snow dominated elevations more sensitive compared to lower rain dominated elevations. Additionally, thinner soils limited snow water storage creating a reliance on summer precipitation refilling depleted soil moisture, while deeper soils were more sensitive to early snowmelt and reduced snowmelt input (Fellows *et al.*, 2019).

The Dry Creek Watershed spans the rain-snow transition where warming temperatures are expected to raise the snow line reducing the seasonal snow extent and changing the timing of snow water inputs (Klos *et al.*, 2014). Within the Dry Creek Watershed, the distribution of snow disappearance and the soil water capacity varies with elevation, aspect, and vegetation. At higher elevations, snowmelt timing is synchronized with areas of high soil water storage capacity and later energy inputs resulting in more

intense ET (Poulos *et al.*, 2021). Warming temperatures will alter the precipitation phase across the rain-snow transition. The effects will propagate into changes in the timing and distribution of snow water availability and synchrony with ET. This research will build off previous studies in a semiarid climate (e.g. Marshall et al., 2019a; Poulos et al., 2021; Kraft and McNamara, 2022) by evaluating the seasonal variability of warming temperatures on snow and ET across the rain-snow transition. This research will address how the seasonal variability of warmer temperatures will affect water availability for ET in a rain dominated, ephemeral snowpack and seasonal snowpack environment. We use a modeling approach to address the following objectives: (1) how will changing temperatures alter snow water input, streamflow, and ET? (2) how does seasonal variability in warming temperatures affect ET?

Methods

Study Site

The Dry Creek watershed drains 27 km^2 in semiarid southern Idaho (Fig. 4.1). The elevation of the watershed spans 1030 m to 2130 m, with low elevations receiving approximately 26% annual precipitation as snow and high elevations receiving 59% annual precipitation as snow and accumulating an average peak seasonal snowpack of 1.8 m. Vegetation in the watershed is predominantly grass at low elevations transitioning to sagebrush and other woody shrubs, and Douglas fir (*Pseudotosuga menziesii*) and Ponderosa pine (*Pinus Ponderosa*) trees at higher elevations. Within the watershed, there are five weather stations located at different elevations. The Lower Weather (LW) station is the lowest elevation weather station at 1151 m, Treeline (TL) is at the edge of the upward tree line at 1610 m, Shingle (SH) is 120 m above TL at 1720 m, followed by

Lower Deer Point (LDP) at 1850 m and Bogus Ridge (BR) at the highest elevation 2114 m. Each weather station records hourly air temperature, relative humidity, incoming and outgoing shortwave and longwave radiation, wind speed and direction, precipitation, and snow depth. We used soil moisture from the TL weather station at 5 cm soil depth and soil moisture measurements at 8 cm depth from the LDP weather station. Streamflow was measured at the Lower Gage (LG) station at the watershed outlet. Sap flux was measured in a Douglas fir tree about 0.75 km from the LDP site. This study was conducted across six years, from water year (WY) 2016 to WY2021.

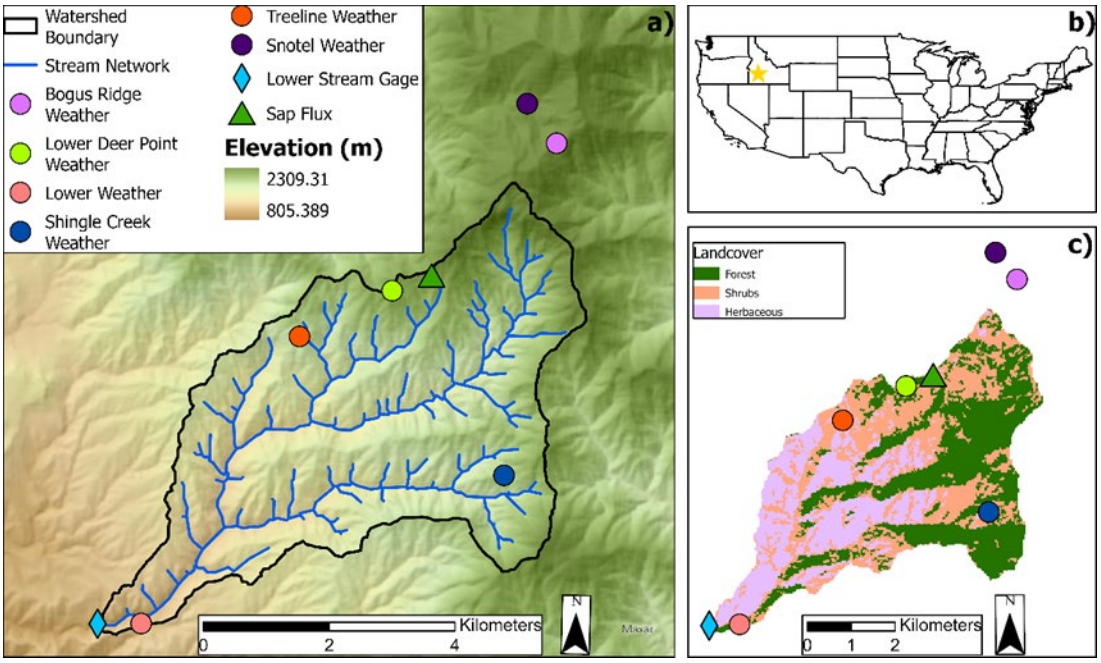

Figure 4.1 Map of the location of Dry Creek Experimental Watershed (DCEW) (a). The location of DCEW in southern Idaho, USA represented by a yellow star (b). The landcover type in DCEW (c). Circles are weather stations, including the Snotel station. The diamond is the stream gage at the stream outlet and the triangle is the sap flux station.

Ech2o Model

We used the EcH_2O model to investigate how surface water inputs (snow or rain) are partitioned into evaporation, transpiration, streamflow, or soil moisture and how this

will change with increased air temperatures. EcH$_2$O is a spatially distributed model that integrates a two-layer (canopy and understory) vertical energy scheme, dynamic vegetation growth that includes carbon uptake, allocation, and transpiration, and a hydrologic component based on the kinematic wave with lateral and vertical water redistribution (Maneta and Silverman, 2013). At each timestep (daily in this study), the EcH$_2$O model requires information on incoming shortwave radiation, incoming longwave radiation, air temperature (maximum, minimum, and average), wind speed, and relative humidity. The spatial domain of EcH$_2$O is on a regular grid defined from digital elevation data with multiple vegetation covers. In each model timestep, the energy balance is solved over the cell for the canopy level and fraction of vegetation types within a cell. The energy components are partitioned into radiative (net radiation) and turbulent (sensible, latent, ground heat, and heat into the snowpack) components as functions of canopy and surface temperatures. The surface energy balance allocates energy available to evaporate water, reduce the cold content of the snowpack, and heat the air and ground.

The model differentiates the latent heat associated with transpiration and evaporation from the canopy and soil. Evaporation from the surface is limited to the upper soil layer and surface of leaves and is limited by water availability, aerodynamic resistances, and soil resistance to gas exchange. The latent heat of transpiration is controlled by a Jarvis-type model and is affected by environmental factors of solar radiation, air temperature, soil moisture, and vapor pressure deficit (VPD). The stomatal conductance depends on the maximum stomatal conductance for the vegetation type. The canopy can alter the surface energy balance by attenuating radiation through the canopy, emitting longwave radiation on the surface, and altering the atmospheric

aerodynamic resistance to latent and sensible heat exchanges between the soil surface and atmosphere.

The water balance includes components of a linear bucket canopy interception, a one-layer snowpack model, surface ponding storage, and three soil layers. If a snowpack exists, fluxes into the snowpack are assumed to increase or decrease the snowpack's cold content. At the melting point temperature, any extra energy generates snowmelt, and the amount of snowmelt water is calculated from the latent heat of melt. Snowmelt water or rain infiltration into the soil is calculated using a form of the Green and Ampt equation. The drainage from upper to lower soil layers occurs when the field capacity is exceeded and can move to deeper layers or the stream (gravitational water and diffusive water effects are assumed negligible). Leakance through the bottom soil boundary follows the same approach but is controlled by a leakance parameter that ranges from free drainage to no drainage. The precipitation phase within the model is differentiated using a user defined threshold and the maximum and minimum daily temperatures. If the maximum temperature is below the threshold, the precipitation phase will be snow; if, the minimum temperature is above the threshold, it will be rain. If the air temperature is between the maximum and minimum daily air temperature, the model divides the fraction of snowfall and rainfall using the maximum and minimum temperatures.

Input Data, model setup

The gridded digital elevation model (DEM) was derived from the USGS 10 m DEM and aggregated to the 30x30 m^2 resolution to match the National Landcover Database (NLCD) vegetation input. The DEM was used to delineate the drainage boundary, obtain slopes and drainage direction, and stream network using the PCRaster

tool suite (http://pcraster.geo.uu.nl/). The drainage network was delineated using the steepest-descent algorithm on the 8-neighbor window around each cell. We split the basin into three elevation ranges using the empirical distribution function of the DEM. The snowmelt coefficient was separated into three bands ranging from below 1418 m, 1418-1619 m, and above 1619 m elevation.

Climate data

Meteorological variables required by EcH_2O were collected at five weather stations distributed at different elevations within the watershed and a Snotel station located just outside the watershed. The model requires the climate data to be distributed across climate zones within the watershed. We discretized the watershed into 12 elevation bands between 1030 m and 2130 m. Each elevation band was split into North, East, South, and West aspects resulting in 44 total climate zones. The highest elevation only had a south aspect and the second highest elevation zone had east, south, and west aspects, while all other elevation bands contained all four aspect categories. Point measurements of meteorological variables were distributed using a method and weather stations suitable for each variable. We used all five weather stations to develop a linear regression model between daily mean air temperature and elevation. The linear regression model was used to distribute mean daily air temperatures across the climate zones, but air temperatures were assumed to remain constant on different slope aspects (Fig. 2a). We used the low and high elevation weather stations to develop a linear regression between precipitation and elevation and distribute the daily precipitation rate. We used only the LW and BR weather stations to distribute the precipitation data due to uncertainty in precipitation under catch at TL, LDP and SH (Fig. 2b). Relative humidity, wind, and

incoming longwave radiation were distributed using all five weather stations and inverse distance weighting methodologies. Incoming shortwave radiation was first distributed using inverse distance weighting (IDW), then scaled by aspect. To scale incoming shortwave radiation by aspect, we used the ArcGIS solar radiation tool to calculate potential daily solar radiation across the watershed. We then used the potential solar radiation to calculate the proportion of potential radiation in each cell for a given day (max daily radiation/cells radiation). The daily proportion of max solar radiation was multiplied by the station IDW distributed incoming shortwave to obtain distributed incoming shortwave radiation across the different aspects and elevations.

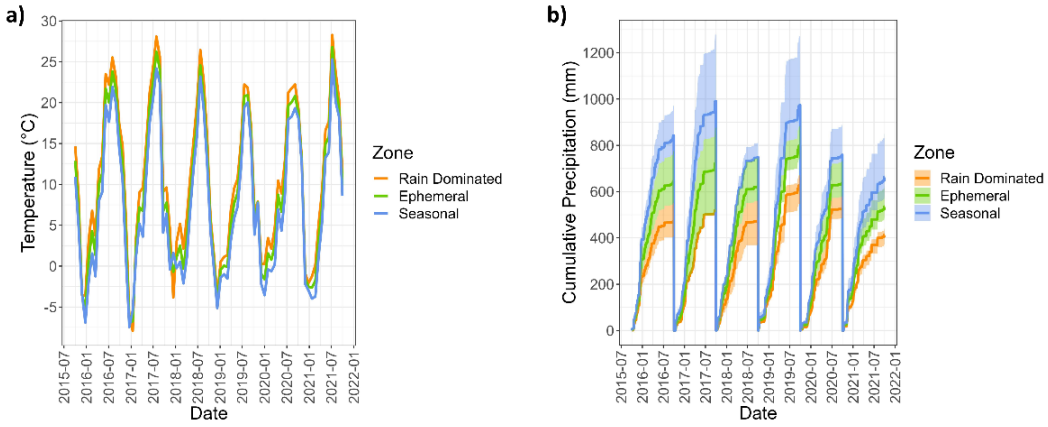

Figure 4.2 Mean daily air temperature in the rain dominated, ephemeral and seasonal zones (a) and mean cumulative precipitation with max and minimum cumulative precipitation in the rain dominated, ephemeral and seasonal zones (b).

Vegetation and soil input data

We used the National Land Cover Database to designate vegetation classes of herbaceous, shrubs, and pine trees. Leaf Area Index (LAI) was measured at multiple point locations in the canopy near the LDP weather station. Following Richardson et al. (2009), we used 2007 LIDAR data to estimate LAI at the watershed scale. The LIDAR

data were used to estimate vegetation height, and following Zhang (1997), empirical relationships were used to estimate the DBH and basal area. We verified the 2007 LIDAR estimated LAI and calculated vegetation fraction with Sentinel 30 m data from the summer of 2021. We used the SNAP – ESA Sentinel Application Platform to calculate LAI and vegetation fraction. Of the watershed area, grasses cover 26.2%, shrubs cover 36.0%, and trees cover 37.9%. Forest LAI was estimated as 2 m^2/m^2 occupying 36% of the surface in forested areas, 5% of the surface in shrub areas, and 2% of the surface in herbaceous areas. Shrub LAI was estimated as 0.8 m^2/m^2 and occupied 30% of the shrub areas and 5% of the surface in both the forested and herbaceous areas. Herbaceous LAI was estimated as 0.1 m^2/m^2 and occupied 30% of the surface in herbaceous areas and 5% in forest and shrub areas. We estimated additional vegetation parameters required by the model using the literature and expert knowledge (Supplemental Table 1).

Soil properties and classes were mapped using SSURGO soil data (Soil Survey Staff). The soil types were aggregated into four classes loam (26.8% of the watershed), sandy loam (58.6% of the watershed), loamy sand (7.3% of the watershed), and bedrock (8.4% of the watershed). Uncalibrated and initial soil parameters were estimated using values from the literature and field data (Supplemental Table 1).

Model Parameterization and Calibration

We used a multi-criteria optimization approach to calibrate the model. The model was calibrated with transpiration, streamflow, soil moisture, and SWE observation data. Transpiration was estimated from a thermal dissipation sap flux measurement in a Doug fir tree located 0.1 km from the LDP weather station. To estimate transpiration from the

sap velocity, we estimated the sapwood area following Mitra et al. (2020) using the DBH of the tree with the sap flux sensors and the average measured DBH of the trees in the area. To calculate SWE at the BR site we used snow density from the Snotel weather station located at 0.7 km distance and 173 m lower elevation from the BR site combined with the BR snow depth to calculate SWE. Previous research in the watershed found snow density was not as spatially variable as snow depth (Anderson et al., 2014). Both the BR and Snotel weather stations are located in similar vegetation covers and relatively similar elevations. Thus, the assumption that snow density is the same at the BR weather station is reasonable. Soil moisture was measured at the LDP weather station using Campbell Scientific CS616 Water Content Reflectometers at 8 cm soil depth. Last, observed streamflow was from the LG station at the watershed outlet. The model was calibrated at a daily timestep from WY2016 – WY2019 and validated during WY2020 and WY2021. The calibration period was chosen based on a combination of wet and dry years and data availability for calibration. Sap flux data was only available for WY2016 and WY2017. Previous research with the Ech$_2$o model found that transpiration data was necessary for the simulation of transpiration. Therefore, we included the transpiration field measurements in the calibration (Kuppel *et al.*, 2018). We used the KGE (Equations 1-3) goodness-of-fit metric for each observation simulation pair for each simulation.

$$KGE = 1 - \sqrt{(r-1)^2 + (\beta-1)^2 + (\alpha-1)^2} \quad \text{Equation 1}$$

$$\beta = \frac{\mu_s}{\mu_o} \quad \text{Equation 2}$$

$$\alpha = \frac{CV_s}{CV_o} \quad \text{Equation 3}$$

where r is the Pearson correlation coefficient, μ is the average, CV is the coefficient of variation for the simulated (s) and observed (o) data. The KGE efficiency was selected as the GOF metric because it combines bias, correlation, and variability into a single equation and is widely used in hydrologic model calibration (Gupta *et al.*, 2009). We combined the GOF from each observation and simulation pair into a single objective function (equation 4).

$$Obj = \left(1 - KGE_Q\right) + (1 - KGE_T) + (1 - KGE_{SM}) + (1 - KGE_{SWE}) \quad \text{Equation 4}$$

where the subscript Q is streamflow, T is transpiration, SM is soil moisture and SWE is the snow water equivalent. The objective function (Obj) was minimized using the Dynamically Dimensioned Search (DDS) algorithm to find an optimum parameter set. The DDS algorithm is robust for calibrating many parameters and avoids a locally optimal solution (Tolson and Shoemaker, 2007).

Snow Zone Classification

We split the basin into categories of rain, ephemeral and seasonal snow zones in each water year. Annual snow zones were defined as rain dominated if bias-adjusted peak snow water equivalent (SWE) was less than 0.14 m, ephemeral snowpack between 0.14 and 0.37 m, and seasonal snowpack above 0.365 m peak SWE. Based on Sturm and Liston (2021) classification categories, we defined the upper bound of the ephemeral zone as 1 m peak snow depth. The model outputs values of SWE rather than snow depth, thus estimated peak snow depth from SWE using a mean density of 365 kg/m^3 from 2016-2021 at the peak snow depth. We calculated the annual peak SWE percent bias between the modeled data and BR SWE and used the annual bias to adjust the upper bound and lower bounds of the ephemeral zone. The lower bound was established so a

single snow storm period would not shift the ephemeral snow zone. The snow zone was set at 0.14 m SWE based on the LW station, where the peak snow accumulation during a 12-day storm period was 39 cm snow depth (2/3/2021 – 2/15/2021), and we assumed a density of 365 kg/m^3 during this period.

Sensitivity analysis

To evaluate how changes in the rain-snow transition will affect ET, we increased temperatures during the potential snow cover season from October through June (8-month scenario) and by individual months in November, December, March, and April. Our goal was to isolate changes in the fall and spring to understand how changes in the seasonal periods will impact hydrologic processes. Climate perturbations were designed by evaluating the mean annual projected surface air temperature under the SSP2-4.5 scenario in the IPCC report (Iturbide et al., 2021). The SSP2-4.5 scenario is an intermediate GHG emission scenario and is considered realistic if action is taken to curb emissions. To represent near-time conditions of climate change, the sensitivity experiments were conducted by increasing historical air temperatures by 2°C in five different scenarios between WY2016 and WY2021. Last, the no change in air temperature scenario represents the historical average base case scenario. In total, we evaluated six model runs and compared the 8 month, November, December, March, and April scenarios to the base case.

Results

Calibration results

The calibration process achieved an average calibration period KGE of 0.80 with values ranging between 0.74 and 0.87 between observation and simulation pairs

(Supplemental Table 2). The modeled SWE follows the observed SWE at BR but modeled peak SWE is biased low (average -13%) and the snow disappearance timing is on average days 24 days later compared to the observed (Fig. 4.3). The modeled streamflow correctly simulates the timing of fall and summer streamflow, but the timing of peak streamflow and the spring declining limb tend to occur later than the observed values (Fig. 4.3). The later snow disappearance timing may contribute to the later peak streamflow timing, however, there are likely other contributing factors because streamflow is an amalgamation of modeled hydrologic processes. The model correctly captures transpiration timing and magnitude through the summer season. Soil moisture is biased low during the winter months, tends to over predict the peaks during the summer period, and is flashier compared to the observed soil moisture. However, overall, the model captures the timing and magnitude of soil moisture at the LDP site and TL sites.

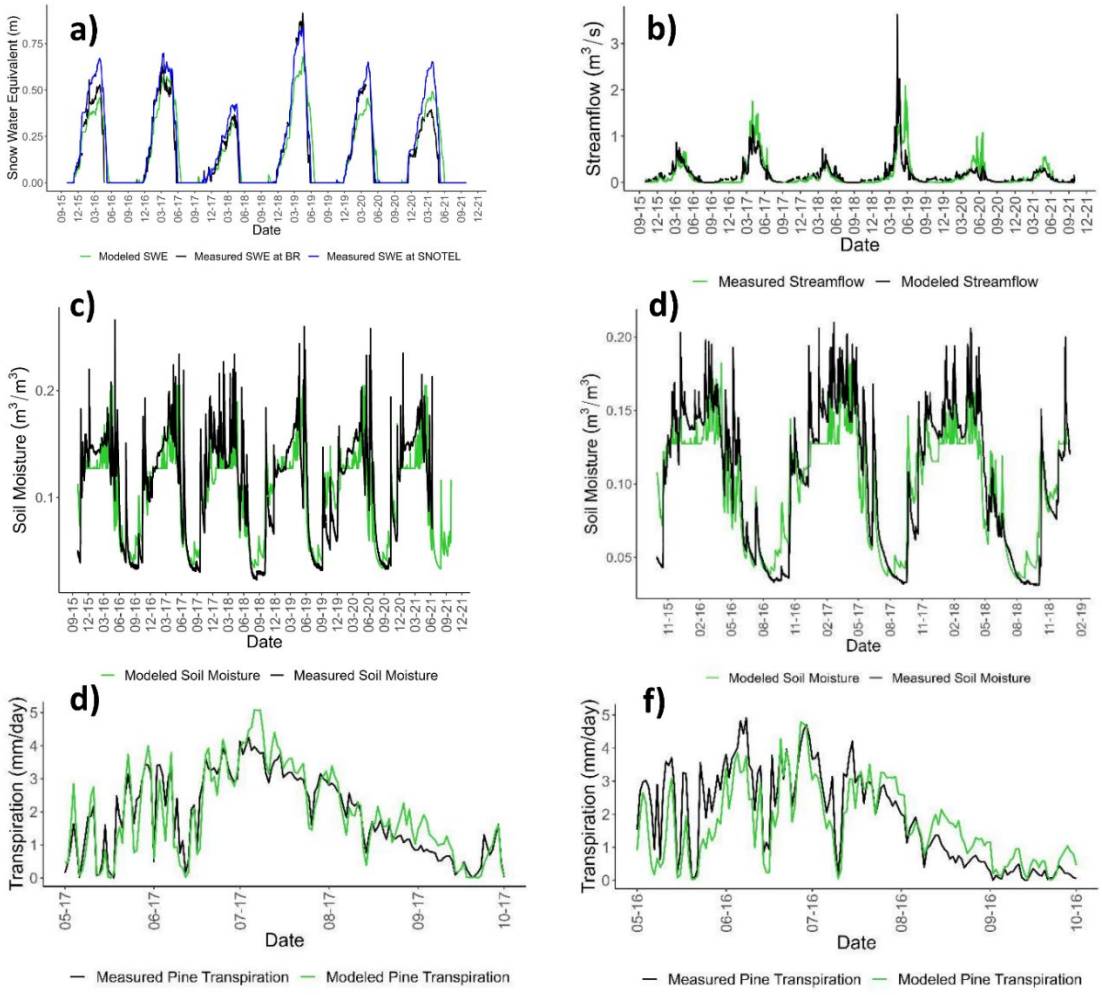

Figure 4.3 Modeled snow water equivalent (SWE) and estimated SWE at BR and measured SWE at the Snotel (a). Modeled streamflow and measured streamflow at the watershed outlet (LG) (b). Modeled layer 1 soil moisture with measured soil moisture at 8cm depth at the LDP site (c). Modeled soil moisture and measured soil moisture at 5cm depth at the TL site (d). Modeled transpiration and measured sap flux transpiration in a Doug Fir tree (d) and (f).

Changes to Rain/Snow phase and zone

We calculated the difference between the change in snow zone areas and precipitation phase between the base case and 8-months scenario (Fig. 4.4). On average, the fraction of area in the rain dominated zone increased by 28% while the ephemeral zone decreased by 17% and the seasonal zone decreased by 10% (Fig. 4.4 b, c, d). The fraction of precipitation phase as snow decreased in all zones with the largest decrease in

the seasonal snow zone of 16% and an average basin wide decrease of 14% (Fig. 4.4a). We did not calculate the difference in rain dominated zone for the other scenarios because peak SWE did not change in all the other scenarios, and the goal was to evaluate the changes within these currently established zones rather than the combined effects.

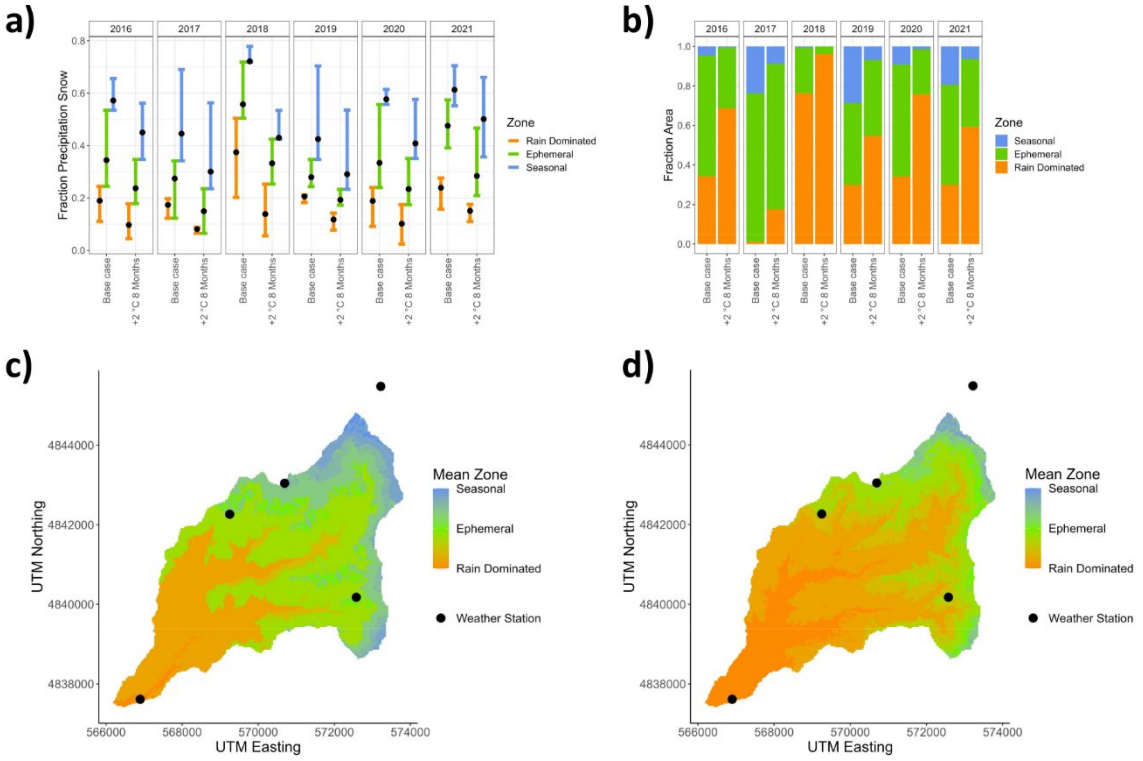

Figure 4.4 The fraction of precipitation as snow in each zone in the base case and 8-month scenarios (a). The fraction area of each zone in the base case and 8-month scenarios for each year (b). Figures (c) and (d) are the mean zones for the base case and 8-month scenario with the weather stations (black dots).

Annual water balance

Annual water balance response to warming

The average annual watershed ET change in the 8-month scenario was 8.03% while the average annual change in streamflow was -14.13% (Table 4.1). Streamflow in the 8-month scenario compared to the base case tended to be higher in the fall and mid-winter and lower in the spring (Fig. 4.5). Similarly, in the March and April scenarios

streamflow began increasing in their respective months of temperatures increase (Fig. 4.5). Streamflow peaked at similar levels to the base case, but the streamflow recession started earlier than the base case scenario. The peak SWE declined in all scenarios with the 8-month scenario having the greatest average change in peak SWE of 37.34% followed by the December scenario with an average change of 9.4%. On average, the snow disappeared four days earlier in December, March, and April scenarios and one day earlier in the November scenario (Table 4.2). Within the individual month scenarios, the April scenario had the greatest mean annual change in ET of 2.49%, while the December scenario had the greatest change in streamflow of -4.93%. Increasing temperatures in December resulted in a decrease in average peak SWE of 9.4% but annual ET in the December scenario on average increased only 0.53%.

Table 4.1 Annual mean watershed evapotranspiration (ET), streamflow (Q) and peak snow water equivalent (SWE) in each scenario and the percent change from base case in each scenario. The standard deviation represents the range between years.

	ET (mm)	Q (mm)	Peak SWE (cm)
	Mean ± STD	Mean ± STD	Mean ± STD
Base Case	343.0 ± 15.54	190.20 ± 96.13	183.19 ± 120.43
+2°C 8-Months	313.34 ± 15.62	165.81 ± 91.98	114.78 ± 94.67
+2°C April	349.53 ± 16.31	190.22 ± 96.23	182.67 ± 118.94
+2°C March	350.36 ± 16.56	189.75 ± 2.19	177.59 ± 115.33
+2°C December	347.10 ± 16.26	181.89 ± 95.22	165.98 ± 117.87
+2°C November	347.60 ± 16.23	186.16 ± 91.98	176.46 ± 117.09
% Change +2°C 8-Months	8.03 ± 0.51	-14.13 ± 6.00	-37.34 ± 21.93
% Change +2°C April	1.91 ± 4.95	0.03 ± 0.81	-0.29 ± 2.39
% Change +2°C March	2.15 ± 6.57	-0.20 ± 1.37	-0.43 ± 2.90
% Change +2°C December	1.20 ± 4.66	-4.93 ± 2.13	-9.40 ± 6.45
% Change +2°C November	1.34 ± 4.48	-2.67 ± 2.55	-3.68 ± 5.21

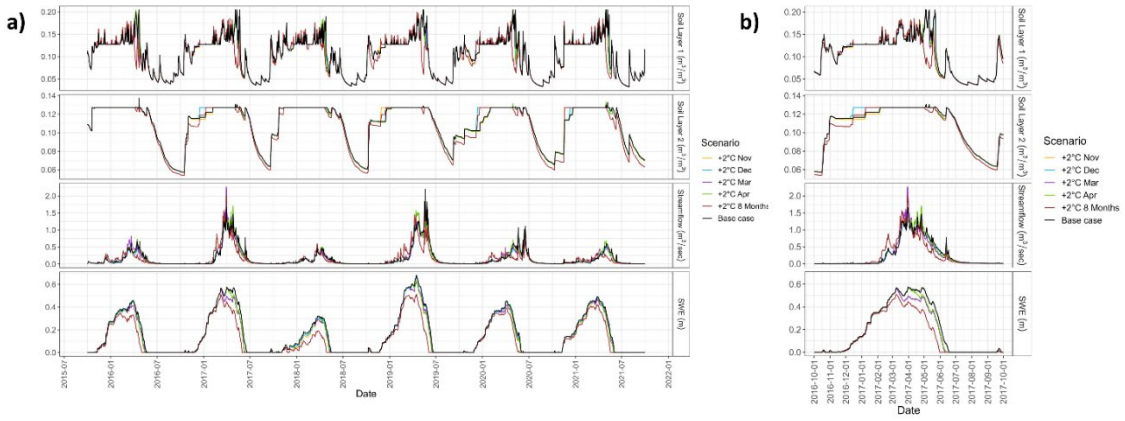

Figure 4.5 Model run output for each scenario at point locations used in the model calibration for all years (a) and WY2017 (b) to help see the differences between model runs. The soil layers 1 and 2 are near the LDP weather station, the streamflow is at LG near the outlet of the watershed and the SWE is in the top elevation band of the model boundary closest to the BR weather station.

Table 4.2 Mean day of snowmelt for each scenario, zone and landcover.

Zone	base	+2°C 8-Months	+2°C April	+2°C March	+2°C December	+2°C November
Rain Dominated	59	20	58	57	52	59
Ephemeral	115	81	111	109	112	114
Seasonal	145	125	139	140	144	144
Herbaceous	72	37	70	69	67	72
Shrub	106	72	102	101	102	105
Tree	112	78	108	106	107	111

The greatest change in annual ET occurred in the seasonal snow zone with a mean annual ET change of 16.42% in WY2020 (Fig. 4.6) and an average annual change of 12.75% in the 8-month scenario. The April and November scenarios also increased the greatest in the seasonal zone with an average annual change of 2.54% and 1.39%. Annual ET in the March scenario increased the most in the ephemeral dominated zone except for WY2016 and WY2020 but on average increased 1.79% and 1.86% in the rain and ephemeral zones and 1.50% in the seasonal zone. The December scenario had the lowest change in ET values in all zones with average ET changes of 0.89%, 0.76%, and 0.66% in the rain, ephemeral and seasonal zone. In all scenarios snow melted earlier. The 8-month scenario had the greatest difference of 39 days earlier in the rain dominated zone, 35 days earlier in the ephemeral zone, and 20 days earlier in the seasonal snow zone. In the single month scenarios, the December scenario had the greatest change in melt timing in the rain zone of 7 days.

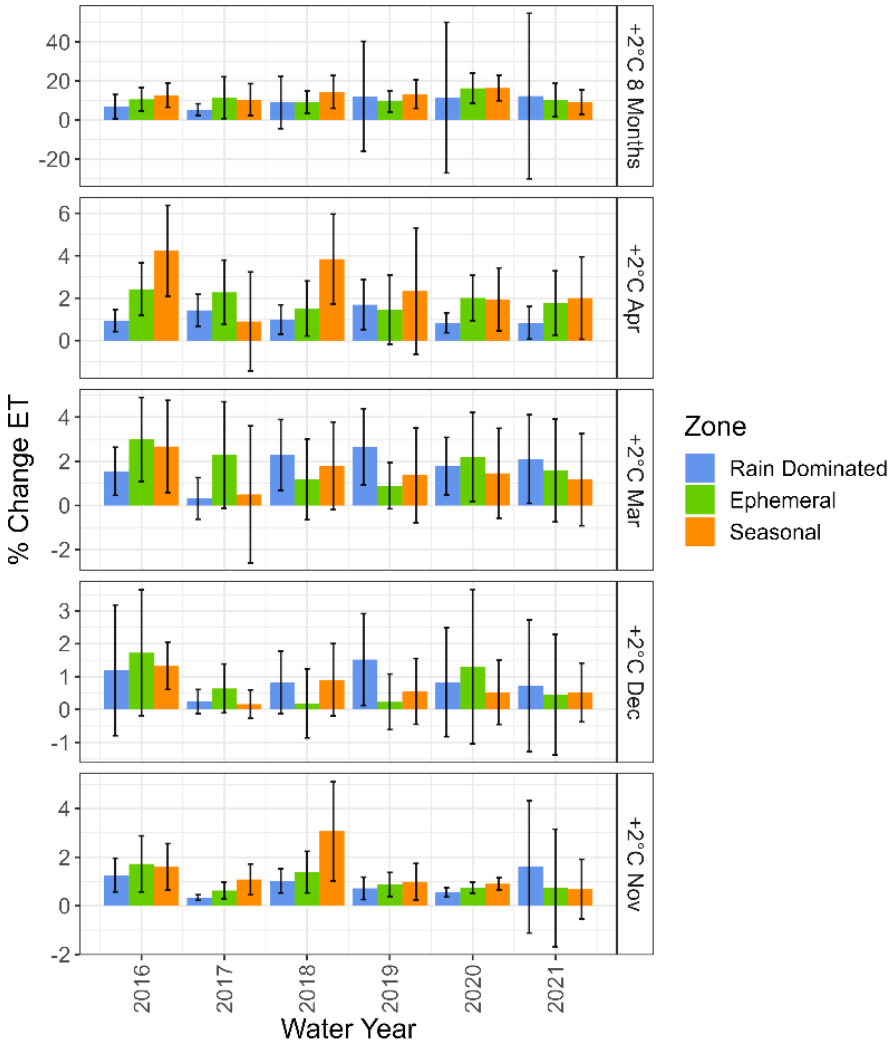

Figure 4.6 Mean percent change ET from the base case with +- one standard deviation error bars for all years and scenarios in each zone.

Water balance ratios

At the watershed scale, the largest change in Q/P (Q is the streamflow and P is precipitation), E/P (E is evaporation), and T/P (T is transpiration) was in WY2020 of -6.32% (Q/P), 4.68% (E/P) and 1.18% (T/P) (Figure 4.7a). Consistently in each scenario, Q/P decreased while E/P and T/P increased. The changes between Q/P, E/P, and T/P did not cancel, rather the GW storage component fluctuated to account for the differences. For example, in WY2019 in the 8-month scenario, ET/P increased by 3.2%, and Q/P

decreased by 4.3% leaving an additional 1.1% of groundwater storage. Interannually, T/P and E/P ratio and the wettest year were in WY2019. There was a negative trend in mean annual ET/P and snow disappearance with an average ET/P increase of 2% per 10-day earlier snow disappearance (Fig. 4.8a). WY2018 had the lowest Q/P ratio, and the highest E/P ratio, and of note, WY2018 also had the highest mean average winter temperatures (Fig. 4.7a) and lowest peak SWE (Fig. 4.5). On average, the highest T/P ratio in all scenarios was in WY2021 while the lowest

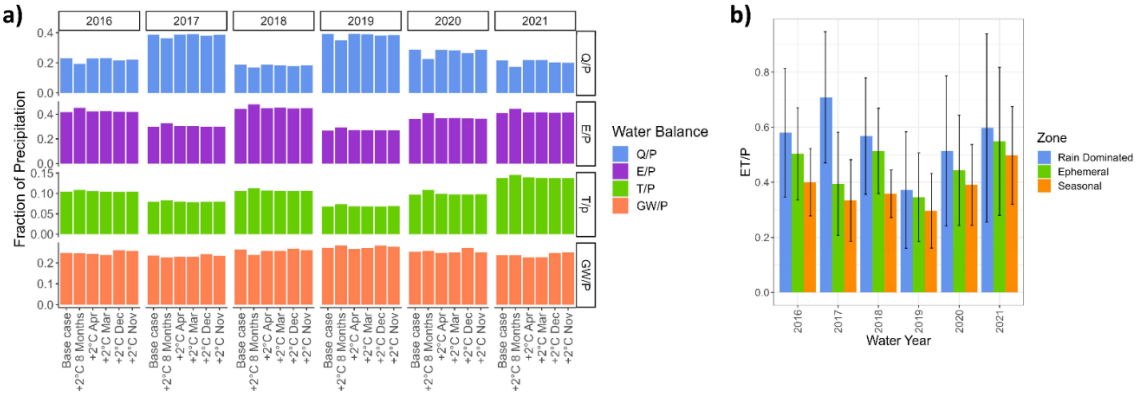

Figure 4.7 Ratios of watershed water year total streamflow (Q), evaporation (E), transpiration (T) and groundwater (GW) with precipitation (P) for each year and scenario (a). Base case scenario ratio of mean water year evapotranspiration (ET) and precipitation (P) with +- one standard deviation error bars in the rain dominated, ephemeral, and seasonal zones.

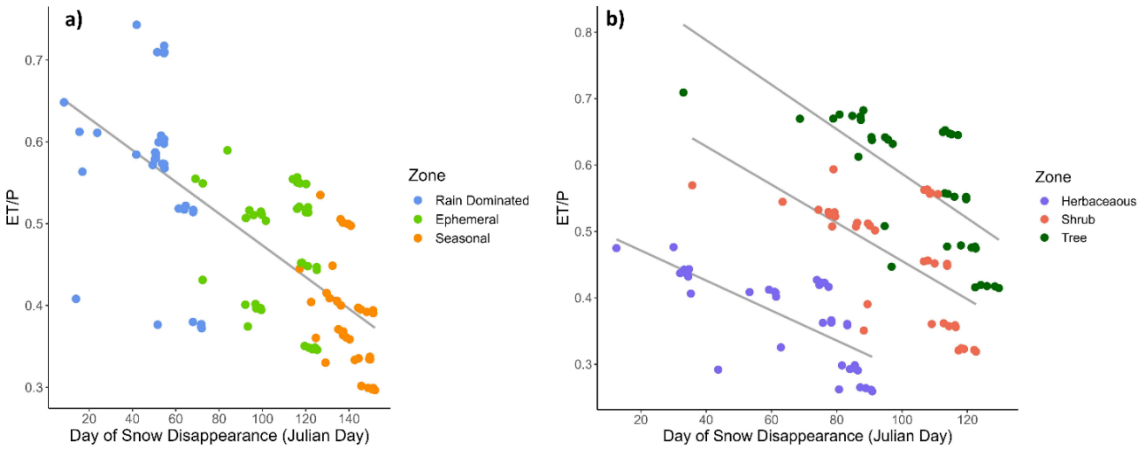

Figure 4.8 Mean day of snow disappearance versus ET/P ratio for each year and scenario colored in the rain dominated, ephemeral, and seasonal snow zones (a). Mean day of snow disappearance versus ET/P ratio for each year and scenario in the herbaceous, shrub, and tree landcover types (b).

The mean ET/P ratio varied between zones with the highest ET/P ratios in the rain dominated zone and the lowest ET/P ratios in the seasonal zone (Fig. 4.7b). Splitting the E and T, the highest mean fraction of E/P and T/P was in the rain dominated zone (0.11 and 0.45) and the greatest increase from the base case was in the E/P component in the rain dominated zone (3.5% increase in the 8-month scenario). The highest ET/P ratio for the ephemeral and seasonal snow zones was in WY2021 which was also the lowest water year cumulative precipitation while the highest ET/P ratio in the rain dominated zone was in WY2017. In all zones and consistent with the watershed averages, the lowest ET/P ratio was in WY2019.

Mean ET/P varied between landcover types with the greatest ET/P ratios in the tree dominated landcover followed by the shrub and herbaceous land covers (Fig. 4.8b). Both the T/P and E/P tended to be highest in the tree landcover. The greatest change was in the E/P component in the herbaceous landcover type (3.6% 8-month scenario) while the T/P component increased the most in the tree zone in the 8-month scenario (0.72%). Mean annual ET/P ratios in each landcover type were negatively correlated with snow the

snow disappearance date. The tree landcover type had the steepest slope with a 3% increase in ET/P for each 10 day earlier snow disappearance.

Daily ET

The seasonal zone had the highest mean daily ET rate of (2.3 - 2.4 mm/day in June) in all scenarios followed by the ephemeral zone in June (1.97 - 2.03 mm/day). The daily ET rates increased the most in all years and months in the 8-month scenario (Figure 4.9). In general, median daily ET rates increased early in the water year and spring but were lower compared to the base case scenario starting in June or July except for WY2020 and WY2021, in the November and 8-month scenario rain zone. The 8-month scenario had the lowest median decline in ET rates in the seasonal zone of -10.92% in September, and on average the median daily ET rate declined -3.34% in August and 3.2% in September in the seasonal zone. March and April scenarios exhibited the most distinct boom and bust cycle with the highest median ET rate increase of 25.18% in the April scenario seasonal zone and 32.84% in the March scenario in the rain zone during the month's respective increase in temperatures. The increase in daily ET rates in April and March scenarios were followed by the greatest decline or bust in median daily ET rate of -4.11% and -5.20% in July in the seasonal snow zone.

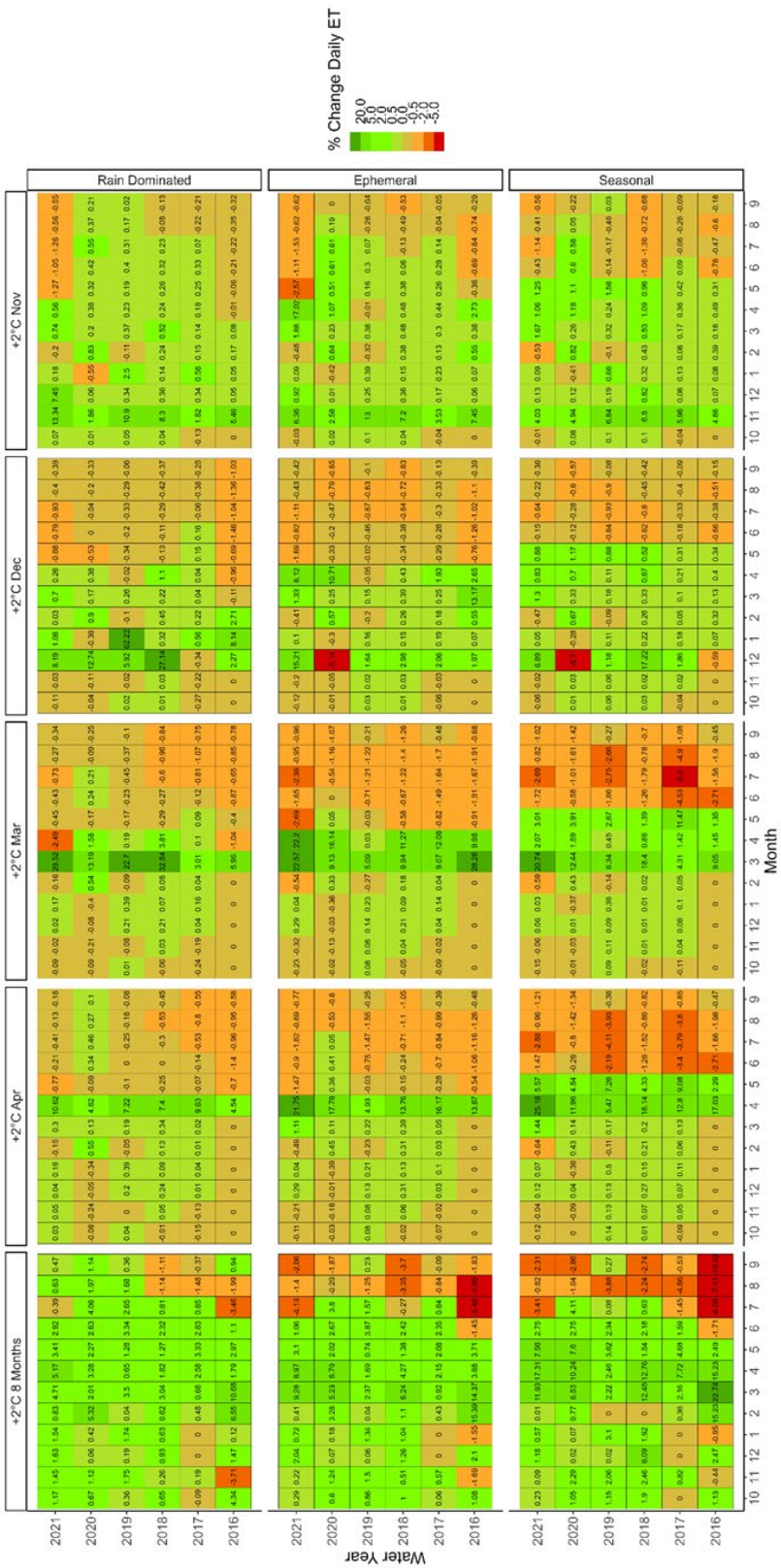

Figure 4.9 Median monthly change from the base case in daily ET rates for each zone and scenario in each model year.

On the monthly scale, daily average median ET rates increased the greatest during April in the seasonal snow zone in the 8-month scenario and April scenario by 10.95% and 15.10%. The March, December, and November scenarios resulted in the greatest increase in average median daily ET rates in the rain dominated zone by 17.87% in March (March scenario), 21.13% in January (December scenario), and 6.95% in November (November scenario). Interannually, the greatest average median daily ET rate increase was in WY2021 in the April scenario seasonal zone, March ephemeral zone, November ephemeral zone, and December rain zone.

Discussion

Climate change sensitivity of ET across the rain-snow transition

The sensitivity of ET to warming suggests that earlier snow disappearance timing will increase ET and reduce streamflow but is sensitive to the timing of warmer temperatures and the precipitation phase. The effect of warmer temperatures depended on the synchrony with energy drivers for ET and snow disappearance initiating the peak soil moisture availability. Increased temperatures early in the fall season led to the lowest change in annual ET compared to the other scenarios because increased temperatures coincided with lower incoming shortwave radiation limiting the energy for ET. The warmer fall temperatures changed the phase of early season precipitation from snow to rain reducing the snow accumulation and water availability for streamflow the following spring. Rain precipitation refilled depleted groundwater stores, increased soil water storage, and increased fall streamflow but lowered spring streamflow. Warmer temperatures in the spring months increased the snowmelt rate shifting snow disappearance earlier in the season and increasing the daily ET rate due to more intense

energy inputs coinciding with peak soil moisture. The total volume of annual streamflow was relatively consistent between the single month scenarios, but the timing of streamflow changed with a higher and earlier peak and earlier start of streamflow recession. The combined effects of increasing temperatures in the fall, winter, and spring merge to reduce annual streamflow due to a combination of increased water used for ET, higher fall streamflow, and less snow accumulation.

The effects of warming in a single month propagated into the following months. Initially, when temperatures were higher, daily ET rates increased but, following the high ET rates, daily ET dropped below the base case in the summer season. Following the summer decline in daily ET rates, fall precipitation replenished soil moisture, and daily ET rates returned to near the base case scenario. At snow disappearance, the soil moisture did not differ between years or scenarios indicating the soil moisture was not limiting the ET rates early in the season. The earlier snow disappearance, due to increased temperatures or reduced snow accumulation led to an earlier soil moisture drawdown and soil moisture limitations later in the summer season. Although, soil moisture limitations were likely not the only limiting variable. Increased temperatures in the 8-month scenario led to the greatest soil moisture drawdown and increased ET/P ratios. The difference is also evident between years with 2021 having the highest June and July average temperatures (23.6°C compared to the multi-year average of 20.1°C). Following snow disappearance, the high early season temperatures combined with water availability resulted in more intense and greater ET rates. The increased temperatures result in both more intense high and low ET rates due to soil moisture limitations.

Warmer temperatures will have the greatest effect on ET in forests and high elevation, seasonal snowpacks. Within forest landcover, ET/P increases at a greater rate with earlier snow disappearance as temperatures warm compared to open landcover types (shrubs and herbaceous). Similarly, the seasonal snowpack had the greatest change in annual ET but the smallest mean change in snow disappearance timing (-20 days) in the 8-month scenario and therefore, the highest rate of increased annual ET per day earlier snow disappearance. Both the seasonal snowpack and forest landcover had the latest snowmelt timing. In these zones, snow disappearance tends to occur when temperatures and shortwave radiation are high, increasing the energy for ET and an earlier snow disappearance extends the period ET is occurring. Previous research in Dry Creek found forests shaded the snow surface resulting in later snowmelt timing (Kraft et al., in Review), and middle and high elevation ET was limited by growing season length (Kraft and McNamara, 2022). These findings support the previous research in Dry Creek, finding increased ET in warm years and tree cover prolonging the snow cover season. This research builds on the previous findings by combining the link between snow disappearance timing and ET in forest cover. The forest cover buffers the snow disappearance timing synchronizing the soil moisture availability and increasing energy for ET. The sensitivity of ET in these zones to earlier snow disappearance suggests that increasing the warm season length will increase ET disproportionately in the tree and seasonal snow covered areas.

Assumptions and Limitations

The results presented are limited by the modeling approach and assumptions within the model framework. For instance, the model uses a one-layer snow model with

an empirical snowmelt coefficient when the snowpack cold content reaches 0°C. Previous research in the watershed found snowmelt rates varied by landcover and aspect (Anderson *et al.*, 2014; Kormos *et al.*, 2014). While the model does account for spatially variable energy input prior to the snowpack reaching an isothermal state, applying a uniform snowmelt rate resulted in underestimating snowmelt rates in the open. The underestimate snowmelt rate likely occurred to account for the slower snowmelt in the forest. Additionally, there are uncertainties due to the meteorological forcing data. The sensors are regularly maintained but there are missing data periods due to battery failure and sensor malfunctions. The transpiration observation was based on one tree and an empirical relationship to estimate basal area.

Summary and Conclusion

This study used a modeling framework to assess the sensitivity of ET and streamflow to warming temperatures across the rain-snow transition in a semiarid watershed. Warmer temperatures will shift snow disappearance timing earlier, resulting in increased annual ET, and decreased streamflow. However, the seasonal timing of warmer temperatures is important for the synchrony of energy and soil moisture. The ET rates were less sensitive to warming fall temperatures because of low overall energy for ET during the fall months. Warmer fall temperatures shift the precipitation from snow to rain, increasing fall streamflow, reducing the early season snow accumulation and peak SWE, and therefore reducing the snow mass to melt and the snow water available for spring ET and streamflow. The earlier snowmelt extended the growing season length resulting in increased annual ET. Warming temperatures in the spring, increased the snowmelt rate, therefore, shifting the snow disappearance timing earlier and streamflow

timing earlier. The warmer spring temperatures were synchronized with the ET energy demand and soil moisture availability resulting in increased ET in the spring. Across the rain-snow transition ET rates in the forest, and seasonal snow zones were the most sensitive to increased temperatures because of the tendency for later snow disappearance timing and synchrony with soil water availability and increased energy for ET. However, increased ET early in the spring came as a tradeoff with lower late summer soil water availability and reduced ET rates.

The results of this study suggest the shift in the rain-snow transition to a more rain dominated and ephemeral snow regime will vary by landcover type and across elevations. Changes in landcover due to forest fires or vegetation succession will alter the snowmelt timing and consequentially how water is partitioned between ET and streamflow. Our results indicate in all vegetation types, increased temperatures will result in increased ET. However, decreasing forest cover potentially results in a greater fraction of water input towards streamflow compared to ET. The sensitivities observed in this study likely exist in other semiarid regions and watersheds spanning the rain-snow transition. Future work will address the origin of vegetation water use to more explicitly understand where, and when vegetation uses snow water. The modeling scenarios presented develop the understanding of how changes in temperature timing will affect hydrologic processes in complex semiarid montane regions spanning the rain-snow transition.

CHAPTER FIVE: CONCLUSIONS

This dissertation advances research in analyzing snow and vegetation interactions in a semiarid mountain climate. This was achieved using field data at point locations in two different watersheds and using a hydrologic model in a watershed spanning the rain-snow transition. We evaluated how vegetation affects the distribution of snow, how snow and climate impact ET, and how warming temperatures will affect ET and streamflow across the rain-snow transition.

Chapter 2 of this dissertation evaluated what processes control snowmelt timing and magnitude at two paired forested and open sites in semiarid southern Idaho, USA. Snow accumulation, snowmelt, and snow energy balance components were measured at low elevation and high elevation locations in forests, sparse vegetation, forest edge, and open environments. At both locations, the snow disappeared either later in the forest or spatially relatively uniformly in the open and forest. At the upper elevation location, a later peak in maximum snow depth resulted in more variable snow disappearance timing between the open and forest sites with later snow disappearance in the forest. The low elevation location was controlled by the magnitude and duration of a late season storm increasing snow depth variability and reducing the shortwave radiation energy input. Here, a shorter duration spring storm resulted in more uniform snowmelt in the forest and open. At both locations, the low-density forests shaded the snow surface into the melt period slowing the melt rate in the forest. However, the forest site had less cold content to overcome before melting started, partially canceling out the forest shading effect.

Chapter 3 of this dissertation estimates actual ET at five sites across an elevational gradient in the Dry Creek Watershed in southern Idaho, USA. We compare annual and daily ET estimates to climate parameters of soil moisture, snow cover, precipitation, air temperature, and vapor pressure deficit. We observed three trends in ET with climate parameters. The first trend is at the low elevation site where the snow cover is not continuous throughout the winter and rain is the dominant precipitation form. The first day of the growing season and ET occurs early in the season when the energy demand is low and soil water is available. Annual ET at the low elevation site is a balance between spring precipitation providing soil water into the summer season and limiting the ET energy demand. The second trend occurs at the middle elevation site located in the rain-snow transition. At this site, ET increases with snow depth and spring precipitation extending the soil water availability into the summer season. At the higher elevation sites, ET is aligned with the energy demand and is limited by growing season length. At the high elevation sites, decreasing snow depth and spring precipitation and increasing spring air temperatures result in greater annual ET rates.

Chapter 4 of this dissertation applied the physically based EcH_2O model to the Dry Creek Watershed in southern Idaho, USA which spans the rain-snow transition. We perturbed observed air temperatures by 2°C in different months to explore how the seasonal variability of warming temperatures will affect SWE, ET, and streamflow. We found that warming temperatures in the fall decreased the peak SWE and therefore shifted the snowmelt timing and streamflow earlier in the spring. There was a limited increase in ET rates because warming temperatures were not synchronized with soil moisture and other energy drivers. Warming temperatures in the spring shifted the

snowmelt earlier, streamflow timing earlier and ET rates increased. Higher temperatures in the spring resulted in synchronized soil moisture availability and energy drivers. However, the higher ET rates in the spring reduced soil moisture availability and therefore water availability later in the summer season. Across the rain-snow transition, ET rates were the most sensitive in the forest and seasonal zones because of the relatively late snow disappearance aligning soil moisture and energy drivers.

Future work is needed to investigate how snowmelt heterogeneity affects snow water input and soil moisture availability for vegetation. In chapter 2 we established that snow melts later in the forest and in chapter 3 we found elevations with later snowmelt have more higher ET rates. Chapter 4 showed that warming temperatures will shift the snowmelt timing earlier and decrease late summer ET rates due to low soil water availability and zones with late snowmelt timing are more sensitive to warming. Given these findings, future work could involve additional analysis looking at small scale (~1m) effects of vegetation structure on snowmelt timing in parallel with soil moisture. The small scale snowmelt heterogeneity and lingering patches of snow may become an increasingly important vegetation water supply for late season ET. Additional future research could use the EcH_2O model isotope module to better understand what water stores vegetation is using. This would support the understanding of how precipitation phase changes will affect deep groundwater storage.

Data Availability

All data presented in this dissertation can be found in online repositories. The repositories can be found below: https://www.boisestate.edu/drycreek/dry-creek-data/; https://www.boisestate.edu/drycreek/dry-creek-data/;

https://github.com/MaggiK/ECH2O_calibration;

https://www.hydroshare.org/resource/39cf58935f944f10b98baad07368449d/;

https://www.hydroshare.org/resource/20d6db6ff9064928803528dcb317dfad/

REFERENCES

Aishlin P, McNamara JP. 2011. Bedrock infiltration and mountain block recharge accounting using chloride mass balance. *Hydrological Processes* **25** (12): 1934–1948 DOI: 10.1002/hyp.7950

Anderson BT, McNamara JP, Marshall HP, Flores AN. 2014. Insights into the physical processes controlling correlations between snow distribution and terrain properties. *Water Resources Research* **50**: 5375–5377 DOI: 10.1002/2013WR014979.Reply

Andreadis KM, Storck P, Lettenmaier DP. 2009. Modeling snow accumulation and ablation processes in forested environments. *Water Resources Research* **45** (5) DOI: 10.1029/2008WR007042

Badger AM, Bjarke N, Molotch NP, Livneh B. 2021. *The sensitivity of runoff generation to spatial snowpack uniformity in an alpine watershed: Green Lakes Valley, Niwot Ridge Long Term Ecological Research Station*. DOI: 10.1002/hyp.14331

Bales RC, Hopmans JW, O'Geen AT, Meadows M, Hartsough PC, Kirchner P, Hunsaker CT, Beaudette D. 2011. Soil moisture response to snowmelt and rainfall in a sierra nevada mixed-conifer forest. *Vadose Zone Journal* **10** (3): 786–799 DOI: 10.2136/vzj2011.0001

Barnard DM, Barnard HR, Molotch NP. 2017. Topoclimate effects on growing season length and montane conifer growth in complex terrain. *Environmental Research Letters* **12**

Bilish S, Callow J, McGrath G, McGowan H. 2019. Spatial controls on the distribution and dynamics of a marginal snowpack in the Australian Alps. *Hydrological Processes* Available at: https://ejournal3.undip.ac.id/index.php/jamt/article/view/5101

Bowling DR, Logan BA, Hufkens K, Aubrecht DM, Richardson AD, Burns SP, Anderegg WRL, Blanken PD, Eiriksson DP. 2018. Limitations to winter and spring photosynthesis of a Rocky Mountain subalpine forest. *Agricultural and Forest Meteorology* **252** (December 2017): 241–255 DOI: 10.1016/j.agrformet.2018.01.025

Breiman L. 1984. *Classification and Regression Trees*. Routledge, New York.

Brown TC, Hobbins MT, Ramirez JA. 2008. Spatial Distribution of Water Supply in the Conterminous United States. *Journal of the American Water Resources Association (JAWRA)* **44** (6) DOI: 10.1111/j.1752-1688.2008.00252.x

Broxton PD, Harpold AA, Biederman JA, Troch PA, Molotch NP, Brooks PD. 2015. Quantifying the effects of vegetation structure on snow accumulation and ablation in mixed-conifer forests. *Ecohydrology* **8** (6): 1073–1094 DOI: 10.1002/eco.1565

Broxton PD, Moeser CD, Harpold A. 2021. Accounting for fine-scale forest structure is necessary to model snowpack mass and energy budgets in montane forests. *Water Resources Research* **57** (12) DOI: 10.1029/2021wr029716

Burles K, Boon S. 2011. Snowmelt energy balance in a burned forest plot, Crowsnest Pass, Alberta, Canada. *Hydrological Processes* **25** (19): 3012–3029 DOI: 10.1002/hyp.8067

Christensen L, Tague CL, Baron JS. 2008. Spatial patterns of simulated transpiration response to climate variability in a snow dominated mountain ecosystem. *Hydrological Processes* **22** (18): 3576–3588 DOI: 10.1002/hyp.6961

Church JE. 1933. Snow Surveying: Its Principles and Possibilities. *Geographical Review* **23** (4): 529–563

Cooper AE, Kirchner JW, Wolf S, Lombardozzi DL, Sullivan BW, Tyler SW, Harpold AA. 2020. Snowmelt causes different limitations on transpiration in a Sierra Nevada conifer forest. *Agricultural and Forest Meteorology* **291**: 108089 DOI: 10.1016/j.agrformet.2020.108089

Cox PM, Huntingford C, Harding RJ. 1998. A canopy conductance and photosynthesis model for use in a GCM land surface scheme. *Journal of Hydrology* **212–213** (1–4): 79–94 DOI: 10.1016/S0022-1694(98)00203-0

Cui G, Bales R, Rice R, Anderson M, Avanzi F, Hartsough P, Conklin M. 2020. Detecting rain-snow-transition elevations in mountain basins using wireless-sensor networks. *Journal of Hydrometeorology*

Currier WR, Lundquist JD. 2018. Snow Depth Variability at the Forest Edge in Multiple Climates in the Western United States. *Water Resources Research* **54** (11): 8756–8773 DOI: 10.1029/2018WR022553

DeBeer CM, Pomeroy JW. 2017. Influence of snowpack and melt energy heterogeneity on snow cover depletion and snowmelt runoff simulation in a cold mountain environment. *Journal of Hydrology* **553**: 199–213 DOI: 10.1016/j.jhydrol.2017.07.051

Dickerson-Lange SE, Gersonde RF, Hubbart JA, Link TE, Nolin AW, Perry GH, Roth TR, Wayand NE, Lundquist JD. 2017. Snow disappearance timing is dominated by forest effects on snow accumulation in warm winter climates of the Pacific Northwest, United States. *Hydrological Processes* **31** (10): 1846–1862 DOI: 10.1002/hyp.11144

Dickerson-Lange SE, Lutz JA, Gersonde R, Martin KA, Forsyth JE, Lundquist JD. 2015. Observations of distributed snow depth and snow duration within diverse forest structures in a maritime mountain watershed. *Water Resources Research* **51** (11): 9353–9366 DOI: 10.1002/2015WR017873

Dickerson-Lange SE, Vano JA, Gersonde R, Lundquist JD. 2021. Ranking Forest Effects on Snow Storage: A Decision Tool for Forest Management. *Water Resources Research* **57** (10) DOI: 10.1029/2020WR027926

Dickerson-Lange SE, Vano JA, Gersonde R, Lundquist JD. 2021. Ranking forest effects on snow storage: a decision tool for forest management. *Water Resources Research* DOI: 10.1029/2020wr027926

Dingman SL. 2015. *Physical hydrology*. DOI: 10.1177/030913338901300106

Eagleson PS. 1978. Climate, Soil, and Vegetation 4.The expected value of annual evapotranspiration. *Water Resources Research* **14** (5)

Ellis C, Pomeroy JW, Link TE. 2013. Modeling increases in snowmelt yield and desynchronization resulting from forest gap-thinning treatments in a northern mountain headwater basin. *Water Resources Research* **49** (2): 936–949 DOI: 10.1002/wrcr.20089

Esri. 2017. World Imagery: basemap Available at: https://services.arcgisonline.com/ArcGIS/rest/services/World_Imagery/MapServer [Accessed 2 February 2022]

Fang X, Pomeroy JW. 2016. Impact of antecedent conditions on simulations of a flood in a mountain headwater basin. *Hydrological Processes* **30** (16): 2754–2772 DOI: 10.1002/hyp.10910

Fellows AW, Flerchinger GN, Seyfried MS, Lohse KA, Patton NR. 2019. Controls on gross production in an aspen–sagebrush vegetation mosaic. *Ecohydrology* **12** (1): 1–14 DOI: 10.1002/eco.2046

Flerchinger GN, Fellows AW, Seyfried MS, Clark PE, Lohse KA. 2020. Water and Carbon Fluxes Along an Elevational Gradient in a Sagebrush Ecosystem. *Ecosystems* **23** (2): 246–263 DOI: 10.1007/s10021-019-00400-x

Garen BDC. 1992. Improved techniques in regression-based streamflow volume forecasting. *Journal of Water Resources Planning* **118** (6): 654–670

Geroy IJ, Gribb MM, Marshall HP, Chandler DG, Benner SG, McNamara JP, Amara JP. 2011. Aspect influences on soil water retention and storage. *Hydrological Processes* **25** (25): 3836–3842 DOI: 10.1002/hyp.8281

Gleason KE, Bradford JB, D'Amato AW, Fraver S, Palik BJ, Battaglia MA. 2021. Forest density intensifies the importance of snowpack to growth in water-limited pine forests. *Ecological Applications* **31** (1): 1–12 DOI: 10.1002/eap.2211

Goulden ML, Bales RC. 2014. Mountain runoff vulnerability to increased evapotranspiration with vegetation expansion. *Proceedings of the National Academy of Sciences of the United States of America* **111** (39): 14071–14075 DOI: 10.1073/pnas.1319316111

Granier A. 1985. Une nouvelle méthode pour la mesure du flux de sève brute dans le tronc des arbres. *Annals of Forest Science* **42** (2): 193–200 Available at: https://doi.org/10.1051/forest:19850204 [Accessed 23 January 2022]

Gray DM, Male DH. 1981. *Handbook of Snow: Principles, Processes, Management & Use*. Blackburn Press.

Grogan DS, Burakowski EA, Contosta AR. 2020. Snowmelt control on spring hydrology declines as the vernal window lengthens. *Environmental Research Letters* DOI: https://doi.org/10.1088/1748-9326/abbd00

Gupta H v., Kling H, Yilmaz KK, Martinez GF. 2009. Decomposition of the mean squared error and NSE performance criteria: Implications for improving hydrological modelling. *Journal of Hydrology* **377** (1–2): 80–91 DOI: 10.1016/j.jhydrol.2009.08.003

Haleakala K, Gebremichael M, Dozier J, Lettenmaier DP. 2021a. Factors Governing Winter Snow Accumulation and Ablation Susceptibility Across the Sierra Nevada, U.S.A. *Journal of Hydrometeorology* **22**: 1455–1472 DOI: 10.1175/jhm-d-20-0257.1

Haleakala K, Gebremichael M, Dozier J, Lettenmaier DP, K. H, M. G, J. D, D.P. L, Haleakala K, Gebremichael M, et al. 2021b. Factors Governing Winter Snow Accumulation and Ablation Susceptibility Across the Sierra Nevada, U.S.A. *Journal of Hydrometeorology* **22** (6): 1455–1472 DOI: DOI 10.1175/JHM-D-20-0257.1

Hamlet AF, Mote PW, Clark MP, Lettenmaier DP. 2005. Effects of Temperature and Precipitation Variability on Snowpack Trends in the Western United States. *Journal of Climate* **18** (21): 4545–4561

Hammond JC, Harpold AA, Weiss S, Kampf SK. 2019. Partitioning snowmelt and rainfall in the critical zone: effects of climate type and soil properties. *Hydrology and Earth System Sciences* **23** (9): 3553–3570 DOI: 10.5194/hess-23-3553-2019

Hammond JC, Saavedra FA, Kampf SK. 2018a. How Does Snow Persistence Relate to Annual Streamflow in Mountain Watersheds of the Western U.S. With Wet Maritime and Dry Continental Climates? *Water Resources Research* **54** (4): 2605–2623 DOI: 10.1002/2017WR021899

Hammond JC, Saavedra FA, Kampf SK. 2018b. How Does Snow Persistence Relate to Annual Streamflow in Mountain Watersheds of the Western U.S. With Wet Maritime and Dry Continental Climates? *Water Resources Research* **54** (4): 2605–2623 DOI: 10.1002/2017WR021899

Hardy JP, Melloh R, Koenig G, Marks D, Winstral A, Pomeroy JW, Link TE. 2004. Solar radiation transmission through conifer canopies. *Agricultural and Forest Meteorology* **126** (3–4): 257–270 DOI: 10.1016/j.agrformet.2004.06.012

Hardy JP, Melloh R, Robinson P, Jordan R. 2000. Incorporating effects of forest litter in a snow process model. *Hydrological Processes* **14** (18): 3227–3237 DOI: 10.1002/1099-1085(20001230)14:18<3227::AID-HYP198>3.0.CO;2-4

Harpold AA. 2016. Diverging sensitivity of soil water stress to changing snowmelt timing in the Western U.S. *Advances in Water Resources* **92**: 116–129 DOI: 10.1016/j.advwatres.2016.03.017

Harris PP, Huntingford C, Cox PM, Gash JHC, Malhi Y. 2004. Effect of soil moisture on canopy conductance of Amazonian rainforest. *Agricultural and Forest Meteorology* **122** (3–4): 215–227 DOI: 10.1016/j.agrformet.2003.09.006

Harrison HN, Hammond JC, Kampf S, Kiewiet L. 2021. On the hydrological difference between catchments above and below the intermittent-persistent snow transition. *Hydrological Processes* **35** (11) DOI: 10.1002/hyp.14411

Harshburger BJ, Humes KS, Walden VP, Blandford TR, Moore BC, Dezzani RJ. 2010. Spatial interpolation of snow water equivalency using surface observations and remotely sensed images of snow-covered area. *Hydrological Processes* **24** (10): 1285–1295 DOI: 10.1002/hyp.7590

Havens S, Marks D, FitzGerald K, Masarik M, Flores AN, Kormos P, Hedrick A. 2019. Approximating Input Data to a Snowmelt Model Using Weather Research and Forecasting Model Outputs in Lieu of Meteorological Measurements. *Journal of Hydrometeorology* **20** (5): 847–862 DOI: 10.1175/jhm-d-18-0146.1

Hedstrom NR, Pomeroy JW. 1998. Measurements and modelling of snow interception in the boreal forest. *Hydrological Processes* **12** (10–11): 1611–1625 DOI: 10.1002/(SICI)1099-1085(199808/09)12:10/11<1611::AID-HYP684>3.0.CO;2-4

Hinckley ES, Ebel BA, Barnes RT, Anderson RS, Williams MW, Anderson SP. 2014. Aspect control of water movement on hillslopes near the rain – snow transition of the Colorado Front Range. **85** (October 2012): 74–85 DOI: 10.1002/hyp.9549

Hojatimalekshah A, Uhlmann Z, Glenn N, Hiemstra C, Tennant C, Graham J, Spaete L, Gelvin A, Marshall H-P, McNamara J, et al. 2020. Tree canopy and snow depth relationships at fine scales with terrestrial laser scanning. *The Cryosphere Discussions*: 1–35 DOI: 10.5194/tc-2020-277

Honjo T, Lin TP, Seo Y. 2019. Sky view factor measurement by using a spherical camera. *Journal of Agricultural Meteorology* **75** (2): 59–66 DOI: 10.2480/agrmet.D-18-00027

Hu J, Moore DJP, Burns SP, Monson R. 2010. Longer growing seasons lead to less carbon sequestration by a subalpine forest. *Global Change Biology* **16** (2): 771–783 DOI: 10.1111/j.1365-2486.2009.01967.x

Hubbart JA, Link TE, Gravelle JA. 2015. Forest canopy reduction and snowpack dynamics in a Northern Idaho watershed of the continental-maritime region, United States. *Forest Science* **61** (5): 882–894 DOI: 10.5849/forsci.14-025

Iturbide, M., Fernández J, Gutiérrez JM, Bedia J, Cimadevilla E, Díez-Sierra J, Manzanas R, Casanueva A, Baño-Medina J, Milovac J, Herrera S, et al. 2021. Repository supporting the implementation of FAIR principles in the IPCC-WG1 Atlas DOI: 10.5281/zenodo.3691645

Jarvis PG. 1976. The Interpretation of the Variations in Leaf Water Potential and Stomatal Conductance Found in Canopies in the Field. *Philosophical Transactions of the Royal Society B: Biological Sciences* **273** (927): 593–610 DOI: 10.1098/rstb.1976.0035

Jennings KS, Molotch NP. 2020. Snowfall Fraction, Cold Content, and Energy Balance Changes Drive Differential Response to Simulated Warming in an Alpine and Subalpine Snowpack. *Frontiers in Earth Science* **8** (June): 1–16 DOI: 10.3389/feart.2020.00186

Jennings KS, Kittel TGF, Molotch NP. 2018. Observations and simulations of the seasonal evolution of snowpack cold content and its relation to snowmelt and the snowpack energy budget. *The Cryosphere* (1): 1595–1614 DOI: https://doi.org/10.5194/tc-12-1595-2018

Kelleners TJ, Chandler DG, McNamara JP, Gribb MM, Seyfried MS. 2010. Modeling Runoff Generation in a Small Snow-Dominated Mountainous Catchment. *Vadose Zone Journal* **9** (3): 517–527 DOI: 10.2136/vzj2009.0033

Kleine L, Tetzlaff D, Smith A, Goldhammer T, Soulsby C. 2021. Using isotopes to understand landscape-scale connectivity in a groundwater-dominated, lowland catchment under drought conditions. *Hydrological Processes* **35** (5): 1–20 DOI: 10.1002/hyp.14197

Klos PZ, Link TE, Abatzoglou JT. 2014. Extent of the rain-snow transition zone in the western U.S. under historic and projected climate. *Geophysical Research Letters* **41**: 4560–4568 DOI: 10.1002/2014GL060500

Knowles JF, Molotch NP, Trujillo E, Litvak ME. 2018. Snowmelt-Driven Trade-Offs Between Early and Late Season Productivity Negatively Impact Forest Carbon Uptake During Drought. *Geophysical Research Letters* **45** (7): 3087–3096 DOI: 10.1002/2017GL076504

Knowles N, Dettinger MD, Cayan DR. 2006. Trends in snowfall versus rainfall in the western United States. *Journal of Climate* **19** (18): 4545–4559 DOI: 10.1175/JCLI3850.1

Kormos PR, Marks D, McNamara JP, Marshall HP, Winstral A, Flores AN. 2014. Snow distribution, melt and surface water inputs to the soil in the mountain rain-snow transition zone. *Journal of Hydrology* **519** (PA): 190–204 DOI: 10.1016/j.jhydrol.2014.06.051

Kormos PR, Marks D, Pierson FB, Williams CJ, Hardegree SP, Havens S, Hedrick A, Bates JD, Svejcar TJ. 2017. Ecosystem water availability in juniper versus sagebrush snow-dominated rangelands. *Rangeland Ecology and Management* **70** (1): 116–128 DOI: 10.1016/j.rama.2016.05.003

Kormos PR, McNamara JP, Seyfried MS, Marshall HP, Marks D, Flores AN. 2015. Bedrock infiltration estimates from a catchment water storage-based modeling approach in the rain snow transition zone. *Journal of Hydrology* **525**: 231–248 DOI: 10.1016/j.jhydrol.2015.03.032

Koutantou K, Mazzotti G, Brunner P, Webster C, Jonas T. 2022. Exploring snow distribution dynamics in steep forested slopes with UAV- borne LiDAR Cold Regions Science and Technology Exploring snow distribution dynamics in steep forested slopes with UAV-borne LiDAR. *Cold Regions Science and Technology* **200** (May): 103587 DOI: 10.1016/j.coldregions.2022.103587

Kraft M, McNamara JP. 2022. Evapotranspiration across the rain–snow transition in a semi-arid watershed. *Hydrological Processes* **36** (3) DOI: 10.1002/hyp.14519

Kuppel S, Tetzlaff D, Maneta MP, Soulsby C. 2018. What can we learn from multi-data calibration of a process-based ecohydrological model? *Environmental Modelling and Software* **101**: 301–316 DOI: 10.1016/j.envsoft.2018.01.001

Lawler RR, Link TE. 2011. Quantification of incoming all-wave radiation in discontinuous forest canopies with application to snowmelt prediction. *Hydrological Processes* **25** (21): 3322–3331 DOI: 10.1002/hyp.8150

Li D, Wrzesien ML, Durand M, Adam J, Lettenmaier DP. 2017. How much runoff originates as snow in the western United States, and how will that change in the future? *Geophysical Research Letters* **44** (12): 6163–6172 DOI: 10.1002/2017GL073551

Looker N, Martin J, Hoylman Z, Jencso K, Hu J. 2018. Diurnal and seasonal coupling of conifer sap flow and vapour pressure deficit across topoclimatic gradients in a subalpine catchment. *Ecohydrology* **11** (7): 1–16 DOI: 10.1002/eco.1994

Looker N, Martin J, Jencso K, Hu J. 2016. Contribution of sapwood traits to uncertainty in conifer sap flow as estimated with the heat-ratio method. *Agricultural and Forest Meteorology* **223**: 60–71 DOI: 10.1016/j.agrformet.2016.03.014

Lopez-Moreno JI, Gascoin S, Herrero J, Sproles EA, Pons M, Alonso-González E, Hanich L, Boudhar A, Musselman KN, Molotch NP, et al. 2017. Different sensitivities of snowpacks to warming in Mediterranean climate mountain areas. *Environmental Research Letters* **12** DOI: https://doi.org/10.1088/1748-9326/aa70cb

Lundquist JD, Loheide SP. 2011. How evaporative water losses vary between wet and dry water years as a function of elevation in the Sierra Nevada, California, and critical factors for modeling. *Water Resources Research* **47** (5): 1–13 DOI: 10.1029/2010WR010050

Lundquist JD, Dickerson-Lange SE, Lutz JA, Cristea N. 2013. Lower forest density enhances snow retention in regions with warmer winters: A global framework developed from plot-scale observations and modeling. *Water Resources Research* **49** (10): 6356–6370 DOI: 10.1002/wrcr.20504

Malle J, Rutter N, Mazzotti G, Jonas T. 2019. Shading by trees and fractional snow cover control the sub-canopy radiation budget. *Journal of Geophysical Research: Atmospheres* **124** (6): 3195–3207 DOI: 10.1029/2018jd029908

Malle J, Rutter N, Webster C, Mazzotti G, Wake L, Jonas T. 2021. Effect of forest canopy structure on wintertime Land Surface Albedo: Evaluating CLM5 simulations with in-situ measurements. *Journal of Geophysical Research: Atmospheres* (April) DOI: 10.1029/2020jd034118

Maneta MP, Silverman NL. 2013. A spatially distributed model to simulate water, energy, and vegetation dynamics using information from regional climate models. *Earth Interactions* **17** (11): 1–44 DOI: 10.1175/2012EI000472.1

Marks D, Winstral A. 2001. Comparison of Snow Deposition , the Snow Cover Energy Balance , and Snowmelt at Two Sites in a Semiarid Mountain Basin. *Journal of Hydrometeorology* **2** (3): 213–227

Marks D, Kimball J, Tingey D, Link TE. 1998. The sensitivity of snowmelt processes to climate conditions and forest cover during rain-on-snow : a case study of the 1996 Pacific Northwest flood. *Hydrological Processes* **12**: 1569–1587

Marks D, Link TE, Winstral A, Garen D. 2001. Simulating snowmelt processes during rain-on-snow over a semi-arid mountain basin. *Annals of Glaciology* **32**: 195–202 DOI: 10.3189/172756401781819751

Marks D, Winstral A, Reba ML, Pomeroy JW, Kumar M. 2013. An evaluation of methods for determining during-storm precipitation phase and the rain/snow transition elevation at the surface in a mountain basin. *Advances in Water Resources* **55**: 98–110 DOI: 10.1016/j.advwatres.2012.11.012

Marshall AM, Link TE, Abatzoglou JT, Flerchinger GN, Marks DG, Tedrow L. 2019a. Warming Alters Hydrologic Heterogeneity: Simulated Climate Sensitivity of Hydrology-Based Microrefugia in the Snow-to-Rain Transition Zone. *Water Resources Research* **55** (3): 2122–2141 DOI: 10.1029/2018WR023063

Marshall HP, Vuyovich C, Hiemstra CA, Brucker L, Elder K, Deems JS, Newlin J. 2019b. NASA SNOWEX 2020 Experiment Plan

Martin J, Looker N, Hoylman Z, Jencso K, Hu J. 2018. Differential use of winter precipitation by upper and lower elevation Douglas fir in the Northern Rockies. *Global Change Biology* **24** (12): 5607–5621 DOI: 10.1111/gcb.14435

Martinec J, Rango A, Major E. 1983. Snowmelt-Runoff Model (Srm) User'S Manual. *NASA Reference Publication* (1100)

Mazzotti G, Currier WR, Deems JS, Pflug JM, Lundquist JD, Jonas T. 2019. Revisiting Snow Cover Variability and Canopy Structure Within Forest Stands: Insights From Airborne Lidar Data. *Water Resources Research* **55** (7): 6198–6216 DOI: 10.1029/2019wr024898

McCutcheon RJ, McNamara JP, Kohn MJ, Evans SL. 2017. An evaluation of the ecohydrological separation hypothesis in a semiarid catchment. *Hydrological Processes* **31** (4): 783–799 DOI: 10.1002/hyp.11052

McNamara JP, Benner SG, Poulos MJ, Pierce JL, Chandler DG, Kormos PR, Marshall H-P, Flores AN, Seyfried M, Glenn NF, et al. 2018. Form and function relationships revealed by long-term research in a semiarid mountain catchment. *Wiley Interdisciplinary Reviews: Water* **5** (2): e1267 DOI: 10.1002/wat2.1267

McNamara JP, Chandler D, Seyfried M, Achet S. 2005. Soil moisture states , lateral flow , and streamflow generation in a semi-arid , snowmelt-driven catchment. *Hydrological Processes* **19** (2005): 4023–4038 DOI: 10.1002/hyp.5869

Milly PCD, Dunne KA. 2020. Colorado River flow dwindles as warming-driven loss of reflective snow energizes evaporation. *Science* **367** (6483): 1252–1255 DOI: 10.1126/science.aax0194

Mitra B, Papuga SA, Alexander MR, Swetnam TL, Abramson N. 2020. Allometric relationships between primary size measures and sapwood area for six common tree species in snow-dependent ecosystems in the Southwest United States. *Journal of Forestry Research* **31** (6): 2171–2180 DOI: 10.1007/s11676-019-01048-y

Moeser D, Roubinek J, Schleppi P, Morsdorf F, Jonas T. 2014. Canopy closure, LAI and radiation transfer from airborne LiDAR synthetic images. *Agricultural and Forest Meteorology* **197**: 158–168 DOI: 10.1016/j.agrformet.2014.06.008

Molotch N, Brooks P, Burns SP, Litvak ME, Monson RK, McConnell JR, Musselman KN. 2009. Ecohydrology controls on snowmelt partitioning in mixed-conifer sub-alpine forests. *Ecohydrology* **2**: 129–142 DOI: 10.1002/eco.48

Moore C, Kampf S, Stone B, Richer E. 2015. A GIS-based method for defining snow zones: application to the western United States. *Geocarto International* **30** (1): 62–81 DOI: 10.1080/10106049.2014.885089

Morris EM. 1989. Turbulent transfer over snow and ice. *Journal of Hydrology* **105** (3–4): 205–223 DOI: 10.1016/0022-1694(89)90105-4

Mote PW, Li S, Lettenmaier DP, Xiao M, Engel R. 2018. Dramatic declines in snowpack in the western US. *npj Climate and Atmospheric Science* **1** (1) DOI: 10.1038/s41612-018-0012-1

Musselman K, Vano J, Molotch N. 2021. Melt trends portend widespread declines in snow water resources. *Nature Climate Change* **11**: 418–424 DOI: https://doi.org/10.21203/rs.3.rs-79081/v1

Musselman KN, Clark MP, Liu C, Ikeda K, Rasmussen R. 2017. Slower snowmelt in a warmer world. *Nature Climate Change* **7** (3): 214–219 DOI: 10.1038/nclimate3225

Musselman KN, Molotch NP, Brooks PD. 2008. Effects of vegetation on snow accumulation and ablation in a mid-latitude sub alpine forest. *Hydrological Processes* **22**: 2767–2776 DOI: 10.1002/hyp.7050

Petersky RS, Shoemaker KT, Weisberg PJ, Harpold AA. 2019. The sensitivity of snow ephemerality to warming climate across an arid to montane vegetation gradient. *Ecohydrology* **12** (2): 1–14 DOI: 10.1002/eco.2060

Petrie MD, Pockman WT, Pangle RE, Limousin JM, Plaut JA, McDowell NG. 2015. Winter climate change promotes an altered spring growing season in piñon pine-juniper woodlands. *Agricultural and Forest Meteorology* **214–215**: 357–368 DOI: 10.1016/j.agrformet.2015.08.269

Pomeroy JW. 1994. Sensitivity of snow relocation and sublimation to climate and surface vegetation. (423)

Pomeroy JW, Marks D, Link TE, Ellis C, Hardy J, Rowlands AA, Granger R. 2009. The Impact of coniferous forest temperature on incoming longwave radiation to melting snow. *Hydrological Processes* **23** (May): 2513–2525 DOI: 10.1002/hyp.7325

Pomeroy JW, Parviainen J, Hedstrom N, Gray DM. 1998. Coupled modelling of forest snow interception and sublimation. *Hydrological Processes* **12** (15): 2317–2337 DOI: 10.1002/(SICI)1099-1085(199812)12:15<2317::AID-HYP799>3.0.CO;2-X

Potter C. 2020. Snowmelt timing impacts on growing season phenology in the northern range of Yellowstone National Park estimated from MODIS satellite data. *Landscape Ecology* **3** DOI: 10.1007/s10980-019-00951-3

Poulos MJ, Smith TJ, Benner SG, Pierce JL, Flores AN, Seyfried MS, McNamara JP. 2021. Topographically Moderated Soil Water Seasons Impact Vegetation Dynamics in Semiarid Mountain Catchments: Illustrations from the Dry Creek Experimental Watershed, Idaho, USA. *Hydrological Processes* **35** (12) DOI: 10.1002/hyp.14421

R Core Team. 2021. R: A language and environment for statistical computing

Rasouli K, Pomeroy JW, Whitfield PH. 2022. The sensitivity of snow hydrology to changes in air temperature and precipitation in three North American headwater basins. *Journal of Hydrology* **606**: 127460 DOI: 10.1016/j.jhydrol.2022.127460

Rice R, Bales RC, Painter TH, Dozier J. 2011. Snow water equivalent along elevation gradients in the Merced and Tuolumne River basins of the Sierra Nevada. *Water Resources Research* **47** (8): 1–11 DOI: 10.1029/2010WR009278

Richardson AD, Keenan TF, Migliavacca M, Ryu Y, Sonnentag O, Toomey M. 2013. Climate change, phenology, and phenological control of vegetation feedbacks to the climate system. *Agricultural and Forest Meteorology* **169**: 156–173 DOI: 10.1016/j.agrformet.2012.09.012

Richardson JJ, Moskal LM, Kim SH. 2009. Modeling approaches to estimate effective leaf area index from aerial discrete-return LIDAR. *Agricultural and Forest Meteorology* **149** (6–7): 1152–1160 DOI: 10.1016/j.agrformet.2009.02.007

Robles MD, Hammond JC, Kampf SK, Biederman JA, Demaria EMC. 2021. Winter Inputs Buffer Streamflow Sensitivity to Snowpack Losses in the Salt River Watershed in the Lower Colorado River Basin. *Water* **13** (3) DOI: https://doi.org/10.3390/w13010003

Rodrigues TR, Vourlitis GL, Lobo F de A, Santanna FB, de Arruda PHZ, Nogueira J de S. 2016. Modeling canopy conductance under contrasting seasonal conditions for a tropical savanna ecosystem of south central Mato Grosso, Brazil. *Agricultural and Forest Meteorology* **218–219** (January): 218–229 DOI: 10.1016/j.agrformet.2015.12.060

Roth TR, Nolin AW. 2017. Forest impacts on snow accumulation and ablation across an elevation gradient in a temperate montane environment. *Hydrology and Earth System Sciences* **21** (11): 5427–5442 DOI: 10.5194/hess-21-5427-2017

Roth TR, Nolin AW. 2019. Characterizing Maritime Snow Canopy Interception in Forested Mountains. *Water Resources Research*: 4564–4581 DOI: 10.1029/2018WR024089

Running SW, Nemani RR. 1988. Relating Seasonal Pattersn of the AVHRR Vegetation Index to Simulated Photosythesis and Transpiration of Forests in Different Climates. *Remote Sensing of Environment* **24**: 347–367

Safa H, Krogh SA, Greenberg J, Kostadinov TS, Harpold AA. 2021. Unraveling the Controls on Snow Disappearance in Montane Conifer Forests Using Multi-Site Lidar. *Water Resources Research*: 1–20 DOI: 10.1029/2020wr027522

Schleppi P, Conedera M, Sedivy I, Thimonier A. 2007. Correcting non-linearity and slope effects in the estimation of the leaf area index of forests from hemispherical photographs. *Agricultural and Forest Meteorology* **144** (3–4): 236–242 DOI: 10.1016/j.agrformet.2007.02.004

Segura C. 2021. Snow drought reduces water transit times in headwater streams. *Hydrological Processes* **35** (12): 1–17 DOI: 10.1002/hyp.14437

Seyednasrollah B, Kumar M. 2014. Net radiation in a snow-covered discontinuous forest gap for a range of gap sizes and topographic configurations. *Journal of Geophysical Research* **119** (17): 10,323-10,342 DOI: 10.1002/2014JD021809

Seyednasrollah B, Kumar M, Link TE. 2013. On the role of vegetation density on net snow cover radiation at the forest floor. *Journal of Geophysical Research: Atmospheres* **118** (15): 8359–8374 DOI: 10.1002/jgrd.50575

Seyfried M, Flerchinger G, Bryden S, Link T, Marks D, McNamara J. 2021. Slope and aspect controls on soil climate: Field documentation and implications for large-scale simulation of critical zone processes. *Vadose Zone Journal* **20** (6): 1–17 DOI: 10.1002/vzj2.20158

Sicart JE, Essery RLH, Pomeroy JW, Hardy J, Link T, Marks D. 2004. A Sensitivity Study of Daytime Net Radiation during Snowmelt to Forest Canopy and Atmospheric Conditions. *Journal of Hydrometeorology* **5**: 774–784 DOI: 10.1175/1525-7541(2004)005<0774:ASSODN>2.0.CO;2

Smith TJJ, McNamara JP, Flores AN, Gribb MM, Aishlin PS, Benner SG. 2011. Small soil storage capacity limits benefit of winter snowpack to upland vegetation. *Hydrological Processes* **25** (25): 3858–3865 DOI: 10.1002/hyp.8340

Soil Survey Staff NRCSUSD of A. Soil Survey Geographic (SSURGO) Database for Idaho

Soil-Survey-Staff. 2013. US General Soil Map. *USDA Natural Resources Conservation Service* Available at: http://websoilsurvey.nrcs.usda.gov/app/WebSoilSurvey.aspx [Accessed 1 January 2022]

Stewart JB. 1988. Modelling surface conductance of pine forest. *Agricultural and Forest Meteorology* **43** (1): 19–35 DOI: 10.1016/0168-1923(88)90003-2

Storck P, Lettenmaier DP, Bolton SM. 2002. Measurement of snow interception and canopy effects on snow accumulation and melt in a mountainous maritime climate, Oregon, United States. *Water Resources Research* **38** (11): 5-1-5–16 DOI: 10.1029/2002wr001281

Sturm M, Liston GE. 2021. Revisiting the Global Seasonal Snow Classification: An Updated Dataset for Earth System Applications. *Journal of Hydrometeorology*: 2917–2938 DOI: 10.1175/jhm-d-21-0070.1

Tague C, Heyn K, Christensen L. 2009. Topographic controls on spatial patterns of conifer transpiration and net primary productivity under climate warming in mountain ecosystems. *Ecohydrology* **2** (4): 541–554 DOI: 10.1002/eco.88

Tague CL, Band LE. 2004. RHESSys: Regional Hydro-Ecologic Simulation System - An object Oriented Approach to Spatially Distributed Modeling of Carbon, Water, and Nutrient Cycling. *Earth Interactions* **8** (19) DOI: 10.1175/1087-3562(2004)8<1:RRHSSO>2.0.CO;2

Tennant CJ, Harpold AA, Lohse KA, Godsey SE, Crosby BT, Larsen LG, Brooks PD, van Kirk RW, Glenn NF. 2017. Regional sensitivities of seasonal snowpack to elevation, aspect, and vegetation cover in western North America. *Water Resources Research* **53** (8): 6908–6926 DOI: 10.1002/2016WR019374

Tetzlaff D, Buttle J, Carey SK, van Huijgevoort MHJ, Laudon H, Mcnamara JP, Mitchell CPJ, Spence C, Gabor RS, Soulsby C. 2015. A preliminary assessment of water partitioning and ecohydrological coupling in northern headwaters using stable isotopes and conceptual runoff models. *Hydrological Processes* **29** (25): 5153–5173 DOI: 10.1002/hyp.10515

Tolson BA, Shoemaker CA. 2007. Dynamically dimensioned search algorithm for computationally efficient watershed model calibration. *Water Resources Research* **43** (1): 1–16 DOI: 10.1029/2005WR004723

Tor-ngern P, Oren R, Oishi AC, Uebelherr JM, Palmroth S, Tarvainen L, Ottosson-Löfvenius M, Linder S, Domec JC, Näsholm T. 2017. Ecophysiological variation of transpiration of pine forests: Synthesis of new and published results. *Ecological Applications* **27** (1): 118–133 DOI: 10.1002/eap.1423

Trujillo E, Molotch NP, Goulden ML, Kelly AE, Bales RC. 2012. Elevation-dependent influence of snow accumulation on forest greening. *Nature Geoscience* **5** (10): 705–709 DOI: 10.1038/ngeo1571

Varhola A, Coops NC, Weiler M, Moore RD. 2010. Forest canopy effects on snow accumulation and ablation: An integrative review of empirical results. *Journal of Hydrology* **392** (3–4): 219–233 DOI: 10.1016/j.jhydrol.2010.08.009

Wang R, Kumar M, Marks D. 2013. Anomalous trend in soil evaporation in a semi-arid, snow-dominated watershed. *Advances in Water Resources* **57**: 32–40 DOI: 10.1016/j.advwatres.2013.03.004

Webster C, Jonas T. 2018. Influence of canopy shading and snow coverage on effective albedo in a snow-dominated evergreen needleleaf forest. *Remote Sensing of Environment* **214** (September 2017): 48–58 DOI: 10.1016/j.rse.2018.05.023

Webster C, Rutter N, Zahner F, Jonas T. 2016. Measurement of Incoming Radiation below Forest Canopies: A Comparison of Different Radiometer Configurations. *Journal of Hydrometeorology* **17** (3): 853–864 DOI: 10.1175/JHM-D-15-0125.1

Williams CJ, McNamara JP, Chandler DG. 2009. Controls on the temporal and spatial variability of soil moisture in a mountainous landscape : the signature of snow and complex terrain. *Hydrology and Earth System Sciences* **13**: 1325–1336

Winstral A, Marks D, Gurney R. 2009. An efficient method for distributing wind speeds over heterogeneous terrain. *Hydrological Processes* **23**: 2523–2535 DOI: 10.1002/hyp.7141

Zeng X, Broxton P, Dawson N. 2018. Snowpack Change From 1982 to 2016 Over Conterminous United States. *Geophysical Research Letters* **45** (23): 12,940-12,947 DOI: 10.1029/2018GL079621

Zhang L. 1997. Cross-validation of non-linear growth functions for modelling tree height-diameter relationships. *Annals of Botany* **79** (3): 251–257 DOI: 10.1006/anbo.1996.0334

APPENDIX A

Chapter 4 Supplemental Material

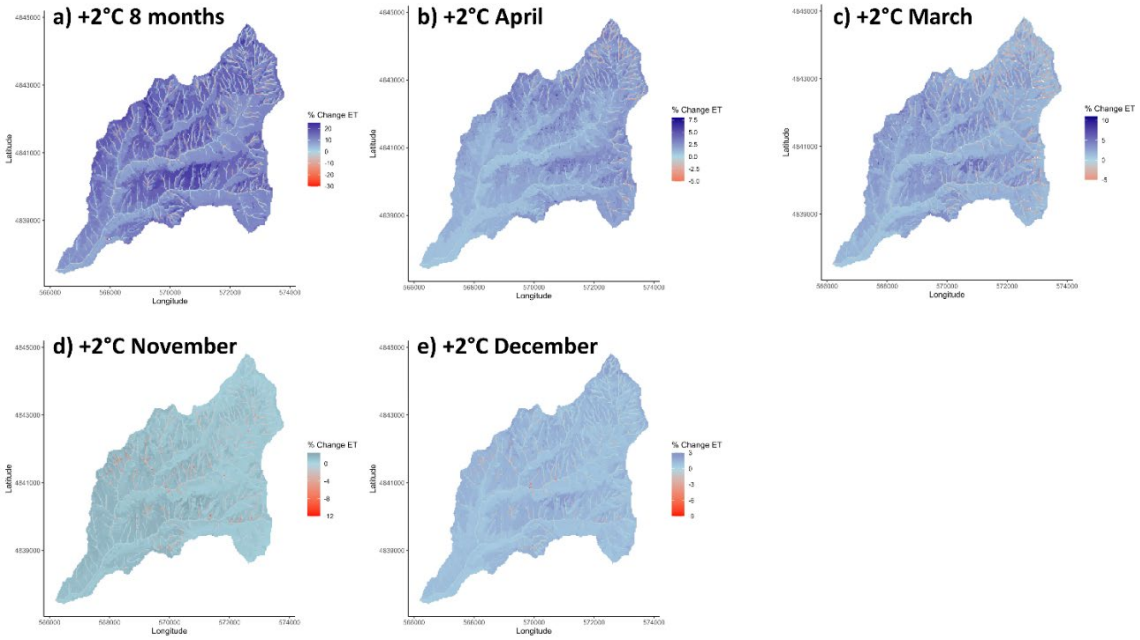

Figure A.1 Percent change in ET from the base case for the 8 months (a), April (b), March (c), November (d), and December (e).

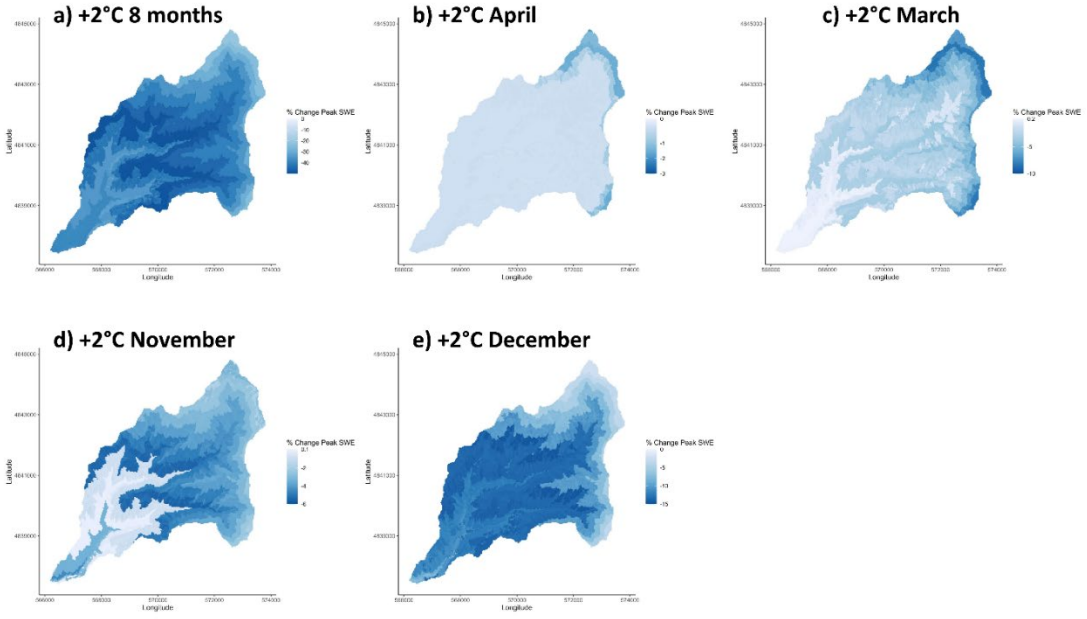

Figure A.2 Percent change in snow water equivalent from the base case 8 months (a), April (b), March (c), November (d), and December (e).

Table A.1 Calibrated parameter values and calibration ranges.

Calibrated Parameters	Calibrated Value				
Soil Parameter	**Sandy Loam**	**Bedrock**	**Loamy Coarse Sand**	**Loam**	**Calibration Range**
Porosity (η, m3/m3)	0.20	0.27	0.30	0.20	0.17 - 0.4
Saturated horizontal hydraulic conductivity (K_{hx}, m/s)	9.45E-05	0.00013	0.0003	0.00083	5E-8 - .009
Ratio of vertical-to-horizontal hydraulic conductivity ($KvKh$, -)	0.0076	0.0011	0.00099	0.0007	5E-05- 1E-2
Brooks-Corey exponent parameter (b, -)	2.76	3.56	3.26	2.97	2.3-10.0
Air-entry pressure head (ψ_{ae}, m)	0.71	0.39	0.14	0.3	0.01 - 0.8
Leakance (L_b)	0.04	0.04	0.04	0.04	3E-20 - .05
Depth of the 1st hydrological layer (m)	0.22	0.081	0.044	0.16	0.01 - 0.2
Depth of the 2nd hydrological layer (m)	0.63	0.42	0.65	0.66	0.01 - 0.5
Total Soil Depth (m)	5.4	2.49	2.44	3.84	0.75 – 6.0
Vegetation Parameter	**Herbaceous**	**Shrubs**	**Forest**		**Calibration Range**
Maximum stomatal conductance (gs_{max}, m/s)	0.00829	0.04	0.031		0.005 - 0.1
Maximum interception storage per unit LAI (m)	5.47E-08	9.67E-06	3.24E-03		5E-10-.004
Optimal Temperature for Stomatal Conductance (deg C)	29.4	28.0	30.0		8.0 - 40.0

Maximum Temperature for Stomatal Conductance (deg C)	49.7	43.4	47.0		40 - 60
Minimum Temperature for Stomatal Conductance (deg C)	2.9	-2	0.8		-5.0 – 5.0
Stomatal Conductance VPD Coefficient	1.12E-13	3.60E-14	1.60E-14		9E-15 - .09
Minimum LWP for Stomatal Conductance (MPa)	0.99	1	0.5		0.5-2.0
Maximum LWP for Stomatal Conductance (MPa)	1.1	0.8	0.54		0.5-5.0
Beer's Law Light Extinction Coefficient (K_b)	0.71	0.54	0.7		0.3-1.0
Parameter Controlling Sensitivity to Light	963	400	800		150 - 1000
	Below 1418 m Elevation	**1418 – 1619 m Elevation**	**Above 1619 m Elevation**		**Calibration Range**
Snowmelt Coefficient (m/°C)	4.43E-08	2.21E-08	2.36E-08		9E-9 - 4.5E-8

Table A.2 Modeled versus measured statistics between point measurements of streamflow, SWE, soil moisture and transpiration for all years, the calibration period (WY2016 – WY2019), validation period (WY2020 – WY2021) and each year. The TL soil moisture site was only used for validation and the transpiration site was only used for calibration.

Timeframe	Bias	R^2	RMSE	KGE	Variable
All Years	0.016	0.536	0.199	0.664	LG Streamflow
Calibration	0.000	0.580	0.211	0.738	LG Streamflow
Validation	0.051	0.429	0.174	-0.550	LG Streamflow
2016	-0.044	0.797	0.090	0.675	LG Streamflow
2017	0.051	0.882	0.166	0.558	LG Streamflow
2018	-0.049	0.833	0.071	0.573	LG Streamflow
2019	0.041	0.401	0.368	0.601	LG Streamflow
2020	0.086	0.346	0.224	-1.119	LG Streamflow
2021	0.013	0.657	0.089	0.317	LG Streamflow
All Years	-0.005	0.735	0.108	0.777	SWE BR
Calibration	-0.018	0.790	0.107	0.788	SWE BR
Validation	0.022	0.538	0.111	0.686	SWE BR
2016	-0.030	0.835	0.070	0.760	SWE BR
2017	0.000	0.701	0.110	0.824	SWE BR
2018	-0.012	0.914	0.038	0.851	SWE BR
2019	-0.037	0.755	0.172	0.676	SWE BR
2020	-0.032	0.837	0.093	0.645	SWE BR
2021	0.075	0.483	0.126	0.532	SWE BR

All Years	-0.004	0.727	0.026	0.772	Soil Moisture LDP
Calibration	-0.003	0.763	0.025	0.788	Soil Moisture LDP
Validation	-0.006	0.623	0.029	0.723	Soil Moisture LDP
2016	-0.005	0.718	0.027	0.760	Soil Moisture LDP
2017	-0.003	0.821	0.021	0.841	Soil Moisture LDP
2018	-0.008	0.847	0.023	0.739	Soil Moisture LDP
2019	0.002	0.696	0.027	0.788	Soil Moisture LDP
2020	-0.003	0.625	0.029	0.741	Soil Moisture LDP
2021	-0.011	0.546	0.028	0.667	Soil Moisture LDP
All Years	-0.005	0.816	0.022	0.776	Soil Moisture TL
2016	-0.005	0.817	0.022	0.776	Soil Moisture TL

2017	-0.008	0.829	0.022	0.791	Soil Moisture TL
2018	-0.006	0.849	0.021	0.769	Soil Moisture TL
All Years	-0.081	0.783	0.636	0.869	Pine Transpiration
2016	-0.216	0.686	0.814	0.737	Pine Transpiration
2017	0.026	0.878	0.479	0.900	Pine Transpiration